Statistical glacier distribution in global- and regional-scale glacier modelling

Submitted to University of Bremen, Fachbereit 8, for the degree of Dr. rer. nat. by

David Parkes

Current affiliation: Earth and Life Institute, Université Catholique de Louvain

supervised by
Prof. Ben Marzeion - Institute of Geography, University of Bremen

Colloquium: June 28, 2018

Reviewers:
Prof. Ben Marzeion - Institute of Geography, University of Bremen
Prof. Olaf Eisen - Alfred Wegener Institute

May 1, 2019

(first submission April 2, 2018)

Contents

Thesis Summary

Changes in the total mass of glaciers globally form a major component of recent – and likely future – global mean sea-level rise (GMSLR), but only a handful of glaciers have detailed and long-term measurements that allow observational estimates of mass change on multi-decadal timescales. Estimating ice mass changes in glaciers on regional and global scales is typically handled with models that run on a per-glacier basis, using an inventory of glaciers collected using satellite mapping. This approach can result in mass change errors resulting from biases in the glacier inventories, particularly relating to small glaciers.

The primary aims of this thesis are to improve our understanding of the distribution of glacierised area on large scales, and to use this information to inform improvements or corrections to regional- and global-scale glacier modelling efforts. Three papers are presented. The first paper examines the link between anthropogenic climate forcing and the response of glaciers on a regional scale, and finds that glacier mass losses can be partly attributed to anthropogenic influences in many regions in the latter part of the 20th century. This highlights the importance of the correct treatment of large-scale glacier modelling for predicting future changes under different anthropogenic forcing scenarios. The second paper uses an observed power-law relationship between glacier area and the number of glaciers globally to estimate under-representation of smaller glaciers in inventories, and uses this to apply an upscaling to mass change estimates produced by an established glacier model, resulting in a sizeable new contribution to GMSLR. The third paper tests the hypothesis that glacierised area, on large scales, has an effective fractal dimension, and finds that a recognisable fractal dimension can be estimated for a majority of regions, which is a potential starting point for understanding the spatial distribution of glaciers accounted for statistically in the second paper.

Zusammenfassung der Arbeit

Änderungen in der Gesamtmasse der Gletscher sind eine Hauptkomponente des globalen Anstiegs des mittleren Meeresspiegels (GMSLR) in der Vergangenheit und wahrscheinlich auch in der Zukunft, aber nur für wenige Gletscher gibt es detaillierte und langfristige direkte Messungen, die eine Abschätzung der Massenänderung auf multidekadischen Zeitskalen ermöglichen. Auf regionaler und globaler Ebene wird die Massenänderungen der Gletscher normalerweise mit Modellen abgeschätzt. Diese Modelle simulieren das Verhalten jedes einzelnen Gletschers, wobei ein Gletscherinventar verwendet wird, das mithilfe von Satellitenkartierungen erstellt wurde. Dieser Ansatz kann zu Fehlern führen, die aus Fehlern des Gletscherinventars stammen, insbesondere bei kleinen Gletschern.

Das Hauptziel dieser Arbeit ist es, unser Verständnis der Verteilung von Gletscherflächen auf großen räumlichen Maßstäben zu verbessern und diese Information zu nutzen, um Verbesserungen der Gletschermodellierung auf regionaler und globaler Ebene zu erreichen. Dazu werden drei Aufsätze vorgestellt: Im ersten Ausatz wird der Zusammenhang zwischen anthropogener Klimaänderung und der Reaktion der Gletschern auf globaler Skala untersucht und festgestellt , dass Gletschermassenverluste in der zweiten Hälfte des 20. Jahrhunderts in vielen Regionen der Erde zum Großteil auf anthropogene Einflüsse zurückzuführen sind. Dieses Ergebnis unterstreicht die Bedeutung der korrekten Modellierung von Gletschern im großen räumlichen Maßstab für die Vorhersage zukünftiger Änderungen unter verschiedenen Szenarien des anthropogenen Antriebs. Der zweite Aufsatz verwendet eine empirische Potenzgesetzbeziehung zwischen Gletscherfläche und der Zahl der Gletscher weltweit, um die Unterrepräsentation kleinerer Gletscher im Inventar abzuschätzen. Diese Beziehung wird dann verwendet, um die mit einem etablierten Gletschermodell bestimmten Massenänderungen hochzuskalieren, was zu einem beachtlichen neuer Beitrag zum GMSLR führt. Der dritte Aufsatz testet die Hypothese, dass die Gletscherfläche in großen Maßstäben eine fraktale Dimension hat. Wir stellen fest, dass eine Schätzung dieser fraktalen Dimension auf regionaler Ebene genutzt werden kann als ein potenzieller Ausgangspunkt, um die räumliche Verteilung der im zweiten Aufsatz hochskalierten Gletscher zu bestimmen.

Preface

This overview and collection of papers is presented as my cumulative thesis for the degree of PhD in physical geography at the University of Bremen, Germany.

The overview section begins with an introduction to the field of large-scale glacier modelling, and an explanation of the motivations behind the original work in the three papers. Next, the papers are summarised individually, then the conclusions from the papers taken together are explored. Finally, there is a discussion of the impacts of the presented work, and of the potential future changes to large-scale glacier modelling that may result from it.

The papers appear next. The first and second are published, and the third is in preparation for submission at the time of writing.

1. Marzeion, B., J.G. Cogley, K. Richter and D.A. Parkes, 2014: Attribution of global glacier mass loss to anthropogenic and natural causes. *Science* **345** (6199), 919-921

2. Parkes, D.A. and B. Marzeion, 2018: Major 20th Century Contribution to Sea-Level Rise from Uncharted Glaciers. *Nature* **563**, 551-554

3. Parkes, D.A. and B. Marzeion, 2018: The Fractal Dimension of Spatial Glacier Distribution on Regional Scales, to be submitted to *The Cryosphere*

This work was funded by the Austrian Science Fund (FWF) project P25362.

Acknowledgements

I would like to thank Ben Marzeion for being a remarkably trusting supervisor, supporting both my ideas and my idiosyncratic working style. His ability to provide consistent insight has been immensely valuable, and our discussions were invariably the most productive parts of my PhD work. I am equally grateful for his understanding on a personal level; without his tolerant attitude towards my need to take time off in the middle of my PhD, this thesis could not have been completed.

A great deal of understanding was also extended to me by my colleagues in Innsbruck, who are too numerous to mention, which I am thankful for.

I would like to thank my parents, Clare and Ben Parkes, for their support of every possible kind, particularly during the time after my contract in Innsbruck was completed. I was difficult to live with for much of the process, and I hope I can repay the kindness and love they have shown through their unwavering belief in me.

Declaration of authorship

I declare that all work presented here is my own, without unauthorised external assistance, and with all sources and aids duly referenced and all reproduced material clearly labelled. No use has been made of material beyond the sources referenced. The electronic copy submitted is identical to the physical copy submitted.

David Parkes, May 1, 2019

Chapter 1

Overview

1.1 Introduction

Global cumulative mass changes for glaciers outside of the Antarctic and Greenland ice sheets are of great interest to the climate science community as one of the most significant contributors to post-industrial global mean sea-level rise (GSMLR) and as a future contributor to GMSLR under a continuation of warming climate [24, 8]. Comprehensive estimates of total glacier mass change on regional and global scales are a necessary part of the GMSLR budget, and their accuracy relies on both the quality of the available data on glacier geometry, and the effectiveness of modelling techniques used to translate this data into mass changes.

Large data sets for glacier location and surface area exist [66, 57], but are only relatively recently available, due to their reliance on large scale, high resolution aerial or satellite mapping techniques. Any mass change hindcasting effort that attempts to go back further than about 3 decades will not have access to comprehensive glacier inventories to validate their choices for modelling or scaling against. By contrast, glacier length measurements go back, in some cases, to the 16th century [65], but exist only for small numbers of glaciers. Direct measurements of glacier properties in general are sparse, and biased towards more accessible glacierised regions [11, 33, 65], and while remote sensing data for differential ice elevation does exist [60] and can be applied over large, flat ice shelves and ice sheets to find changes in the ice surface elevation [21], it is unreliable for the smaller length-scales and steeper ice surfaces of mountain glaciers. Ultimately, better direct glacier measurements are an integral part of improving our ability to forecast and hindcast glacier mass changes, but the generation of new data sets requires expensive, time-consuming mapping efforts, and is often contingent on improvements in remote-sensing technology.

Because data from which mass changes can be directly derived are so rare, estimation of glacier mass changes on regional or global scales are usually the result of glacier modelling of various levels of complexity, from scaling relationships based on length, area, and volume [4, 34], through degree-day proxies of available melt energy over simplified geography [29, 39], to sophisticated models of glacier flow [15, 40]. Simpler models are typically computationally cheap, and not susceptible to overparameterisation, while more sophisticated models can represent more of the physical processes involved, and can better potray complex, non-linear responses if they are initialised and validated properly. Different models are applicable for different purposes, as we see later when discussing the integration of glacier modelling into global circulation models (GCMs).

One of the unifying factors across almost all forms of glacier model currently available is the treatment of glaciers as discretised phenomena; each glacier is modelled separately from an inventory of data for individual glaciers. In reality, glaciers are not permanent,

fixed-location structures. Under changing climates, glaciers can disappear, appear in new locations, split into separate ice masses, or multiple glaciers can combine into a single ice mass. This causes glacier modelling based on an existing inventory to run into a number of potential issues with systematic bias. The ability to entirely melt away glaciers in a region biased warmer under the model conditions than in reality, but not to generate new glaciers in regions colder under the model conditions results in an underestimate of actual ice mass even under climate scenarios with no overall bias. The inability to identify glaciers that are separate in a modern inventory but were historically part of a contiguous ice mass when they were larger can skew our historical distribution of glaciers towards smaller glacier sizes (see paper 2). These biases exist on top of any issues with the data used to generate the inventory; there are reasons to believe that, in many regions, the most up-to-date glacier inventories still have considerable numbers of missing glaciers amongst the smallest sizes [17] (see also paper 2).

Methods do exist for more dynamic simulation of glaciers across a landscape in a way that is not dependent on a pre-existing glacier location data set [10], but these are computationally expensive, especially over large regions, and are already known to underestimate the number of small glaciers when modelling glaciers under realistic climate scenarios. Small glaciers are particularly susceptible to the biases mentioned above, as they typically see the most rapid proportional changes (see paper 2), so a poor representation of the smallest glaciers will limit the ability of non-discretised glacier models to address the bias issues. Global application of high-resolution models that generate ice masses in response to climate and topography is likely a long-term goal in the same vein as improved remote-sensing inventories; limited by technology and the time/expense taken to develop and run.

1.2 Motivation

In the most general sense, the core goal of this thesis is to ensure that glacier distributions are represented as well as possible on regional and global scales for the purpose of glacier modelling, particularly with regard to mass changes for the purpose of calculating GMSLR contributions. No model can generate the best possible results if it does not have the access to the best possible data.

One of the main objectives is to look for a 'middle way' between the reliance on glacier inventory data of traditional glacier models, and the high model complexity and computational requirements of a model that deterministically builds up a distribution of glaciers given a topography and climate by representing the physical processes involved. If the issues of incompleteness in inventories and of systematic bias can be accounted for by modifications to discretised glacier models, representing discepancies between glacier inventories

and the actual distribution of glaciers statistically but without trying to explicitly 'create' new glaciers for the models to work with, this can help to improve total mass change estimates in the short term. In the longer term, such improvements to current models will allow for a smoother transition into models that are not reliant explicitly on glacier inventories; inevitably such models will be compared to and validated against discretised models, and this comparison will be more productive if both model types are trying to faithfully represent actual distributions rather than observed distributions with known deficiencies.

Particularly in papers 2 and 3, the goal is to characterise the properties of glacier distribution (the power law for frequency density, and the fractal dimension, in these papers respectively) in a way that allows for the augmentation of modern glacier inventories, or the reconstruction of analogous inventories for different regions, climates, or time periods. Paper 1 is not directly focused on the same aims of representativity, but is a strong argument for the fact that accurate glacier mass change modelling on large scales is critical to quantifying a major impact of anthropogenic climate change that is responsible for a significant portion of recent sea-level rise.

1.3 Paper summary

1.3.1 Paper 1: Attribution of global glacier mass loss to anthropogenic and natural causes

Using an established glacier mass balance model [39], the evolution of global glacier mass is calculated for the period 1851-2010 using two different modelled climate scenarios: one including all relevant forcings, both natural and anthropogenic, and the other including only natural forcings. The difference in glacier mass change between these two models is taken to represent the anthropogenic influence on glacier mass change, and is found to constitute a minor part of the total glacier mass change for 1851-2010 (25±35%), rising to the major part more recently for 1991-2010 (69±24%).

The modelled glacier mass changes between 1960 and 2010 are compared to an observational data set of pentadal mass changes [11]. Globally, the modelled changes using natural and anthropogenic forcings are more consistent with observations than the modelled changes using only natural forcings, with the disagreement between the model with only natural forcings and the observations becoming most pronounced from 1990 onwards. Across a majority of RGI regions, the model using natural and anthropogenic forcings is more consistent with observations than the model with only natural forcings, but there are regions where the opposite is true.

Conclusions

Glacier mass changes are the result of changes in climate, but the mechanisms by which they are affected are complex; there is a response time for glaciers to adjust to any changes, and the relationship with climate variables such as mean temperature is non-linear. Nevertheless, glacier mass changes in recent decades clearly show the impact of anthropogenic influences on climate, to the extent that they are now the primary drivers of glacier mass loss. Adjustments in response to the end of the Litte Ice Age were more significant in the early part of the post-industrial period, but more recently this cannot explain most of the observed mass changes. With anthropogenic influence on climate expected to grow over the coming decades, this suggests that significant glacier mass loss - and associated contributions to GMSLR - will continue and possibly accelerate. This makes it all the more important that the results from large-scale glacier models are as accurate as possible, in order to properly forecast a very significant impact of man-made climate change.

Personal contribution

D. Parkes performed the analysis of errors in the ensemble model outputs, and contributed to the manuscript.

1.3.2 Paper 2: Major 20th Century Contribution to Sea-Level Rise from Uncharted Glaciers

A significant global underrepresentation of small glaciers in the RGIv5 [1] inventory is quantified, using a power law established theoretically and through observations on smaller scales. Upscaling to account for these missing glaciers does not produce a large increase in present-day ice volume, but because the smallest glaciers today have typically changed the most over the last century, they are likely to have contributed a significant amount of the total mass loss from glaciers historically. A similar upscaling is used to account for glaciers which are not present today (and so will not be present even in a theoretically perfect current inventory) but have disappeared since 1901, meaning they have contributed to total glacier mass change over the 20th century.

Between 1901 and 2015, a total upper bound additional glacier mass change of 48.0±8.9 mm SLE (sea level equivalent) is calculated from all of the glaciers 'repopulated' thanks to the two upscalings applied (lower bound 16.7±3.0). This upper bound represents between 29.6% and 40.0% (lower bound between 12.8% and 18.8%) of the total glacier mass change over the same period, calculated using the same model. The contribution from the upscaling is largest - both in absolute terms and proportionally - earlier in the 20th century, as the

rapid shrinkage of small glaciers over the 20th century means they were typically larger (greater surface area, and therefore greater mass loss potential, even with a constant specific mass balance) then than in the later part of the 20th century/early 21st century. For the 1901-1990 period, the upper bound annual SLE mass change of 0.53 mm yr^{-1} from this upscaling compares favourably to the discrepancy of 0.5 mm yr^{-1} in GMSLR noted for this period in up-to-date sea level budgets [9], though the lower bound (and the upper bound for the earlier part of the 20th century) are not large enough to completely explain the observed discrepancies.

Conclusions

While modern, remote-sensing based glacier inventories are much more representative of glacierised area than many other collections of information about glaciers, they are still lacking at the smallest scales. Glaciers which are tiny today cannot be ignored for the purpose of historical modelling just because of their small current mass, and it should be recognised that estimates of the number of small glaciers in existence are likely to be too low, often by large margins. The same applies to disappeared glaciers, but even more so; these glaciers never feature in modern inventories, so any historical modelling based on modern inventories cannot represent them at all, without deliberate modifications. The most significant takeaway from this paper is that a large potential contributor to GMSLR exists but is not accounted for by previous sea-level budgets, and future efforts to quantify glacier contributions to sea-level change should be aware of the missing and disappeared glaciers defined in the paper and account for them in some way.

Personal contribution

D. Parkes developed the concept and design of the study with B. Marzeion. D. Parkes designed and implemented the method for upscaling glacier area, and performed the analysis of the results. D. Parkes wrote the manuscript with contributions from B. Marzeion.

1.3.3 Paper 3: The Fractal Dimension of Spatial Glacier Distribution on Regional Scales

A method to estimate fractal dimension for glacierised regions is implemented, based on the idea that glacierised area shows similarity to other earth system phenomena which have already been shown to have fractal dimension, such as rivers, which are - like glaciers - dependent on a combination of local climate and topography. Glaciers from the RGIv6 [57] are mapped onto square grids of varying side length, and a 'box counting' approach is applied; the number of grid squares, N, containing glacierised area is totalled, and compared

to the grid cell side length L. A linear relationship between $log(N)$ and $log(L)$ is indicative of a meaningful fractal dimension for the shape being measured, and this method results in estimated fractal dimension values for 14 of 19 RGIv6 regions. The estimated fractal dimension varies considerably between regions, and a moderate positive correlation between regional estimated fractal dimension and the total glacierised area in the region is found.

It is found that the regions where most measurements of glaciers are available - regions which disproportionately influence any observed scaling relationships - are not representative, in terms of fractal dimension, of the distribution of glaciers globally. Weighted by the total glacierised area in the region, the mean of regional estimated fractal dimension is much higher than it is when weighted by the number of available length, glaciological mass balance, or geodetic mass balance measurements.

Characterisation of glacier distribution using fractal dimension shows a limitation in an existing percolation theory based approach to understanding the statistical distribution of glaciers. A simple example of an enhanced approach, using knowledge of a region's fractal dimension to constrain a percolation theory model, is shown, but it is found that parameterisations of correlation length and directionality beyond the scope of the paper are likely needed before a significantly improved method for generating quantitatively and qualitatively realistic glacier distributions can be developed.

Conclusions

Good evidence exists for the spatial distribution of glaciers on regional scales displaying fractal properties. While the fractal dimension of a region does not directly impact properties such as glacier volume and mass balance, it is a metric that tells us something qualitative about the spatial characteristics of the regional distribution; how densely or sparsely clustered the glaciers are. The measurements which are used to calibrate and validate any glacier model aiming to estimate regional or global scale mass changes - in particular, mass balance - are heavily skewed towards regions which are not representative of the fractal dimension in regions that contain the most total glacier area. With fractal dimension reliant on the topography that constrains glacier geometry, models tuned to these measurements may be less representative than previously hoped.

Personal contribution

D. Parkes developed the concept and design of the study with B. Marzeion. D. Parkes designed and implemented the process for analysing multi-scale spatial distribution and estimating fractal dimension. D. Parkes wrote the manuscript with contributions from B. Marzeion.

Chapter 2

Paper 1: Attribution of global glacier mass loss to anthropogenic and natural causes

Ben Marzeion[1], J. Graham Cogley[2], Kristin Richter[1], & David Parkes[1]

[1]Institute of Meteorology and Geophysics, University of Innsbruck, Austria
[2]Department of Geography, Trent University, Peterborough, Canada

Published 2014 in *Science* **345** (6199), pages 919-921

2.1 Abstract

The ongoing global glacier retreat is impacting human societies by causing sea-level rise, changing seasonal water availability, and increasing geohazards. Melting glaciers are an icon of anthropogenic climate change. However, glacier response times are typically decades or longer, which implies that the present day glacier retreat is a mixed response to past and current natural climate variability and current anthropogenic forcing. Here we show that only 25±35% of the global glacier mass loss during the period 1851 to 2010 is attributable to anthropogenic causes. Nevertheless, the anthropogenic signal is detectable with high confidence in glacier mass balance observations during 1991 to 2010, and the anthropogenic fraction of global glacier mass loss rates during that period has increased to 69±24 %.

2.2 Main Text

While glaciers store less than 1 % of global ice mass [64], their mass loss has been a major cause of sea-level rise during the 20th century [24]. Glaciers are important regulators of the seasonal water cycle, providing melt water during dry seasons in many regions of the world [30, 32]. Glacier retreat often leads to the destabilization of mountain slopes and the formation of unstably dammed melt water lakes, increasing the risk of rock slides and catastrophic outburst floods [58]. The world wide glacier retreat over the past decades has therefore had many impacts on human societies, which should increase over the 21st century due to continued mass losses [39, 23, 53].

Even though warming accelerated over recent decades [27], glaciers have contributed to sea level rise during most of the 20th century with relatively constant mass loss rates [39, 24, 34]. The mass loss during the first decades of the 20th century presumably was governed by loss of ice at low altitudes, when glaciers retreated from their 19th century maxima at the end of the Little Ice Age [38]. Since glacier extent responds to changes in the glacier mass balance with a lag of decades to centuries [31, 26, 47], glaciers provide an opportunity to directly perceive long term climate change, not obscured by interannual variability. For this reason, images of retreating glaciers have become widely publicized illustrations for anthropogenic climate change. At the same time, the lagged response of glacier extents to climate changes complicates the attribution of the observed changes to any particular cause, since glacier mass change at any time is in part an ongoing adjustment of the glacier to previous climate change. The global retreat of glaciers observed today started around

the middle of the 19th century, coinciding with the end of the Little Ice Age [34], when the anthropogenic forcing of the climate system was very weak compared to today [44]. Given the response times of glaciers it is therefore reasonable to hypothesize that glaciers at present are responding both to naturally caused climate change of past centuries, and to the anthropogenic warming which has become stronger in recent decades. There is evidence that the recent mass loss of individual glaciers exceeds values expected from internal variability [56] and a rough estimate has been made of the influence of anthropogenic warming on global glacier mass loss [46], but explicit attribution of observed changes of individual glaciers is also complicated by the dynamic response of glaciers' geometries to climate forcing, since internal variability alone may cause glacier changes of the magnitude observed since the end of the Little Ice Age [59].

Here we quantify the evidence for a causal link between anthropogenic climate forcing and observed glacier surface mass balances, not of individual glaciers but of all the world's glaciers outside of Antarctica combined. We then attribute the global glacier retreat since 1851 to natural and anthropogenic causes. We use a model of global glacier evolution that treats the mass balance of each of the world's glaciers contained in the Randolph Glacier Inventory [2, 52] (RGI) individually, including a simple parametrization of ice dynamics leading to glacier hypsometry change [39]. Forced by observed climate [45, 43], the glacier model has been independently validated against both annual surface mass balance observations (Fig. 2.4) and observed, temporally accumulated volume changes of hundreds of glaciers [11], and has been used to reconstruct and project the global glacier mass change from 1851 to 2300 [39] based on climate reconstructions and projections from the Coupled Model Intercomparison Project phase 5 (CMIP5). See the supplementary online material for a comprehensive description of the model.

For each of twelve reconstructions of the global climate between 1851 and 2010, produced by general circulation models (GCMs) from the CMIP5 ensemble (see Table 2.1 for the list of the experiments used), we reconstructed the area and volume of each glacier in 1851 [39]. From this reconstructed glacier state, we modeled the evolution of each glacier forward in time. This forward model was run twice for each GCM: once subject to all known forcings (i.e., solar variability, volcanic eruptions, land use change, anthropogenic aerosols and greenhouse gas emissions; we call these model runs the FULL runs below), and once subject to only natural forcings (i.e., solar variability and volcanic eruptions; we call these model runs the NAT runs below). Figure 2.1a shows the ensemble mean and standard deviation of the global mean specific mass balances for the FULL and NAT runs. Since the global mean specific mass balance interpolated from observations [11] (we call these OBS below) is available as pentadal means only (black lines in Fig. 2.1a), we determined the pentadal means of the model runs (thick solid lines in Fig. 2.1a). In order to determine whether the modeled glacier mass balances (MBs) are consistent with observed MBs, we calculated the confidence level of the difference between modeled and observed MBs for

each pentad. High confidence in this difference (i.e., red shading) thus indicates model results that are inconsistent with observations.

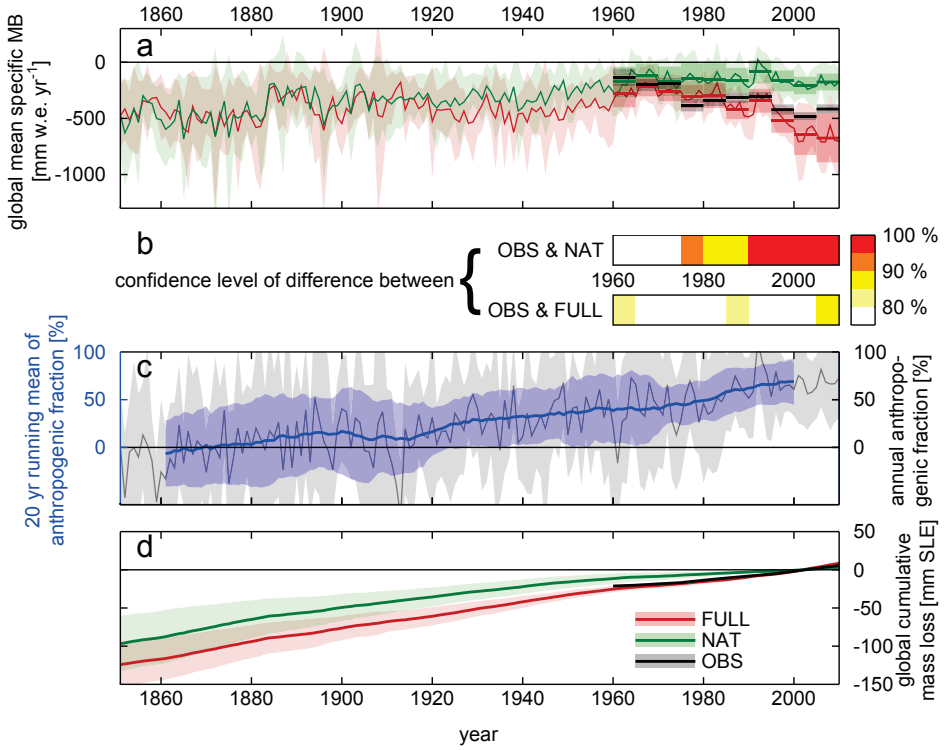

Figure 2.1: Attribution of the anthropogenic signal in global mean glacier mass balances. **a:** Global mean specific MB time series (thin lines are the ensemble mean, shading indicates one ensemble standard deviation), and pentadal means (thick lines are the ensemble mean, shading indicates one standard error, see supplement for the derivation of the error). Green: NAT results; red: FULL results; black: observations. **b:** Confidence level of the difference between interpolated observations (OBS) updated from Cogley (2009) [11] and model results for the NAT and FULL models for each pentad. **c:** Anthropogenic fraction of total glacier mass loss, annual values (gray) and running mean over 20-year periods (blue); solid line is ensemble mean, shading indicates one ensemble standard deviation. **d:** Glacier contribution to global mean sea-level rise, relative to the mean of 1991 to 2010. Modeled results include modeled glacier area change; observations assume constant glacier area, as in the RGI [2] (solid line is ensemble mean, shading indicates one ensemble standard deviation).

Table 2.1: CMIP5 model runs used in the study. From each model, the runs historical_r1i1p1 and historicalNat_r1i1p1 were used.

Modelling Center or Group	Model Name
Beijing Climate Center, China Meteorological Administration	BCC-CSM1.1
Canadian Centre for Climate Modelling and Analysis	CanESM2
National Center for Atmospheric Research	CCSM4
Centre National de Recherches Météorologiques/Centre Européen de Recherche et Formation Avancée en Calcul Scientifique	CNRM-CM5
Commonwealth Scientific and Industrial Research Organization in collaboration with Queensland Climate Change Centre of Excellence	CSIRO-Mk3.6.0
NOAA Geophysical Fluid Dynamics Laboratory	GFDL-CM3
NASA Goddard Institute for Space Studies	GISS-E2-R
Met Office Hadley Centre (additional HadGEM2-ES realizations contributed by Instituto Nacional de Pesquisas Espaciais)	HadGEM2-ES
Institut Pierre-Simon Laplace	IPSL-CM5A-LR
Japan Agency for Marine-Earth Science and Technology, Atmosphere and Ocean Research Institute (The University of Tokyo), and National Institute for Environmental Studies	MIROC-ESM
Meteorological Research Institute	MRI-CGCM3
Norwegian Climate Centre	NorESM1-M

Modeled MBs in both the FULL and NAT runs are negative over essentially the entire considered period. However, a difference emerges over the course of the 20th century: while the MB of the NAT runs becomes less negative as glaciers retreat to higher altitudes, thus stabilizing their mass balances, there is a clear trend towards more negative MBs of glaciers in the FULL runs after 1965. Modeled MBs in the FULL runs are generally consistent with observations during the entire period covered by the latter, while the NAT runs are inconsistent with observations for at least the four pentads spanning 1991 to 2010

(Fig. 2.1b). This means that the anthropogenic signal is detectable in observed MBs over these four pentads with high confidence, unaffected by the result that MBs would have been negative during this period even without anthropogenic climate forcing. The anthropogenic fraction of global specific glacier mass loss rates increased from -6±35 % during the period 1851 to 1870 to 69±24 % during the period 1991 to 2010 (Fig. 2.1c, uncertainties correspond to one ensemble standard deviation). Without anthropogenic influence, glaciers would have contributed 99±36 mm to global mean sea-level rise during 1851 to 2010. With anthropogenic influence, this number increases to 133±30 mm (Fig. 2.1d, uncertainties correspond to one ensemble standard deviation).

When global mean MBs over longer periods than pentads are considered, it becomes evident that the NAT runs are inconsistent with observations for any period spanning five to fifty years and ending in 2010 (Fig. 2.2). The FULL runs are generally consistent with observations, but the simulated MBs are more negative than the observations during 2001 to 2010 (Fig. 2.1b), resulting in a difference between FULL runs and observations above the 85% confidence level for periods spanning five to fifteen years and ending in 2010 (Fig. 2.2). This difference is caused by the FULL MBs for Svalbard and the Russian Arctic, which are too negative compared to the observations (see below).

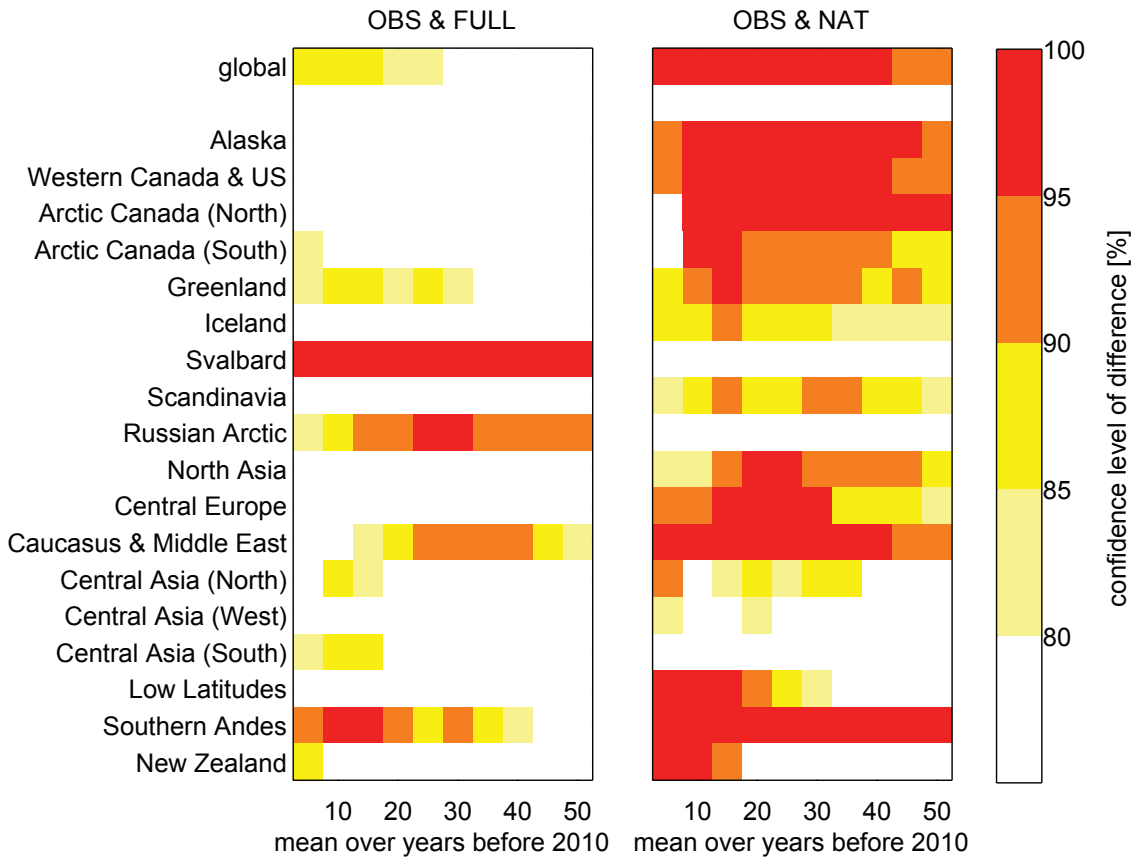

Figure 2.2: Detection of the anthropogenic signal in global and regional glacier mass balances over longer time intervals. Confidence levels of difference between observations [11] and model results for the NAT and FULL models for periods of different length ending in 2010. Regions as defined in the RGI [2]

Glacier mass losses attributable to human activity (shown as a fraction in Fig. 2.1c) have increased nearly steadily since 1860. In Fig. 2.3 we plot the year-by-year anthropogenic global mean specific mass balance $\mathrm{MB_{ANTH}} = \mathrm{MB_{FULL}} - \mathrm{MB_{NAT}}$ against the concurrent anthropogenic radiative forcing R [11], and find a sensitivity $d\mathrm{MB_{ANTH}}/dR$ of -209±33 kg yr^{-1} W^{-1} (uncertainty corresponds to the 95% confidence interval). This is about twice as much as a direct calculation based on the latent heat of fusion of ice would give (-94 kg yr^{-1} W^{-1}), indicating that feedbacks and the spatial distribution of anthropogenic climate change play an important role.

On the regional scale, the increased signal from internal climate variability, and greater uncertainty of GCM results [19], reduce the detectability of the anthropogenic signal. While

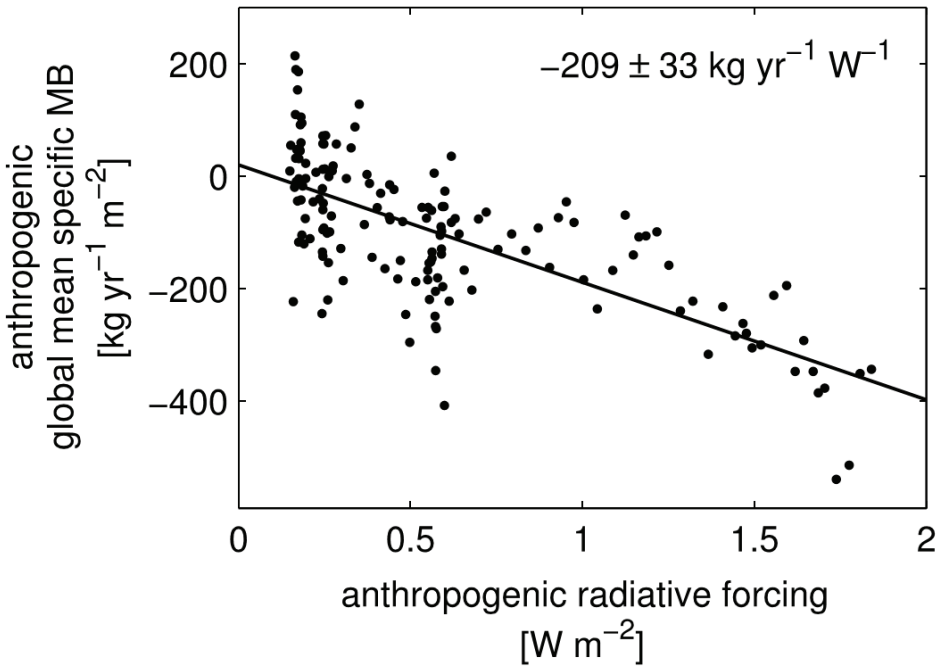

Figure 2.3: Sensitivity of the instantaneous anthropogenic global mean specific MB to global mean anthropogenic radiative forcing. Annual values of $\mathrm{MB}_{\mathrm{ANTH}}$ plotted against concurrent anthropogenic radiative forcing R [42]. The Pearson correlation coefficient between the two is -0.71.

there are some regions where the anthropogenic signal is detectable (i.e., FULL runs are consistent with observations, while NAT runs are inconsistent), there is also a number of regions where the FULL runs are not consistent with observations (Fig. 2.2). The anthropogenic signal is detectable with high confidence in Alaska, Western Canada & US, Arctic Canada North & South, Greenland (note that only peripheral glaciers and not the ice sheet are considered here), North Asia, Central Europe, Low Latitudes, and New Zealand (nine out of eighteen regions), and with lesser confidence in Iceland, Scandinavia, and Central Asia North (three out of eighteen regions). In Svalbard, the Russian Arctic, Caucasus & Middle East, and the Southern Andes, the FULL runs are inconsistent with observations (four out of eighteen regions), and in Central Asia South and West both FULL and NAT runs are consistent with observations (two out of eighteen regions). A closer look at those regions where our method fails reveals that in Caucasus & Middle East and the Southern Andes both the FULL and NAT runs underestimate the mass losses (in both cases, the FULL runs are closer to observations than the NAT runs).

In Svalbard and the Russian Arctic the FULL run overestimates the mass loss, while the NAT run is consistent with observations (Figure 2.5). GCMs tend to have greater errors in this region than on global average [19], but they do not generally exhibit a stronger warming during summer months or reduced precipitation compared to observations [43], which could explain too negative modeled MBs. When we exclude calving glaciers from the observational data set (calving is not accounted for in the glacier model, but does affect the observational estimate), the difference is reduced slightly, but not enough to lead to consistent results in these regions. Since validation of the glacier model on individual glaciers, as opposed to the regional mean, does not indicate a general underestimation of the modeled MBs in this region [39], the reason for this regional inconsistency has to be related to the sampling of glacier mass balance observations [22], but ultimately remains unclear.

Since the glaciers are considerably out of balance with both modeled FULL and NAT climate at the beginning of the simulation period, it is not possible to distinguish between glacier mass losses caused by internal variability and natural forcing. In order to address this question, it would be necessary to identify the causes that led to the build-up of glacier mass during the Little Ice Age, i.e. a period not covered by the CMIP5 experiments. However, our results indicate that a considerable fraction of 20th-century glacier mass loss, and therefore also of observed sea-level rise, was independent of anthropogenic climate forcing. At the same time we find unambiguous evidence of anthropogenic glacier mass loss in recent decades.

2.3 Supporting Online Material

Methods

Glacier model and forcing

The glacier model is set out in full in Marzeion et al. (2012, 2014) [39, 38], on which the following description relies heavily. We refer the reader to that source for further detail.

The glacier model is based on calculating the annual specific climatic mass balance B for each of the world's individual glaciers as

$$B = \left[\sum_{i=1}^{12} \left[P_i^{\text{solid}} - \mu^\star \cdot \max\left(T_i^{\text{terminus}} - T_{\text{melt}}, 0\right)\right]\right] - \beta^\star \tag{2.1}$$

where P_i^{solid} is the monthly solid precipitation onto the glacier surface per unit area, which depends on the monthly mean total precipitation and the temperature range between the glacier's terminus and highest elevations (i.e., temperature at terminus elevation below a certain threshold implies all precipitation is solid, temperature at the glacier's maximum elevation above the threshold implies all precipitation is liquid, and within that temperature range, the precipitation fraction is interpolated linearly, see Marzeion et al. (2012) [39] for a detailed description), $\mu^\star$ is the glacier's temperature sensitivity, T_i^{terminus} is the monthly mean air temperature at the glacier's terminus, T_{melt} is the monthly mean air temperature above which ice melt is assumed to occur, and $\beta^\star$ is a bias correction (see below). The model thus does not attempt to capture the full energy balance at the ice surface, but relies on air temperature as a proxy for the energy available for melt [49, 29, 61]. P_i^{solid} and T_i^{terminus} are determined based on gridded climate observations [45, 43], to which temperature and precipitation anomaly fields from the CMIP5 models are added (see Table S1). Changes affecting the glacier hypsometry (i.e. changes in its volume, surface area, and elevation range) are reflected in the determination of P_i^{solid} and T_i^{terminus}, which are modeled based on B, and on linearly adjusting the glacier's surface area and length towards their respective values obtained from volume-area and volume-length scaling [4, 3]. I.e., the surface area change $\mathrm{d}A$ of a glacier during each mass balance year t is calculated as

$$\mathrm{d}A(t) = \frac{1}{\tau_A(t)} \left(\left(\frac{V(t+1)}{c_A} \right)^{1/\gamma} - A(t) \right) \tag{2.2}$$

where $\tau_A(t)$ is the area relaxation time scale (see Eq. 2.5), $V(t+1)$ is the glacier's volume at the end of the mass balance year, $c_A = 0.0340$ km$^{3-2\gamma}$ (for glaciers), $c_A = 0.0538$ km$^{3-2\gamma}$

(for ice caps), $\gamma = 1.375$ (for glaciers), $\gamma = 1.25$ (for ice caps) are scaling parameters [4, 3], and $A(t)$ is the surface area of the glacier at the end of the preceding mass balance year. Similarly, length changes $\mathrm{d}L$ (and terminus elevation changes associated with them) during each mass balance year are estimated as

$$\mathrm{d}L(t) = \frac{1}{\tau_L(t)} \left(\left(\frac{V(t+1)}{c_L} \right)^{1/q} - L(t) \right) \tag{2.3}$$

where $\tau_L(t)$ is the length relaxation time scale (see Eq. 2.4), $c_L = 0.0180$ km^{3-q} (for glaciers), $c_L = 0.2252$ km^{3-q} (for ice caps), $q = 2.2$ (for glaciers), $q = 2.5$ (for ice caps) are scaling parameters [4, 3], and $L(t)$ is the glacier's length at the start of the mass balance year. The glacier length response time scale τ_L is estimated following roughly Johannesson et al. (1989) [31] as

$$\tau_L(t) = \frac{V(t)}{\sum_{i=1}^{12} \int P_{i,\mathrm{clim}}^{\mathrm{solid}}} \tag{2.4}$$

where $\int P_{i,\mathrm{clim}}^{\mathrm{solid}}$ is the monthly climatological solid precipitation integrated over the glacier surface area, calculated over the preceding 30 years. The glacier area response time scale is estimated as

$$\tau_A(t) = \tau_L(t) \frac{A(t)}{L(t)^2} \tag{2.5}$$

based on the assumption that area changes caused by glacier width changes occur instantaneously, while area changes caused by glacier length changes occur with the time scale of glacier length response.

The volume change dV of a glacier in year t is calculated as

$$dV(t) = B(t) \cdot A(t). \tag{2.6}$$

The temperature sensitivity $\mu^\star$ is determined from observed past variations for each of the glaciers with available mass balance in Cogley (2009) [11]. In that data set (see section *Mass balance observations* below), there is a global total of 255 glaciers that have all the metadata needed for the parameter estimation, that are covered by the temperature and precipitation data set we use (see below), that are indicated to be reliable by the status flag of the data set, and that have at least two annual mass balance measurements. The procedure is as follows. We assume that there exists some 31-year reference period, centered on year $t^\star$, whose climatology is such that the glacier with its present-day hypsometry would be in equilibrium, i.e. with its mass not changing. For this reference period, by construction

$$B = \sum_{i=1}^{12} \left[P(t^\star)_{i,\mathrm{clim}}^{\mathrm{solid}} - \mu(t^\star) \cdot \left(\max \left(T(t^\star)_{i,\mathrm{clim}}^{\mathrm{terminus}} - T_{\mathrm{melt}}, 0 \right) \right) \right] = 0 \tag{2.7}$$

where $P(t^\star)^{\text{solid}}_{i,\text{clim}}$ and $T(t^\star)^{\text{terminus}}_{i,\text{clim}}$ are the monthly climatological values of P_i^{solid} and T_i^{terminus}, during the 31 year period centered around the year $t^\star$. Note that we do not assume $t^\star$ to be a time at which the glacier was actually in balance. If the climate has been warming and the glacier retreating, as is generally the case, $t^\star$ would be in the past, and the glacier actually would have had a negative mass balance at time $t^\star$. The assumption is that if the climate of time $t^\star$ had been maintained, the glacier eventually would have contracted until it reached its present-day hypsometry.

We obtain a total of 109 monthly climatologies of precipitation and temperature (the data set of Mitchell and Jones (2005) [43] provides 109 years of monthly precipitation and temperature; at the end and beginning of the time series, the climatologies are calculated over shorter time periods), and subsequently obtain an estimate of μ from Eq. 2.7 for each of the 109 choices of $t^\star$. We then apply the glacier model to all glaciers for which direct mass balance observations are available, for each of the 109 possible values of $\mu(t)$. For each of these glaciers, we identify $t^\star$ as that time, for which applying the corresponding temperature sensitivity $\mu^\star \equiv \mu(t^\star)$ yields the smallest mean error of the modeled mass balances. This minimum difference is denoted by $\beta^\star$.

For glaciers without observed mass balances (i.e., the vast majority of glaciers), $t^\star$ is interpolated from surrounding glaciers with mass balance observations, and $\mu^\star$ is subsequently determined from solving Eq. 2.7 for $\mu^\star$, using precipitation and temperature obtained from the climatology centered around the interpolated value of $t^\star$.

The bias correction $\beta^\star$ is determined by interpolating the minimized bias obtained during the determination of $t^\star$ from surrounding glaciers with mass balance observations. A cross validation of the determination of $\mu^\star$ shows that the spatial interpolation of $t^\star$ leads to substantially smaller errors than the spatial interpolation of $\mu^\star$ [39]. This can be understood as an effect of neighboring glaciers experiencing a similar history of climate forcing, but having potentially very different temperature sensitivities.

Initial values for surface area and elevation distribution of each glacier are obtained by draping ice outlines from the Randolph Glacier Inventory [52] version 1 over version 2 of the ASTER global digital elevation model (GDEM), applying a suitable watershed algorithm [14] to separate ice complexes into individual glaciers, and extracting glacier elevation statistics (minimum, mean and maximum elevation) from the GDEM. The model accounts for the differing dates of surface area measurement in the Randolph Glacier Inventory by ensuring that the observed glacier extent is reproduced in the year of observation.

Treatment of uncertainty

Glacier model Uncertainty estimates of the glacier model are obtained by (i) performing a leave-one-glacier-out cross-validation that allows to determine the model's performance on glaciers without direct mass balance observations; (ii) propagating these uncertainties of the modeled mass balances through the entire glacier model, also taking into account uncertainties of the representation of the dynamic glacier response to volume changes; and (iii) validating these propagated and temporally accumulated uncertainties themselves using independent geodetically measured volume and surface area changes. Figure S1 shows the result of the cross-validation. The systematic, global mean bias of the glacier model is 5 mm w.e.

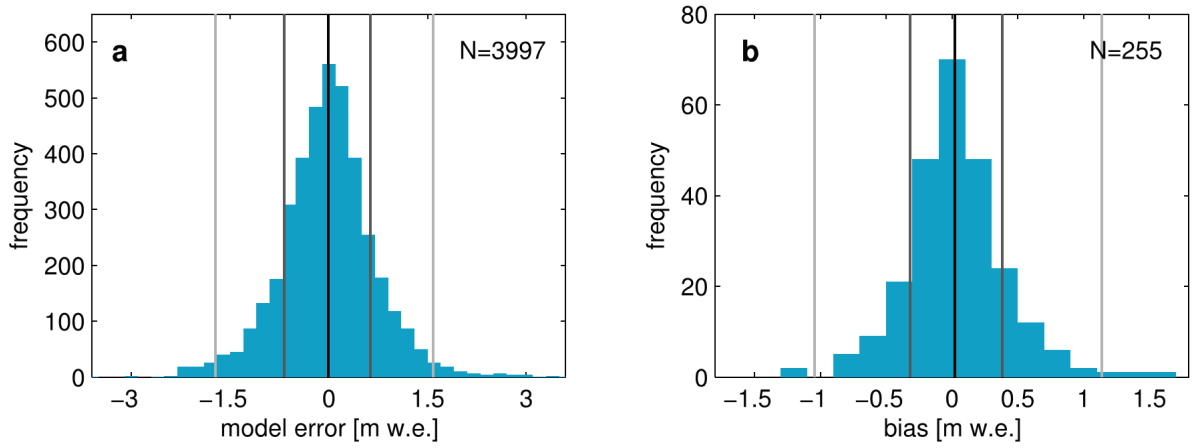

Figure 2.4: Results from the leave-one-glacier-out cross-validation; **(a)** distribution of the errors of the modeled individual mass balance years; **(b)** distribution of the systematic model bias for each individual glacier; vertical lines indicate the 2nd and 98th percentiles (light gray), 15th and 85th percentiles (dark gray), and median (black).

Given any pair of glaciers for which the cross-validation is carried out, we may calculate the temporal correlation between the annual time series for those two glaciers of the errors in the modeled mass balance. Considering all such pairs, we can calculate the correlation of this temporal error correlation with the distance between the two glaciers. This latter correlation is < 0.01 (not significant), indicating that the model errors for the individual glaciers can be treated as independent of each other. The global and regional model errors are thus taken as the root of the sum of the squared errors of the individual glaciers.

A more detailed and complete description of the determination of the model's parameters, both glacier-specific and global, and of the comprehensive validation of the model, can be found in Marzeion et al. (2012) [39].

Mass balance observations To correct for their uneven spatial distribution, all available in-situ (glaciological) measurements and measurements based on repeated surveys of elevation change from aircraft and satellites are interpolated to the glacierized cells of a $1^\circ \times 1^\circ$ global grid. For brevity we call these interpolated estimates *observations* (OBS), although in some regions there are few or even no actual measurements. The measurements, updated from those of Cogley (2009) [11] and available at `http://people.trentu.ca/~gcogley/glaciology/index.htm` as Release R1301, are too few for global estimation before 1960. Uncertainty estimates are obtained from a comprehensive error analysis [11].

Attribution of mass loss to anthropogenic forcing The global uncertainties of the glacier model, obtained as described above, are very small compared to the ensemble spread caused by using different global climate models for forcing the glacier model (see Marzeion et al. (2012) [39]; similar results are found by others [23, 53]. The uncertainty of the entire model chain is therefore dominated by the ensemble spread, and we base the uncertainty estimates of the entire model chain on ensemble spread rather than glacier model uncertainty.

To estimate the uncertainty σ of the modeled ensemble-mean pentadal MBs, we first determine the mean MB μ_i and uncertainty of the mean MB σ_i for each ensemble member i, based on the five annual values, as well as the ensemble-mean pentadal MB μ. We then estimate

$$\sigma = \left[\left(\sum_{i=1}^{n} \frac{\mu_i^2 + \sigma_i^2}{n} \right) - \mu^2 \right]^{1/2}$$

where $n = 12$ is the number of ensemble members, thus taking into account both ensemble spread and interannual variability as sources of uncertainty. We then obtain the confidence level of the difference between model results and observations by performing a paired t-test on the difference of the pentadal means; observed time series of annual MB are found to be serially independent and normally distributed [12], and we assume that the same holds for modeled MBs.

The anthropogenic fraction of global specific glacier mass loss rates (Fig. 1c) is taken as $1 - \frac{\mathrm{NAT}}{\mathrm{FULL}}$, and is therefore not limited between 0 and 100 % if NAT and FULL differ in sign, or if they have the same sign and NAT is greater than FULL.

Figure 2.5: Attribution of the anthropogenic signal in regional mean glacier mass balances. a: Regional mean specific MB time series (thin lines are the ensemble mean, shading indicates one ensemble standard deviation), and pentadal means (thick lines, shading indicates one standard error). Green: NAT results; red: FULL results; black: observations. b: Confidence level of the difference between interpolated observations (OBS) updated from Cogley (2009) [11] and model results for the NAT and FULL models for each pentad. c: Glacier contribution to global mean sea-level rise, relative to the mean of 1991 to 2010. Modeled results include modeled glacier area change; observations assume constant glacier area, as in the Randolph Glacier Inventory (solid line is ensemble mean, shading indicates one ensemble standard deviation).

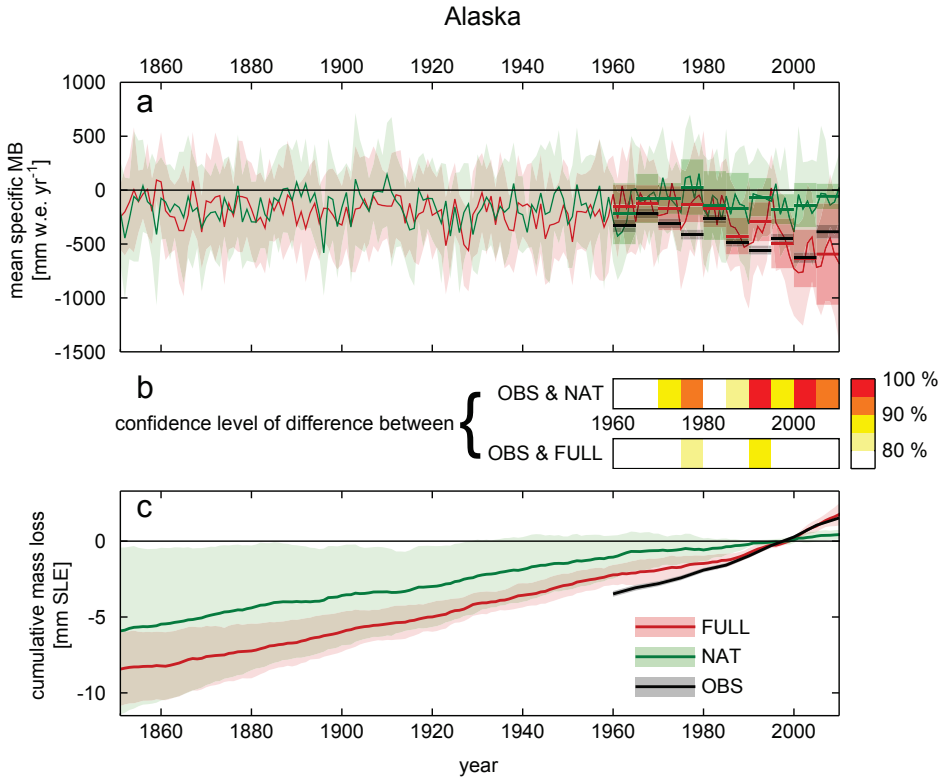

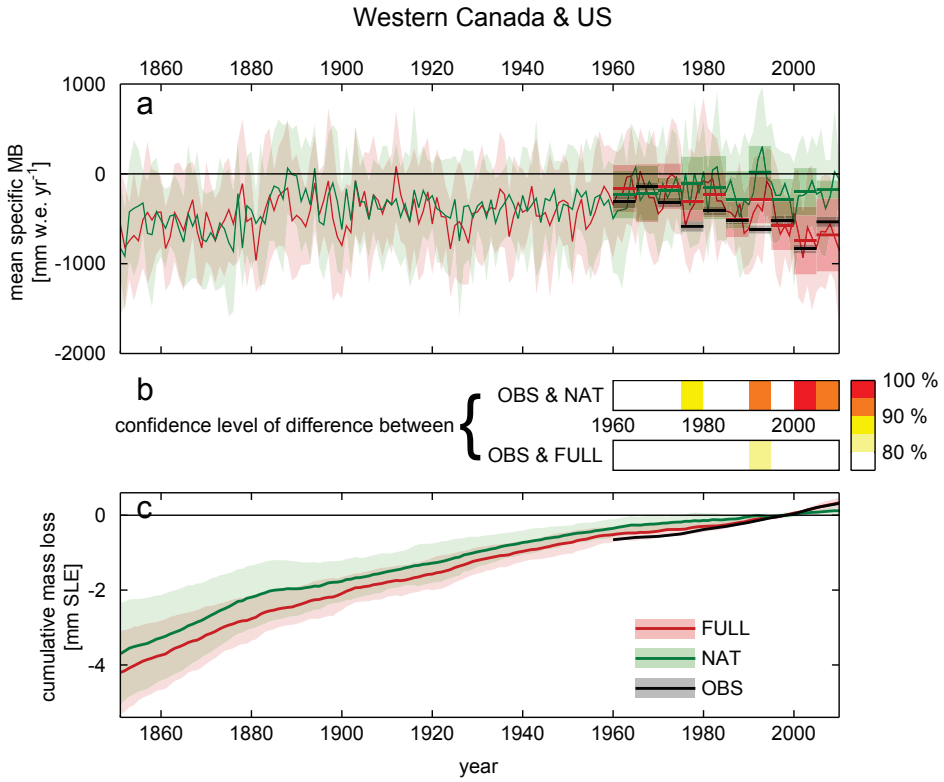
Western Canada & US
a
mean specific MB
[mm w.e. yr-1]
1000
0
-1000
-2000
1860
1880
1900
1920
1940
1960
1980
2000
b
confidence level of difference between
OBS & NAT
OBS & FULL
1960
1980
2000
100 %
90 %
80 %
c
cumulative mass loss
[mm SLE]
0
-2
-4
FULL
NAT
OBS
year

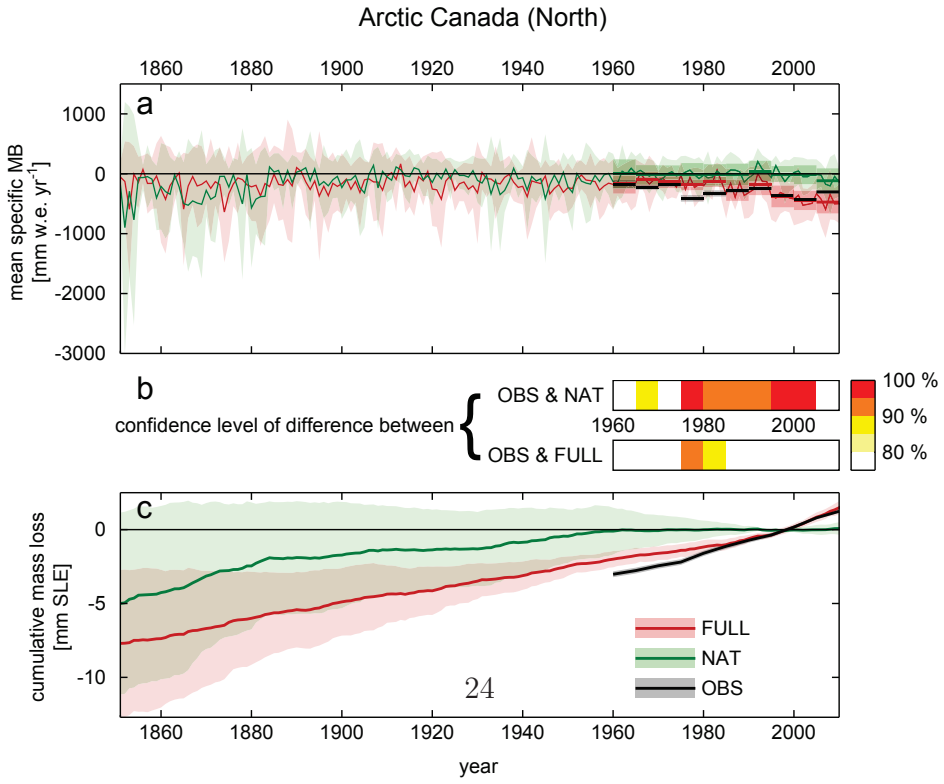
Arctic Canada (North)
a
mean specific MB
[mm w.e. yr-1]
1000
0
-1000
-2000
-3000
1860
1880
1900
1920
1940
1960
1980
2000
b
confidence level of difference between
OBS & NAT
OBS & FULL
1960
1980
2000
100 %
90 %
80 %
c
cumulative mass loss
[mm SLE]
0
-5
-10
FULL
NAT
OBS
year

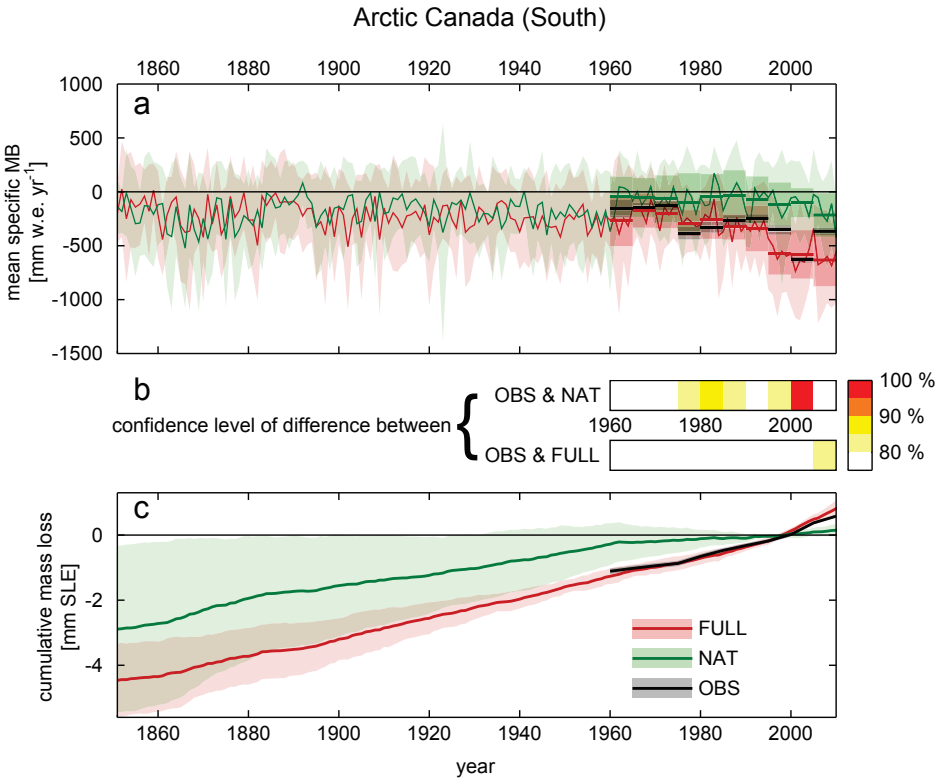
Arctic Canada (South)
a
mean specific MB
[mm w.e. yr-1]
1000
500
0
-500
-1000
-1500
1860
1880
1900
1920
1940
1960
1980
2000
b
confidence level of difference between
OBS & NAT
OBS & FULL
1960
1980
2000
100 %
90 %
80 %
c
cumulative mass loss
[mm SLE]
0
-2
-4
FULL
NAT
OBS
year

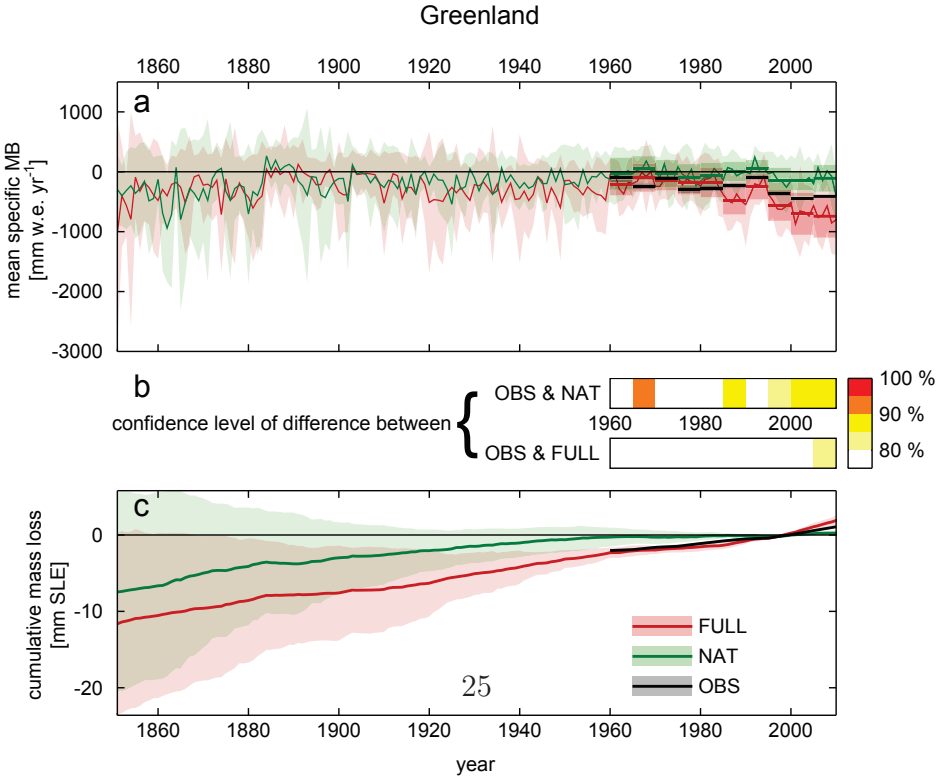
Greenland
a
mean specific MB
[mm w.e. yr-1]
1000
0
-1000
-2000
-3000
1860
1880
1900
1920
1940
1960
1980
2000
b
confidence level of difference between
OBS & NAT
OBS & FULL
1960
1980
2000
100 %
90 %
80 %
c
cumulative mass loss
[mm SLE]
0
-10
-20
FULL
NAT
OBS
year

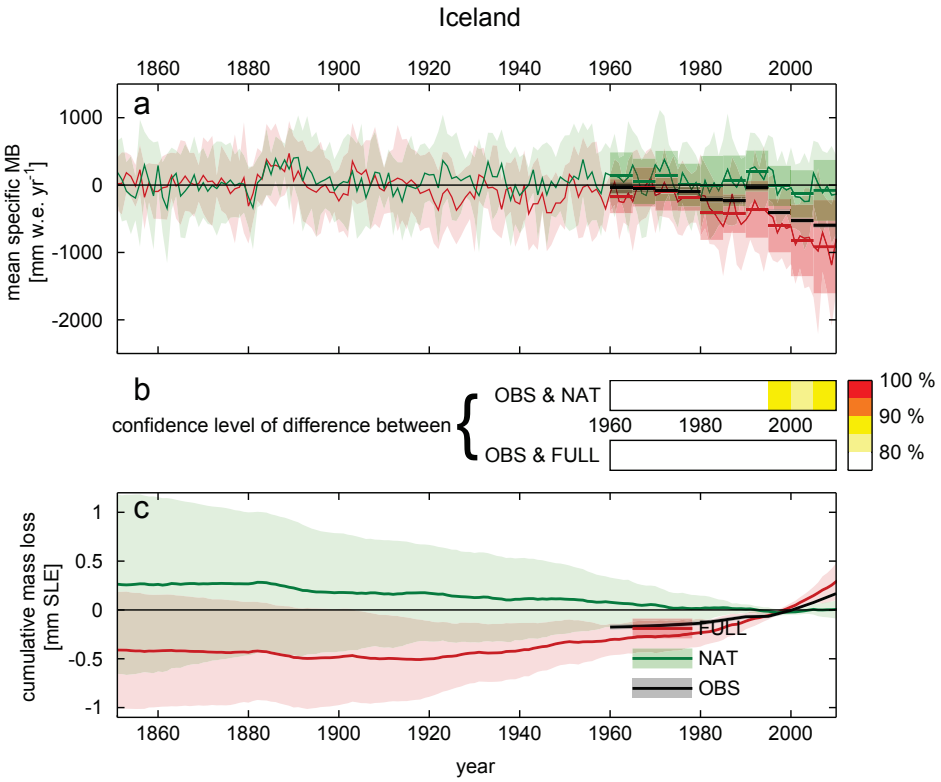
Iceland
a
mean specific MB
[mm w.e. yr-1]
1000
0
-1000
-2000
1860
1880
1900
1920
1940
1960
1980
2000
b
confidence level of difference between
OBS & NAT
OBS & FULL
1960
1980
2000
100 %
90 %
80 %
c
cumulative mass loss
[mm SLE]
1
0.5
0
-0.5
-1
FULL
NAT
OBS
year

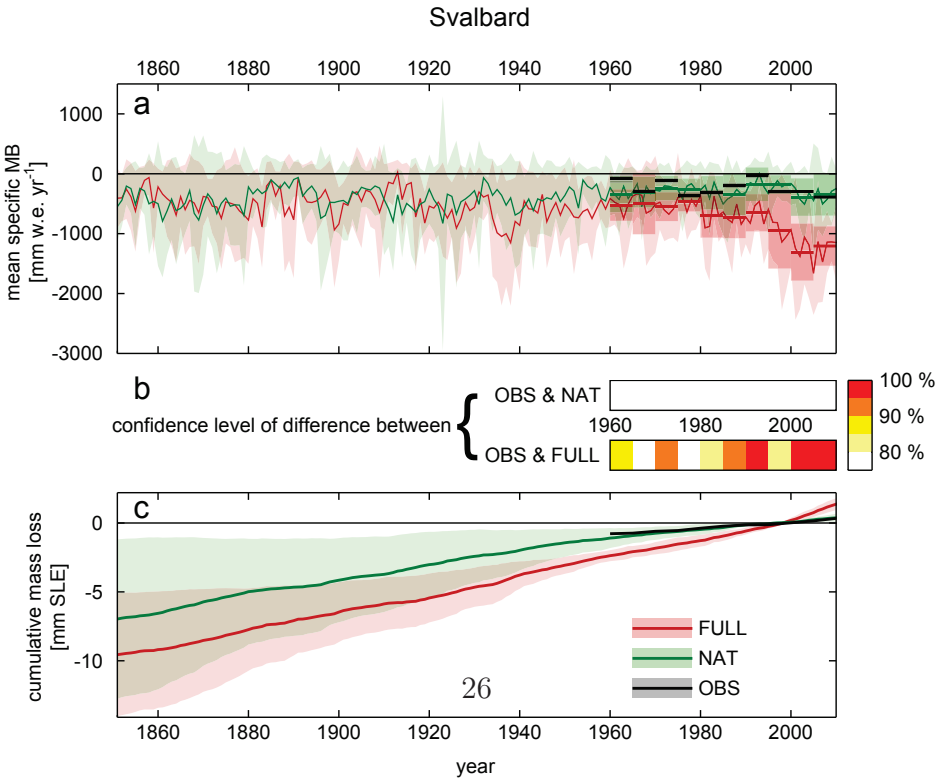
Svalbard
a
mean specific MB
[mm w.e. yr-1]
1000
0
-1000
-2000
-3000
1860
1880
1900
1920
1940
1960
1980
2000
b
confidence level of difference between
OBS & NAT
OBS & FULL
1960
1980
2000
100 %
90 %
80 %
c
cumulative mass loss
[mm SLE]
0
-5
-10
FULL
NAT
OBS
year

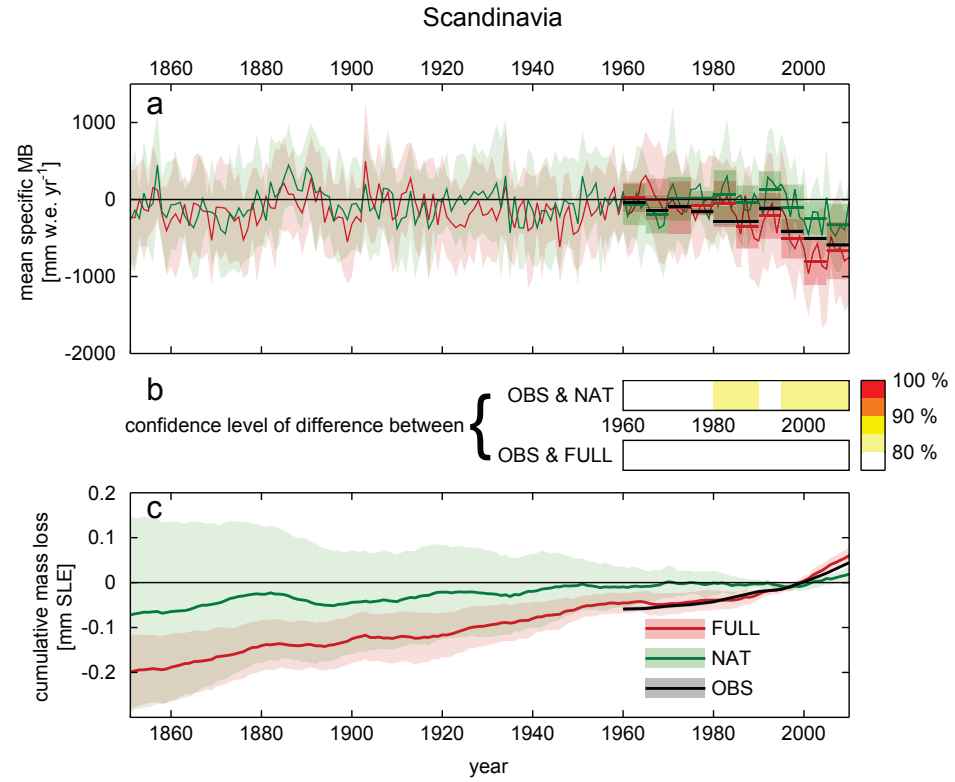
Scandinavia
a
mean specific MB
[mm w.e. yr-1]
1000
0
-1000
-2000
b
confidence level of difference between
OBS & NAT
OBS & FULL
1960
1980
2000
100 %
90 %
80 %
c
cumulative mass loss
[mm SLE]
0.2
0.1
0
-0.1
-0.2
FULL
NAT
OBS
1860
1880
1900
1920
1940
1960
1980
2000
year

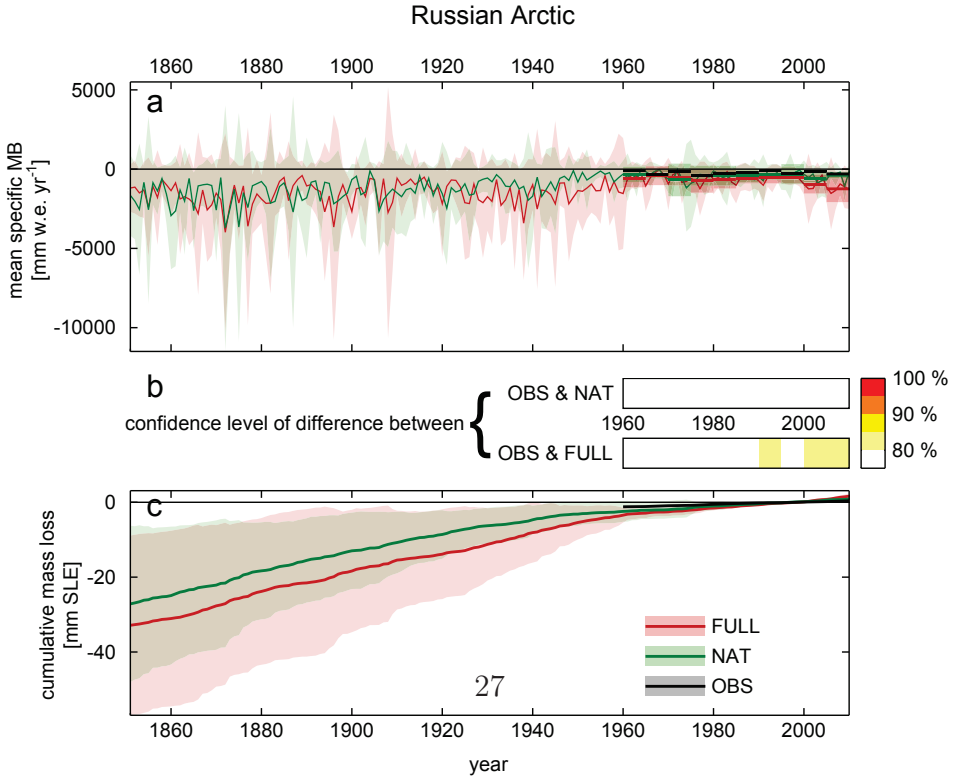
Russian Arctic
a
mean specific MB
[mm w.e. yr-1]
5000
0
-5000
-10000
b
confidence level of difference between
OBS & NAT
OBS & FULL
1960
1980
2000
100 %
90 %
80 %
c
cumulative mass loss
[mm SLE]
0
-20
-40
FULL
NAT
OBS
1860
1880
1900
1920
1940
1960
1980
2000
year

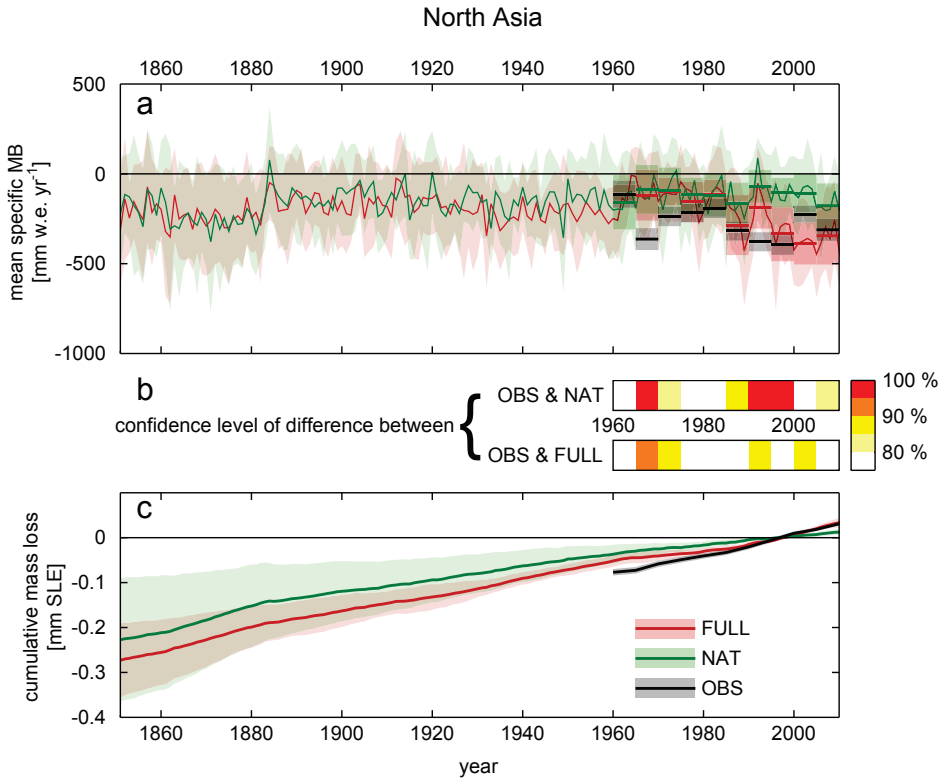
North Asia
a
b
c
mean specific MB
[mm w.e. yr-1]
confidence level of difference between
OBS & NAT
OBS & FULL
100 %
90 %
80 %
cumulative mass loss
[mm SLE]
FULL
NAT
OBS
year

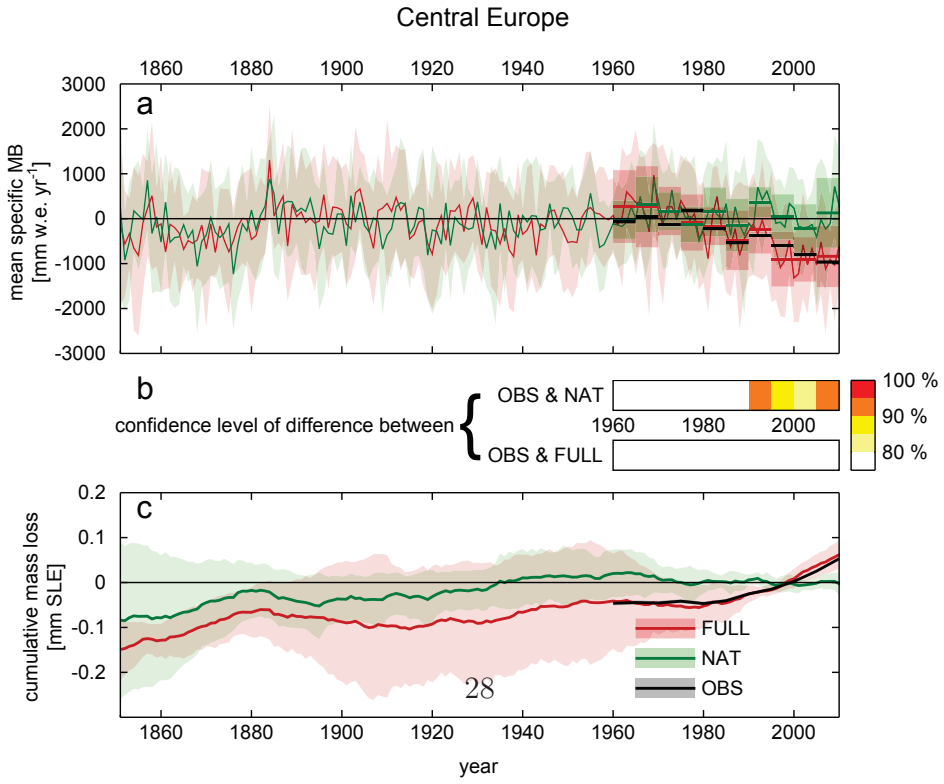
Central Europe
a
b
c
mean specific MB
[mm w.e. yr-1]
confidence level of difference between
OBS & NAT
OBS & FULL
100 %
90 %
80 %
cumulative mass loss
[mm SLE]
FULL
NAT
OBS
year

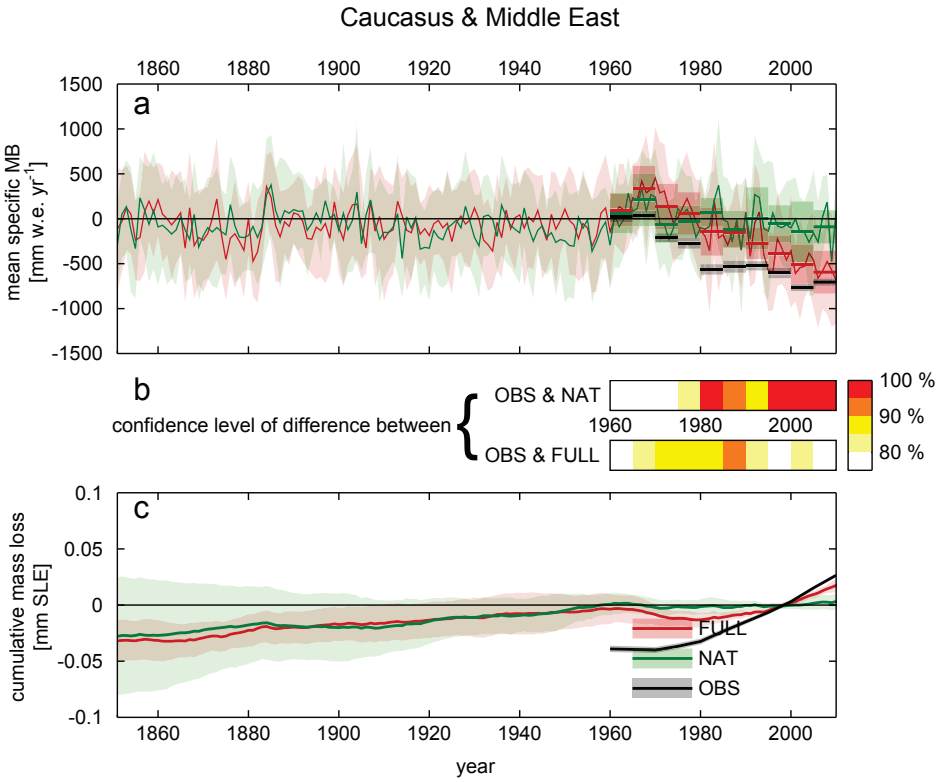
Caucasus & Middle East
a
mean specific MB
[mm w.e. yr-1]
1500
1000
500
0
-500
-1000
-1500
1860
1880
1900
1920
1940
1960
1980
2000
b
confidence level of difference between
OBS & NAT
OBS & FULL
100 %
90 %
80 %
c
cumulative mass loss
[mm SLE]
0.1
0.05
0
-0.05
-0.1
FULL
NAT
OBS
year

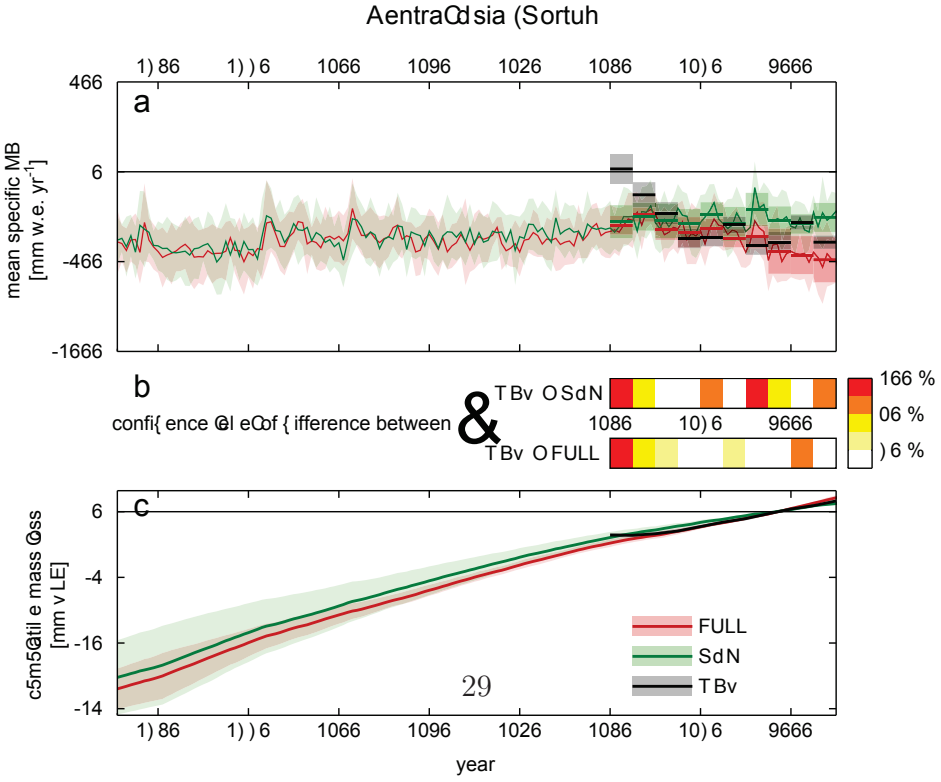
AentraCdsia (Sortuh
a
mean specific MB
[mm w.e. yr-1]
466
6
-466
-1666
1) 86
1)) 6
1066
1096
1026
1086
10) 6
9666
b
confi{ ence @l eCof { ifference between
&
TBv OSdN
TBv OFULL
166 %
06 %
) 6 %
c
c5m5@til e mass @ss
[mm v LE]
6
-4
-16
-14
FULL
SdN
TBv
year

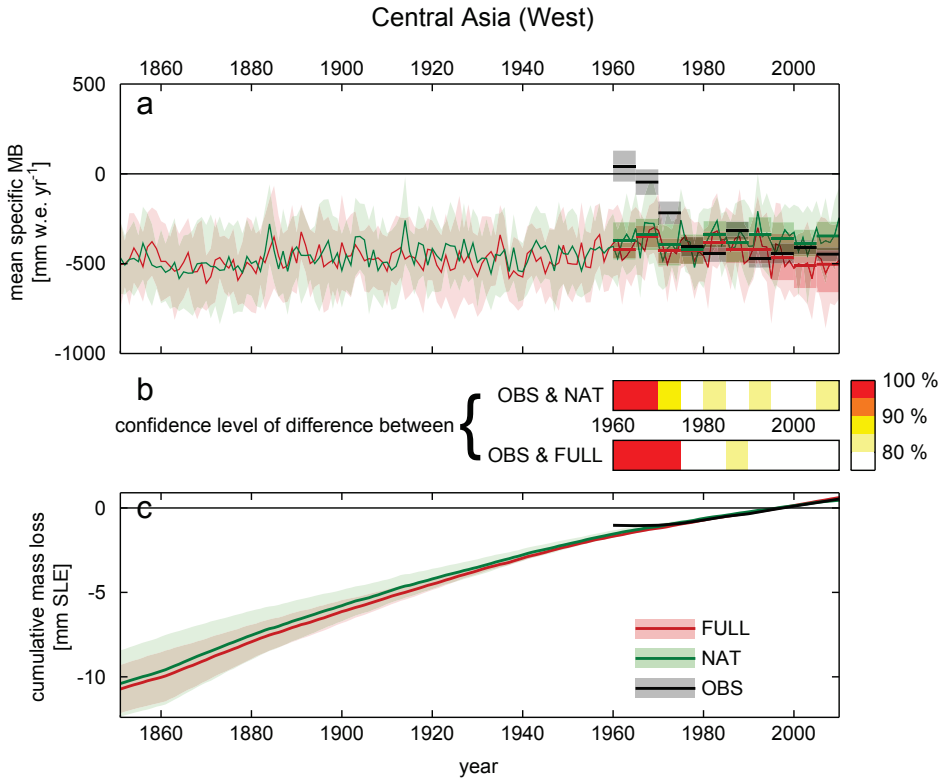
Central Asia (West)
a
mean specific MB
[mm w.e. yr-1]
500
0
-500
-1000
1860
1880
1900
1920
1940
1960
1980
2000
b
confidence level of difference between
OBS & NAT
OBS & FULL
100 %
90 %
80 %
c
cumulative mass loss
[mm SLE]
0
-5
-10
FULL
NAT
OBS
year

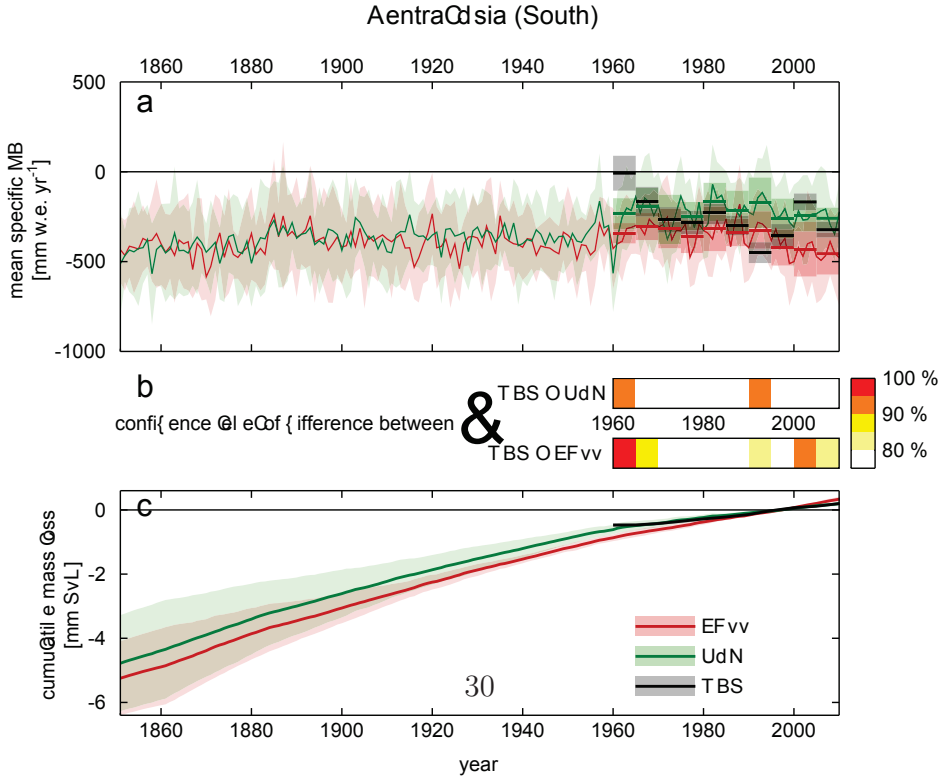
Aentra Cd sia (South)
a
mean specific MB
[mm w.e. yr-1]
500
0
-500
-1000
1860
1880
1900
1920
1940
1960
1980
2000
b
&
100 %
90 %
80 %
c
0
-2
-4
-6
EFvv
UdN
TBS
year

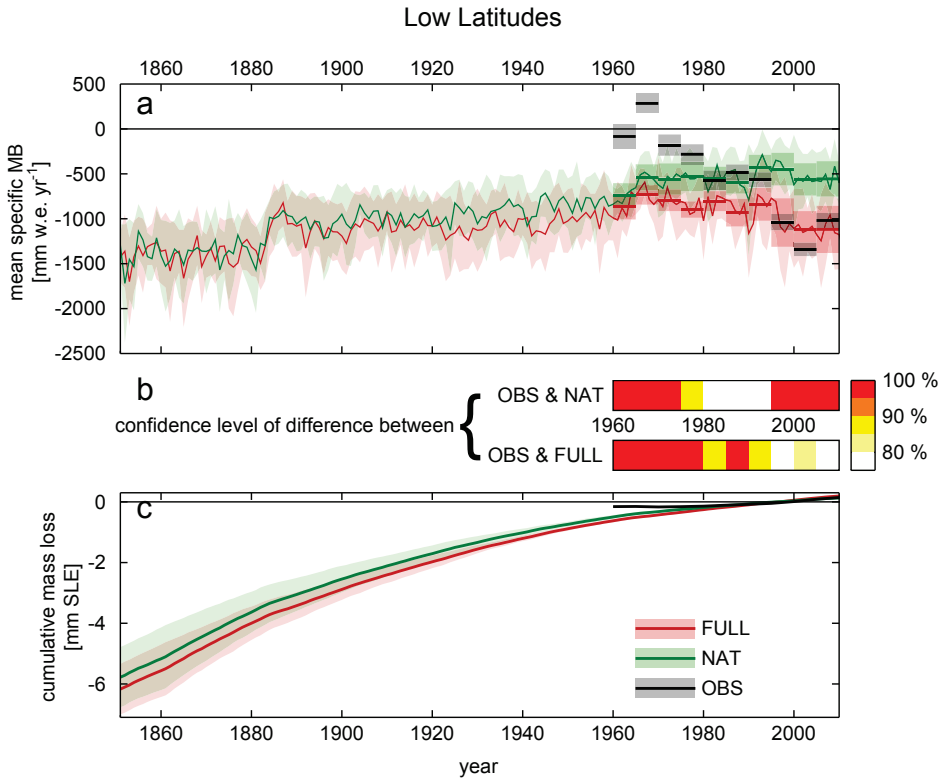
Low Latitudes
a
mean specific MB
[mm w.e. yr-1]
b
confidence level of difference between
OBS & NAT
OBS & FULL
100 %
90 %
80 %
c
cumulative mass loss
[mm SLE]
FULL
NAT
OBS
year

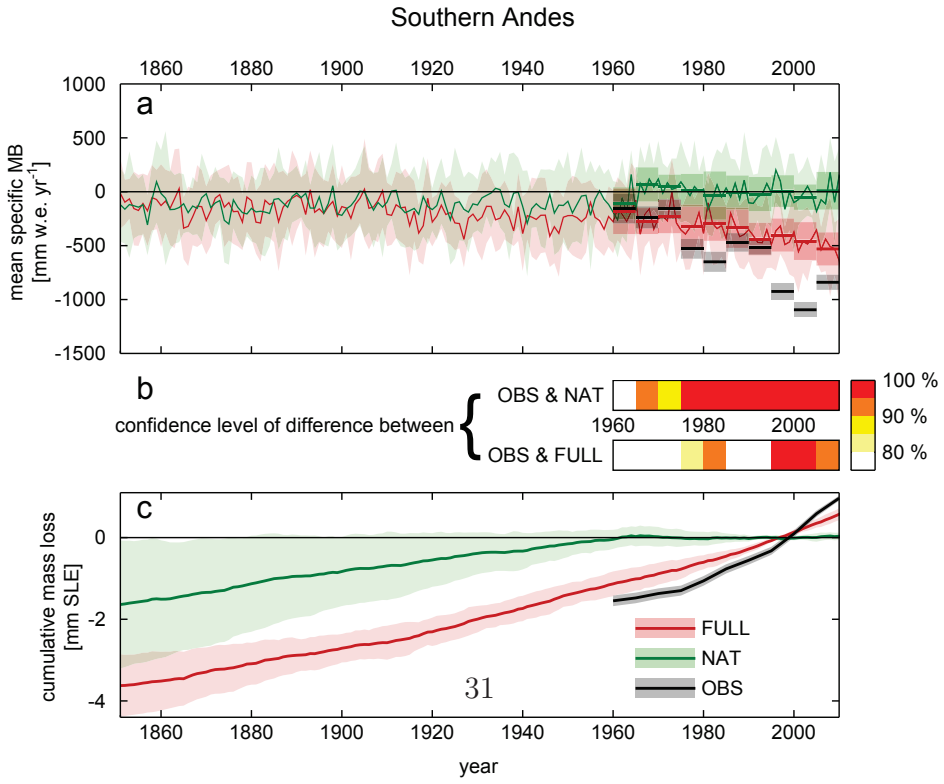
Southern Andes
a
mean specific MB
[mm w.e. yr-1]
b
confidence level of difference between
OBS & NAT
OBS & FULL
100 %
90 %
80 %
c
cumulative mass loss
[mm SLE]
FULL
NAT
OBS
year

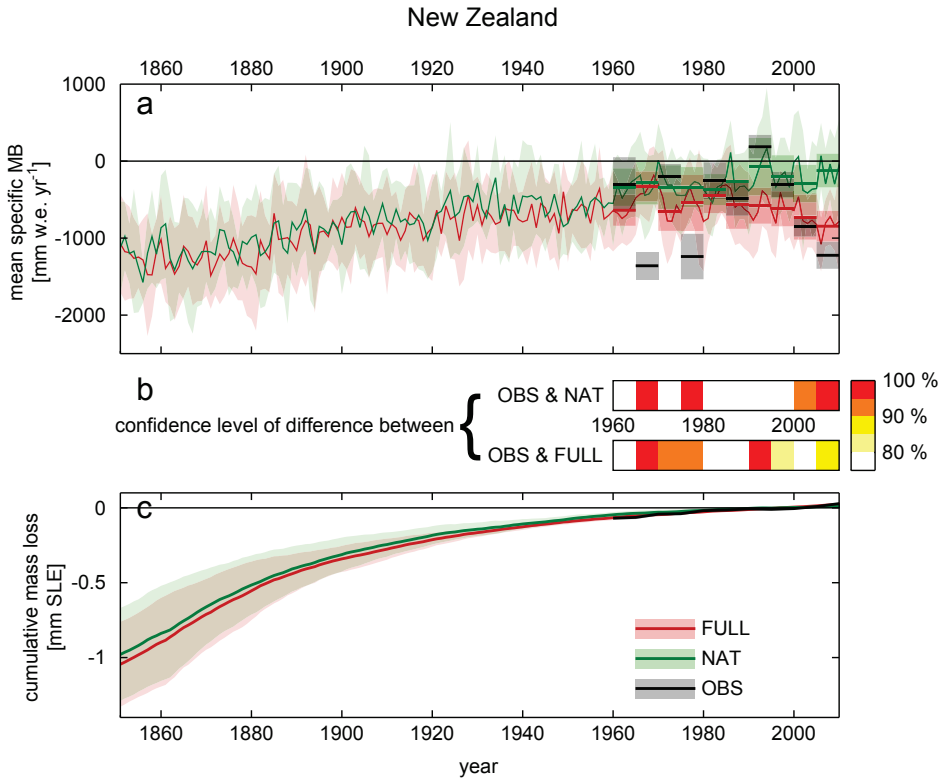
New Zealand
a
mean specific MB
[mm w.e. yr-1]
1000
0
-1000
-2000
1860
1880
1900
1920
1940
1960
1980
2000
b
confidence level of difference between
OBS & NAT
OBS & FULL
1960
1980
2000
100 %
90 %
80 %
c
cumulative mass loss
[mm SLE]
0
-0.5
-1
FULL
NAT
OBS
year

2.4 Addendum

This work was funded by the Austrian Science Fund (FWF): PP25362-N26, and supported by the Austrian Ministry of Science BMWF as part of the UniInfrastrukturprogramm of the Research Platform Scientific Computing at the University of Innsbruck. We acknowledge the World Climate Research Programme's Working Group on Coupled Modelling, which is responsible for CMIP, and we thank the climate modeling groups (listed in the Extended Data Table 2.1) for producing and making available their model output. For CMIP the U.S. Department of Energy's Program for Climate Model Diagnosis and Intercomparison provided coordinating support and led development of software infrastructure in partnership with the Global Organization for Earth System Science Portals.

Chapter 3

Paper 2: Major 20th Century Contribution to Sea-Level Rise from Uncharted Glaciers

David Parkes[1,2] & Ben Marzeion[2]

[1]Institute of Meteorology and Geophysics, University of Innsbruck, Austria
[2]Institute of Geography, University of Bremen, Bremen, Germany

Published 2018 in *Nature* **563**, pages 551-554

3.1 Abstract

Global mean sea-level rise (GMSLR) during the 20th century was primarily caused by glacier and ice sheet mass loss, thermal expansion of ocean water, and change of terrestrial water storage [8]. Whether based on observations [24] or results of climate models [9, 62], the sum of estimates of each of these contributors tends to fall short of the observed GMSLR. All estimates of the glacier contribution to GMSLR rely on the application of glacier inventory data, which are known to under-sample the smallest glacier size classes [6, 52]. Here we show that *missing* glaciers (those small glaciers that we expect to exist today, but which are not represented in the inventories) have contributed a substantial amount of water to GMSLR. During the period 1901 to 2015, we estimate a lower bound of their contribution at 12.3±1.6 mm SLE (sea-level equivalent), and an upper bound at 42.7±6.5 mm SLE. Because their total 2015 ice mass is estimated to be very small, between 2.1±0.3 mm SLE and 2.4±0.4 mm SLE, their potential to impact future GMSLR is much smaller.

Additionally, *disappeared* glaciers that existed in 1901, but had completely melted away by 2015, and which are therefore not included in modern global glacier inventories, are estimated to have contributed between 4.4±1.4 mm SLE and 5.3±2.4 mm SLE. Together, these *uncharted* glaciers (missing glaciers and disappeared glaciers combined) made an estimated contribution between 16.7±3.0 mm SLE and 48.0±8.9 mm SLE. Failure to consider these glaciers may be an important cause of difficulties in closing the GMSLR budget during the 20th century: their contribution is on average between 0.17 mm SLE yr^{-1} and 0.53 mm SLE yr^{-1}, compared to a budget discrepancy of about 0.5 mm GMSLR yr^{-1} considering the period 1901 to 1990. During the period 1993 to 2010, their average contribution is between 0.08 mm SLE yr^{-1} and 0.21 mm SLE yr^{-1}, compared to a discrepancy of 0.4 mm GMSLR yr^{-1} in the budget [9]. We suggest that accounting for uncharted glaciers in some fashion is essential for accurate historical glacier GMLSR contribution estimations.

3.2 Main Text

Mass loss from glaciers forms a major component of GMSLR during the 20th century [8]. Direct historical records of glacier mass changes are small in number compared to the total number of glaciers globally [67, 11], such that methods for upscaling these observations to

the global scale are necessary for assessing the GMSLR budget [24, 9, 62]. Available methods cover a wide range of complexity, from geographically weighted interpolation [11], to scaling from glacier length change observations [48, 34], to numerical modeling of each individual glacier based on climate observations [39]. All these methods rely on comprehensive global inventories of glaciers, which are a relatively recent development made possible by large-scale aerial mapping [66] and satellite-based earth observation techniques [52]. Glacier inventories are therefore only reasonably representative of current or recent glacier states, with information not sufficiently available for historical states. Accuracy in reconstructed SLE mass change contribution from glaciers is limited by the effective 'resolution' of the glacier inventory (the minimal glacier size the inventory can faithfully represent) which underpins the reconstructive method. Accuracy is further limited by the possibility that glaciers which have already completely disappeared contributed to mass change in the past. There is strong evidence that small glaciers are underrepresented also in the most up-to-date inventories, compared to expected glacier distributions [7, 6, 52]. In some regions, glaciers sized below a certain threshold are deliberately excluded from the inventories. [55] Improvements in remote observation techniques alone are not an efficient way to reduce the limitation that glacier inventory resolution places on global glacier reconstructions: new and improved data sets are expensive, time consuming to collect (requiring lots of manual labour) [51], and limited by available sensing technologies and the missions that employ them. Furthermore, reducing the error in global or regional total glacier mass by an order of magnitude could require improving the effective resolution of glacier inventories by almost 4 orders of magnitude [6], which would necessitate a huge advance in remote sensing. It is important to note that any error in the present-day representation of small glaciers results in proportionally larger errors in reconstructions of these glaciers' change during the past, because small glaciers tend to have experienced much greater proportional changes in volume and area since pre-industrial times than larger glaciers (supplementary fig. 3.3b). Methods to account for the limitations of glacier inventories without explicitly collecting the missing data are therefore of great interest for improving global glacier mass change estimates, and as we suggest here, for closing the GMSLR budget.

First, we define two new classes of glaciers which need to be considered for estimating the glaciers' SLE mass change. *Missing* glaciers are those that we expect to exist in 2015, but which are not contained in the Randolph Glacier Inventory version 5 (RGIv5 [1], the 2015 release of the RGI, with data for over 200,000 glaciers): they represent current undersampling due to limitations in remote sensing methods. *Disappeared* glaciers are those that we expect to have existed in 1901, but entirely melted away between 1901 and 2015: they are a contribution systematically left out by glacier reconstruction reliant explicitly on modern inventories, regardless of the quality of remote sensing data. We use the term *uncharted* glaciers to refer to both these classes of glaciers combined.

We then combine glacier modeling and empirically determined global power laws relating

glacier frequency density and glacier surface area S to estimate the 1901-2015 SLE mass loss contribution for *missing* and *disappeared* glaciers. The existence of a power law relationship between glacier surface area and frequency density is supported by theoretical evidence [7] and observational evidence on a regional scale [6], as well as evidence of a similar power law holding for smaller snow-deposition-based phenomena like snow patches [7]. We find strong evidence for the same form of power law holding globally (fig. 3.1). Based on RGIv5 data, the power law holds globally for glaciers between $10^{0.3}$ (≈ 2) and $10^{2.6}$ (≈ 398) km^2, with the fall off in frequency density for large glaciers a consequence of the limitations in size and topography of glacierized regions. The fall off in frequency density for small glaciers ($10^{-2.0}$ ($= 0.01$) km^2 $<= S < 10^{0.3}$ km^2 - the lower limit of $10^{-2.0}$ km^2 being the minimum glacier size in RGIv5), however, does not have a known physical justification. As the power law holds both for a wide range of mid-sized glaciers, and also for smaller but similarly distributed phenomena such as snow patches [6], and since there is no posited mechanism reducing the occurrence of small glaciers, the fall-off at small glacier sizes has been hypothesized to be explained by underrepresentation in the global inventory [52, 6]. Based on this hypothesis, we derive an upper bound estimate of the contribution of *uncharted* glaciers.

Since the hypothesis that the power law holds down to the smallest glacier size classes remains to be tested, we derive a lower bound estimate of the contribution of *uncharted* glaciers by using an alternative assumption that there is a lower cut-off in glacier size for which the power law holds, and that the frequency density of glaciers smaller than the cut-off, as a function of area, is constant. The chosen cut-off of 0.1 km^2 is an order of magnitude larger than the minimum glacier size recorded in RGIv5, implying that the lower bound estimate is considerably less affected by potential effects from ice bodies at the glacier/snow patch transition, which are not necessarily dominated by the same physical processes as larger glaciers and for which scaling relationships may be less certain. In Switzerland, where we expect the RGI to be better than average in its representation of small glaciers thanks to high resolution mapping efforts such as the SGI [17] (see supplementary fig. 3.4) we find a power law still applies - albeit with a smaller exponent - down to the smallest glacier sizes. The existence of a hard cut-off is a strong assumption, but it serves to derive a credible lower bound to the mass contribution that can be expected from *uncharted* glaciers. These bounds account for a range of possibilities of partial flattening/tailing-off of the power law at the smallest glacier sizes.

To account for *missing* glaciers, we upscale mass change from small glacier size classes in RGIv5: For the upper bound, using the power law observed for glaciers between $10^{0.3}$ and $10^{2.6}$ km^2, we generate an upscaling factor for each glacier size class below $10^{0.3}$ km^2 equal to the ratio of the power-law-predicted 2015 frequency density to the 2015 RGIv5 frequency density. For the lower bound, we generate an upscaling factor as described above for size classes of 0.1 km^2 and above. Below 0.1 km^2, we scale to the same frequency density as glaciers at 0.1 km^2. By hindcasting annual mass change of each glacier contained in RGIv5

back to 1901 using an established global glacier model [39] that has been used extensively in sea level budget assessment [24, 9, 20, 62, 37], and applying these upscaling factors to the contribution of each small glacier (small being based on their 2015 size), we generate upper and lower bound mass change estimates for *missing* glaciers between 1901 and 2015. As the 1901 glaciers are also expected to be distributed following the same power law (with a potential cut-off), we independently fit a power law to the RGIv5 + *missing* glaciers in 1901, and this time upscale the 1901 mass, using newly generated upscaling factors, to account for the total mass of *disappeared* glaciers. The glacier mass added by this second upscaling is expected to have entirely disappeared by 2015, so combining the total mass of *disappeared* glaciers and the 1901-2015 mass change from *missing* glaciers we arrive at upper and lower bound total mass change estimates for all *uncharted* glaciers during the period 1901 to 2015.

The RGIv5 glacier frequency distribution for 2015 (fig. 3.1a and d, dark green line) gives a power law exponent of -1.80±0.01 (fig. 3.1a and d, purple line), resulting in an upper bound of 42.7±6.5 mm (95% confidence interval - see 'Estimation of errors' in extended methods for details) SLE mass loss between 1901 and 2015 from *missing* glaciers (assuming global sea surface area of 3.619 x 10^{14} m^2), or a lower bound of 12.3±1.6 mm. The secondary power law fit applied to the 1901 glacier distribution after complete upscaling (fig. 3.1b, pink line) gives a power law exponent of -1.98±0.04 (fig. 3.1c, light green line), resulting in an expected upper bound of 5.3±2.4 mm SLE mass loss over the same period from *disappeared* glaciers. The secondary power law applied to the 1901 glacier distribution for the lower bound estimate (fig. 3.1e, pink line) gives a power law exponent of -1.96±0.03 (fig. 3.1f, light green line), resulting in a lower bound of 4.4±1.4 mm SLE mass loss from *uncharted* glaciers. We note that the different exponents for 2015 and 1901 may be due to the state of glaciers relative to equilibrium, as the response of smaller glaciers is faster than the response of large glaciers, resulting in a 'flattening' of the distribution as glaciers in general shrink. Bahr and Radic [6] find a regionally averaged (different to calculating a single exponent for all regions, and only across 10 glacierized regions) exponent of -2.10 ± 0.09, and the theoretical exponent given by Bahr and Meier [7] is -2.05, implicitly for an equilibrium scenario. We see a slightly flatter distribution in 1901 and a flatter distribution still in in 2015, qualitatively in agreement with general glacier shrinkage during the 20th century.

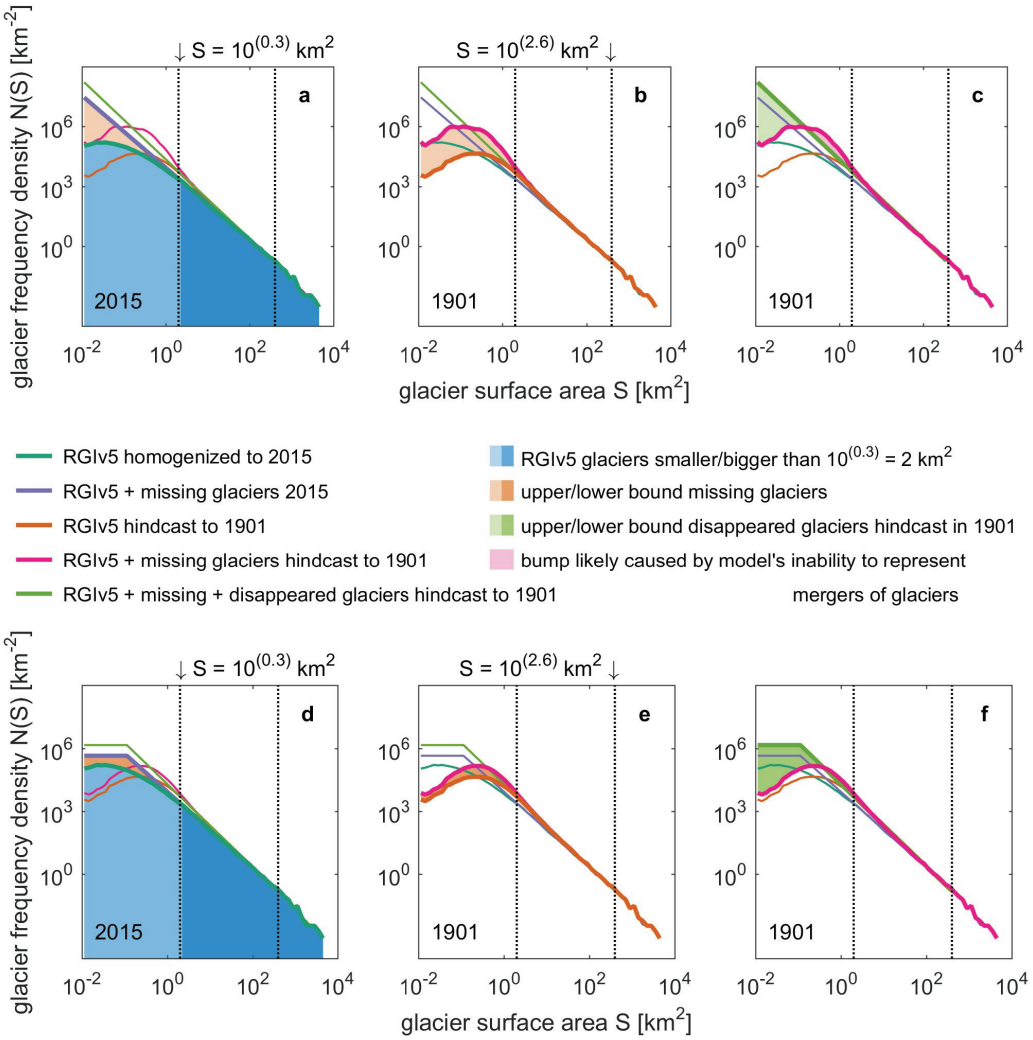
glacier frequency density N(S) [km^{-2}]
↓ S = 10$^{(0.3)}$ km^2
S = 10$^{(2.6)}$ km^2 ↓
a
b
c
d
e
f
2015
1901
10^6
10^3
10^0
10^{-2}
10^0
10^2
10^4
glacier surface area S [km^2]
RGIv5 homogenized to 2015
RGIv5 + missing glaciers 2015
RGIv5 hindcast to 1901
RGIv5 + missing glaciers hindcast to 1901
RGIv5 + missing + disappeared glaciers hindcast to 1901
RGIv5 glaciers smaller/bigger than 10$^{(0.3)}$ = 2 km^2
upper/lower bound missing glaciers
upper/lower bound disappeared glaciers hindcast in 1901
bump likely caused by model's inability to represent
mergers of glaciers

Figure 3.1: Frequency density function of glaciers as a function of glacier size. The top row (panels a, b, and c) shows the upper bound, while the bottom row (panels d, e, and f) shows the lower bound. Within each row, each panel shows the same set of distributions, but highlights a different area of the graph, representative of a different set of glaciers. The left panels (a and d) show RGIv5 glacier distribution in 2015 ('homogenized' in that the actual RGIv5 observation years differ between glaciers, so we model forward to provide a 2015 snapshot of glacier distribution) in blue, split into light and dark sections to reflect the distinction between small ($10^{-2.0}$ km^2 $< S <$ $10^{0.3}$ km^2) and other glaciers, with the same colours representing this distinction in fig. 3.2. The left panels also show the power-law-derived distribution of *missing* glaciers in 2015, shaded in orange. The middle panels (b and e) show the distribution of *missing* glaciers in 1901 (shaded orange). The right panels (c and f) show the distribution of *disappeared* glaciers shaded in green, from a power law derived from the 1901 RGIv5 + *missing* glaciers' distribution, as well as a 'bump' that we consider to be a modeling artefact (see online Methods section), shaded in pink.

Combining the contributions of *missing* and *disappeared* glaciers, we derive a total mass loss upper bound of 48.0±8.9 mm SLE from *uncharted* glaciers, and a lower bound of 16.7±3.0 mm SLE, on top of a revised figure of 89.1±3.9 mm SLE from the reconstruction of all RGIv5 glaciers using the unmodified glacier model [39] forced with the climate observations [25] (CRU version 3.24) and initialized using RGIv5 [1]. This implies that we estimate *uncharted* glaciers to have contributed up to between 29.6% and 40.0% of a total 137.1±12.8 mm SLE glacier mass loss between 1901 and 2015 (upper bond), and at least between 12.8% and 18.8% of a total 105.8±6.9 mm SLE (lower bound). The SLE 2015 mass and 1901-2015 mass loss contribution for each class of glaciers is summarized in tab. 3.1.

The *uncharted* glacier contribution to GMSLR over the period 1901 to 2015 is estimated to be between 0.15 mm SLE yr^{-1} and 0.42 mm SLE yr^{-1}, and the total glacier contribution during the same period to be between 0.93 mm SLE yr^{-1} and 1.20 mm SLE yr^{-1}. The upper bound *uncharted* contribution may close the sea-level budget discrepancy identified in the IPCC's 5th assessment report [9] during the period 1901 to 1990 (0.53 mm SLE yr^{-1} upper bound / 0.17 mm SLE yr^{-1} lower bound contribution compared to a discrepancy of 0.5 mm GMSLR yr^{-1}), but not completely so during the period 1993 to 2010 (0.21 mm SLE yr^{-1} upper bound / 0.08 mm SLE yr^{-1} lower bound contribution compared to a discrepancy of 0.4 mm GMSLR yr^{-1}). Smaller estimates of 20th century GMSLR have been published after the 5th assessment report [28, 13]. However, since their methods (to different degrees) depend on the sea-level fingerprint of glacier mass loss, the impact of our results on a sea-level budget closure based on these recent GMSLR estimates is not immediately obvious.

	Total ice mass in 2015 [mm SLE]	**Mass loss contribution 1901-2015 [mm SLE]**
RGIv5 glaciers >= $10^{0.3}$ km^2	489.3±21.4	75.1±3.3
RGIv5 glaciers < $10^{0.3}$ km^2	3.2±0.1	14.0±0.6
RGIv5 total	**492.5±21.6**	**89.1±3.9**
Missing glaciers - upper bound	2.4±0.4	42.7±6.5
Disappeared glaciers - upper bound	0	5.3±2.4
Uncharted glaciers - upper bound	**2.4±0.4**	**48.0±8.9**
Missing glaciers - lower bound	2.1±0.3	12.3±1.6
Disappeared glaciers - lower bound	0	4.4±1.4
Uncharted glaciers - lower bound	**2.1±0.3**	**16.7±3.0**

Table 3.1: Breakdown of current ice masses and 1901-2015 SLE mass loss contributions from different glacier classes. In the RGIv5 results - as in the *missing* glaciers - we see that a small glacier mass in 2015 was responsible for a much larger proportion of historical glacier mass loss than their 2015 mass may suggest, as these glaciers have typically seen a much greater proportionate mass change than large glaciers (see also supplementary fig. 3.3b). *Disappeared* glaciers, by definition, do not exist in 2015, but still contributed a modest amount to SLE mass loss.

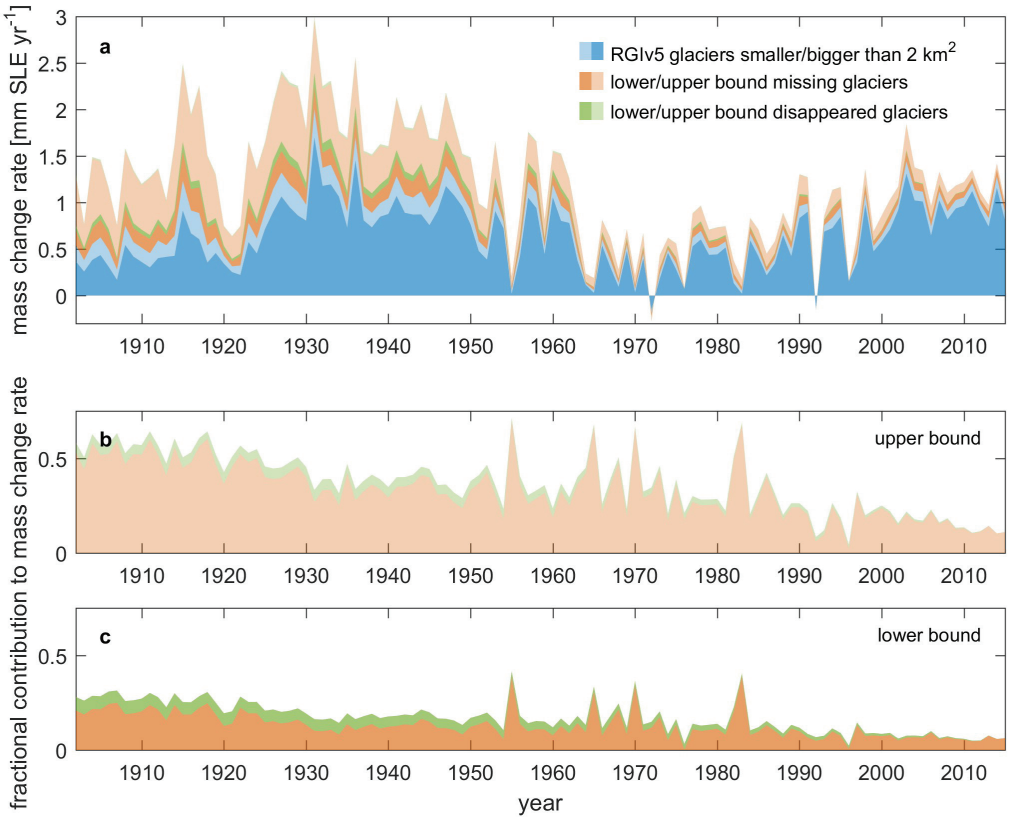

Figure 3.2: Annual glacier mass loss time series. The light and dark blue sections show the hindcast mass loss from RGIv5 glaciers (colours see fig. refp2:1). The additional contribution from *missing* glaciers is shown in orange, that of *disappeared* glaciers is shown in green. In panel a, the lower and upper bounds are stacked (light orange and dark orange combined give upper bound of the *missing* glaciers' contribution, light green and dark green combined that of the *disappeared* glaciers). In panels b and c the *missing* and *disappeared* glaciers' contributions are separated, and the fractional mass changes are calculated based on the separate totals.

The modeled annual SLE mass loss contribution between 1901 and 2015 for RGIv5, *missing*, and *disappeared* glaciers is shown in fig. 3.2. The data from RGIv5 glaciers is split into the contribution from small glaciers (which contribute to the *uncharted* glacier upscaling) and large glaciers. This shows that the contribution of *uncharted* glaciers, both in absolute terms and as a proportion of total glacier contribution, is largest early in the 20th century. The contribution decreases gradually to the point where it is negligible by 2015, with the total remaining volume of *missing* glaciers in 2015 comprising only between 2.1±0.3 mm

SLE and 2.4±0.4 mm SLE ice mass. This potential contribution is likely to be realized in the very near future, as *missing* glaciers are very small, and extending past surface mass balances (supplementary fig. 3.3a), small glaciers will see much more rapid proportionate mass changes. The small glacier effects are largely separate from the overall pattern of increasing mass loss rates up to a peak in the 1930s, decreasing to a minimum around 1970, and subsequent increase until the 2010s (this temporal pattern is the result of spatially inhomogeneous climate variability during the 20th century [39]); the rapid decrease in surface area and resulting decrease in volume loss for small glaciers dominates over the temporal variability seen in the RGIv5 population as a whole.

The consideration of *uncharted* glaciers adds a significant amount to hindcast SLE mass loss contributions from glaciers between 1901 and 2015, with the strongest effect in the first half of the 20th century. This additional contribution is comparable to the existing discrepancy between known GMSLR contributors and observed sea-level change. It is therefore imperative for the closure of the 20th century GMSLR budget that these glaciers are considered. Improved coverage of small glaciers in glacier inventory data sets can reduce the size of the expected contribution from *uncharted* glaciers by decreasing the extent to which small glacier size classes need to be upscaled, but the required glacier inventory resolution improvements to account for most of the *uncharted* glacier contribution calculated here would likely be prohibitively expensive and time consuming. There is also a component of the contribution from *uncharted* glaciers that will exist even with a theoretically perfect modern glacier inventory: the contribution from *disappeared* glaciers is small in comparison to the total contribution from all *uncharted* glaciers, but not vanishingly so. Accounting for *uncharted* glaciers thus cannot be done exclusively through improvements in glacier inventories, and upscaling (or other methods) of contributions from known glaciers to account for glaciers outside of either the resolution or scope of current glacier inventories must form an integral part of accurate GMSLR hindcasting. With only a small remaining potential contribution from *uncharted* glaciers in the future (an upper bound of 2.4±0.4 mm SLE), it is less important to consider these glaciers in projections.

3.3 Extended Methods

The mass balance model used for hindcasting glacier evolution is the same as that described in Marzeion et al [39], with the output updated for the RGIv5 [1] and CRU 3.24 climate observations [25]. The only modification is a change to the handling of data gaps to make it consistent with the treatment of *uncharted* glaciers: instead of assuming regional mean rates of glacier volume and area change for glaciers which cannot be explicitly modelled (22.7% of all glacier area globally, of which 76.8% comes from Antarctic and Subantarctic peripheral glaciers (PGs). See supplementary tab. 3.2 for breakdown), the regional mean

rates for glaciers within the same size class (as defined below) are assumed. For Antarctic and Subantarctic PGs, where CRU data are not available so no glaciers can be explicitly modelled, global mean rates for glaciers within the same size class are assumed. See the section 'Impact of Antarctic glaciers' for detailed consideration of the validity of using Antarctic PGs in this study.

A 'base' run of the glacier model is established first. We require a snapshot of global glacier area distribution for a single point in time, but the observation years for RGIv5 glaciers differ. We model each glacier forward to 2015 if it has an observation year before 2015, to homogenize the data to a single snapshot in 2015 (distributed as shown in the dark green line in fig. 3.1a and d), as well as hindcasting their sizes in 1901 (distributed as shown by the orange line in fig. 3.1b and e).

The results for all glaciers are separated into size classes based on their modelled areas in 1901 and 2015. Size classes are logarithmic, defined as each set of glaciers with surface area S such that $10^{i \cdot 0.1}$ km^2 $\leq S < 10^{(i+1) \cdot 0.1}$ km^2 for each integer i with -20 $\leq$ i $<$ 40 (resulting in size classes that span from 0.01 km^2 to 10,000 km^2). As these size classes do not cover equal area ranges, we divide the glacier count in each size class (unitless) by the width of each size class (upper area limit minus lower area limit - km^2) to get the glacier frequency density , $N(S)$, (km^{-2}). It is glacier frequency that we work with for the power law.

From the distribution of glaciers in 2015, we can determine a power law of the form $N(S) = aS^b$ (with a and b coefficients to be determined) for glacier frequency density by surface area that holds for glaciers not at either extreme end of the area distribution, with the theoretical basis in Ref. 13, and extending a regional method [6]. In this specific case, we fit the regression line (purple line in fig. 3.1a and d) for glaciers between $10^{0.3}$ and $10^{2.6}$ km^2, with this range selected based on the section of the graph which best fits a straight line while encompassing as many size classes as possible. We note that the regression coefficient is only generated once, globally, rather than for individual regions: this is because the distribution of differently sized glacierized regions is also part of the underlying distribution, and the power law exponent calculated globally is not necessarily the same as the mean of exponents calculated for each region. Thus, the mass of *uncharted* glaciers calculated globally is not necessarily the same as the sum of the masses of *uncharted* glaciers if they were calculated for individual regions. In the context of SLE mass loss contributions, it is important to consider the entirety of glacierized area rather than focusing on individual regions selected based on geographical convenience.

3.3.1 Estimation of errors

We generate the error values on the regression coefficients by varying the size classes over which the regression is calculated; the upper and lower limits are varied by one size class in each direction, independently, and the resulting distribution of 9 regression coefficients (lower limits of 23rd, 24th, and 25th size classes, upper limits of 45th, 46th, and 47th size classes in each possible combination) is used as a sample for generation a 95% confidence interval. The regression coefficient error is generated independently for each of the two regressions performed (one to account for *missing* glaciers, one to account for *disappeared* glaciers), which results in a larger proportionate error for *disappeared* glacier SLE mass loss contribution. The 4.4% proportionate error from the original Marzeion 2012 model is is assumed to hold also for *missing* and *disappeared* glaciers and thus added to the error due to the power laws, to determine total error for these mass loss contributions.

3.3.2 Missing glaciers

In this paper, 'small glaciers' is taken to mean glaciers with area $10^{-2.0}$ km^2 $< S <$ $10^{0.3}$ km^2, i.e. glaciers below the size of those to which the power law is fitted. We determine a scaling factor for each small glacier size class equal to the ratio of the power law-predicted frequency density in 2015 to the observed frequency density in 2015 (with a lower cut-off in glacier size for the lower bound estimate). To obtain an estimate of the *missing* glacier mass change, the contribution of each RGIv5 small glacier is multiplied by the scaling factor for the 2015 size class it occupies (regardless of what size class the same glacier may have occupied historically). *Missing* glaciers are defined as those small glaciers that are not included in RGIv5, but are expected to exist in 2015 from this power law upscaling. The hindcast 1901 glacier distribution with missing glacier scaling applied is shown by the pink line in fig. 3.1b and e. The annual GMLSR contribution from *missing* glaciers is then found by applying the upscaling factors based on 2015 glacier size class to each glacier's mass change timeseries for RGIv5 small glaciers.

3.3.3 Disappeared glaciers

We fit the *disappeared* glacier power law (light green line in fig. 3.1c and f) in the same manner as the power law for *missing* glacier upscaling, but with the pink line (RGIv5 + *missing* glaciers, hindcast to 1901) as the basis for the calculation of the power law constant and exponent. However, a correction is needed for the 'bump' in the hindcast RGIv5 + *missing* glaciers. In large part, we believe this 'bump' to be due to the fact that the glacier

model is unable to resolve the merging of two glaciers within a larger valley if they grow (or correspondingly, recombine glaciers, when hindcasting, that were previously the same glacier but split as they shrank); modern separate glaciers in adjoining valleys may have historically been part of a single larger glacier, but the fact that in the 1901 hindcast they are always represented as two separate glaciers artificially inflates some of the smaller size classes in the RGIv5 + *missing* glacier 1901 distribution, while reducing the glacier count in larger size classes. For this reason, we do not apply any scaling to small glacier size classes for which the *disappeared* power law predicted glacier frequency is lower than the RGIv5 + *missing* 1901 glacier frequency. The impact of this omission is not expected to be large, and we expect that it results in an overall underestimation of *disappeared* glacier SLE mass loss contribution as the artificial inflation of size classes below $10^{0.3}$ km^2 and reduction of larger size classes is expected to result in a smaller power law exponent. The smaller the power law exponent (i.e. the 'flatter' the distribution for the size classes on which the power law is calculated), the smaller the *disappeared* glacier mass added through our upscaling.

The time series shown in fig. 3.2 (light and dark green) is not explicitly calculated for *disappeared* glaciers. While *missing* glaciers are upscaled based on existing RGIv5 glaciers, *disappeared* glaciers have no existing analogues for time series upscaling. It is theoretically possible to generate a time series of mass loss by recalculating the power law on a yearly basis and determining how much of the original 1901 *disappeared* glacier mass is remaining, but the variability in the power law exponent is almost certain to dominate over actual climate-driven variability. As we know that the contribution is zero in 2015 due to these glaciers being entirely melted away, we instead show a linear decrease from a maximum in 1901, which is close to what we observe in *missing* glaciers.

3.3.4 Upper and lower bound estimates

We refer to the scaling of all small glacier size classes up to the power laws as the *upper bound* contribution estimate. To obtain the *lower bound* contribution estimates, we include an additional step: instead of upscaling all small glacier size classes to the calculated power law, we impose a cap on glacier frequency density based on the frequency density at 0.1 km^2, and upscale only to this cap for size classes between 0.01 km^2 and 0.1 km^2. In fig. 3.1, this modified upscaling can be seen in panels d (for *missing* glaciers) and f (for *disappeared* glaciers).

In supplementary fig. 3.4, we show the glacier distribution for Switzerland alone, in order to examine the apparent power law for a region where we expect the available glacier inventories to be much more complete. The Swiss Glacier Inventory [17] is based on 25 cm

resolution aerial orthophotographs, and as we see in supp. fig. 3.4, it gives us an apparent power law of exponent 1.16 down to the smallest measured glaciers sizes in the RGI. In fact, the RGI itself also exhibits such a power law - with exponent 1.26 - across small glaciers, and is apparently no less complete for this region than the SGI. With the limited number of glaciers in the SGI (1420 in total) and in the RGI restricted to Switzerland, we do not have enough data to determine a power law for larger glaciers, so we are unable to say whether this lower-exponent power law is a characteristic of the region, or a characteristic of the distribution of smaller glaciers with a transition into a steeper power law for larger glaciers. As a compromise, instead of guessing at transitions between power laws for different glacier size scales, we suggest a lower bound estimate of the *uncharted* glaciers' contribution by assuming a cut-off at 0.1 km^2, so the power law observed for larger glaciers continues down to 0.1 km^2, and below this the distribution is flat. The exponent observed in Switzerland lies somewhere between the lower bound (effectively an exponent of 0) and the upper bound, with the exponent of around 1.8 derived from larger glaciers globally.

For *missing* glaciers, the upper and lower bound estimates are based on the same power law, calculated for RGIv5 glaciers homogenised to 2015, but for *disappeared* glaciers, as the power law is based on the distribution of RGIv5 + *missing* glaciers hindcast to 1901 and this differs based on the upscaling used for *missing* glaciers, the upper and lower bound estimates are based on separately calculated power laws, with different exponents. In practice, we note a slightly smaller exponent (but not significantly so) for the lower bound estimate, likely due to the lessened effect of the merging of glaciers when hindcasting due to the model not accounting for glaciers coming together as their area increases (see 'bump' in fig. refp2:1c, with much less significant bump in fig. 3.1f). We also note that the lower bound contribution for *missing* glaciers is by definition smaller than the upper bound, as the upscaling is from the same base glacier distribution to a strictly smaller-than-pure-power-law distribution. This is not the case for the lower bound contribution of *disappeared* glaciers. Due to the potentially different power law exponents and the different distributions that are being upscaled from, it is possible that the lower bound *disappeared* glacier contribution is larger than the upper bound contribution, although in practice this is not the case.

3.3.5 Impact of Antarctic Peripheral Glaciers

Glaciers in the RGIv5 Antarctic and Subantarctic (A&S) region are unique in this study, as our climate data does not extend to these latitudes. This means that none of the glaciers in this region can be explicitly modeled (supplementary tab. 3.2), so global mean mass balance within each size class is assumed for each glacier. This is a strong and not well-justified assumption, so it is worthwhile to consider both why it is still valuable to include

these glaciers in our analysis, and what the impact on the results is if the region is removed.

Inclusion of A&S peripheral glaciers (PGs) is desirable, if possible, because the basis for a global upscaling of small glaciers must be a global glacier inventory. Generation of independent power laws on a regional basis and summing the upscaling for *uncharted* glaciers over these regions does not yield the same results as performing the upscaling based on global glacier distribution, and the distribution of glaciers across regions containing different sized glacier populations is fundamentally part of the global distribution we are trying to represent. Furthermore, the definition of the RGI regions is largely a matter of convenience, and the ability to artificially partition the world's glaciers into geographically separate boxes does not reflect the fact that the overall distribution of glaciers is the result of the interaction of much less separable factors like topography, precipitation, and surface energy balance, which are variables that are more continuous across glaciated and non-glaciated areas. In the same way that individual glaciers within a region are part of a larger pattern of glacierised area within that region, individual regions are part of a larger pattern of glaciated regions across the globe. A&S PGs are part of this global distribution, so we consider their inclusion worthwhile despite the additional modeling assumption, provided they do not have a clearly destabilising influence on the overall results.

While the A&S region comprises a large amount of overall glacier mass, it does not represent a large proportion of the total area of small glaciers (4.7%, as compared to 43.1% and 19.3% in the Greenland Periphery and Central Asia regions, respectively). Small glaciers are the ones which contribute to the upscaling for *uncharted* glaciers, so lack of explicit surface mass balance modeling for A&S PGs does not have a significant effect on the upscaled glacier SLE mass loss contribution. Nevertheless, for completeness we provide figures for the global modeling and upscaling with the A&S region removed, corresponding to the same figures included in the main text including the region. Only the upper bound estimate is compared, as the intention is to give an impression of the maximal effect of including or removing A&S glaciers. Removing A&S glaciers, RGIv5 SLE mass loss contribution is reduced to 75.8±3.3 mm SLE (from 89.1±3.9 mm including A&S PGs), but the *missing* and *disappeared* glacier contributions actually increase (insignificantly) to 49.1±5.2 mm and 6.3±2.5 mm SLE respectively (from 42.7±6.5 mm and 5.3±2.4 mm SLE respectively including A&S PGs). The reason for these contributions increasing when A&S glaciers are removed appears to be a change in power law exponents to -1.83±0.01 for the initial *missing* glacier upscaling and -2.01±0.04 for the *disappeared* glacier upscaling (from -1.80±0.01 and -1.98±0.04 respectively); these increase the amount of upscaling applied for small glacier size classes by enough to more than account for the reduced overall number of RGIv5 small glaciers used in the data set, given the aforementioned small proportion of small glaciers that are found in the A&S region.

RGI Region	**Percentage of glacierized area that cannot be modeled**	**Percentage of global small glacier area in this region**
Alaska	0.2%	2.2%
Western Canada and US	0.7%	0.1%
Arctic Canada North	3.4%	8.5%
Arctic Canada South	0.7%	3.3%
Greenland Periphery	12.3%	43.1%
Iceland	0.0%	0.0%
Svalbard	6.2%	0.5%
Scandinavia	0.0%	0.0%
Russian Arctic	28.4%	1.4%
North Asia	4.7%	0.5%
Central Europe	2.7%	0.9%
Caucasus and Middle East	14.1%	2.4%
Central Asia	2.3%	19.3%
South Asia West	0.7%	3.6%
South Asia East	0.8%	1.6%
Low Latitudes	15.0%	4.8%
Southern Andes	0.8%	2.9%
New Zealand	0.9%	0.2%
Antarctic and Subantarctic	100.0%	4.7%

Table 3.2: Each RGI region may contain glaciers for which the model fails. A&S PGs all fail due to the absence of CRU data for the appropriate latitudes, while in other regions the iteration to find an initial 1901 glacier area fails in a minority of cases. The percentage of glacierized area in each region that cannot be modeled is shown alongside the percentage of global small glacier area (all glaciers less than $10^{0.3}$ km^2 in size) in each region (which relates to how significantly the region affects upscaling of small glaciers to account for *uncharted* glaciers). Notably, the Greenland Periphery region contains disproportionately much of the world's total small glacier area, while A&S contains relatively little. At present, we are unable to determine whether this is primarily due to differing regional distributions (e.g. Antarctica has more large glaciers but fewer small glaciers than Greenland) or differing data quality.

3.3.6 Exponent Constraints

The nature of the power law explanation of glacier distribution places certain constraints on the power law in order for the outcome to be physically plausible. We concern ourselves with three integrals that relate to the distribution:

$$\int_m^n N(S)\ dS \tag{3.1}$$

giving the total number of glaciers with area between m and n,

$$\int_m^n S \cdot N(S)\ dS \tag{3.2}$$

giving total area of all glaciers with areas between m and n, and

$$\int_m^n jS^k \cdot N(S)\ dS \tag{3.3}$$

giving the total volume of all glaciers between m and n, with the exponent k and constant j being volume/area scaling factors $k = 1.375$ and $j = 0.0340km^{3-2k}$ taken from literature [4, 3]. In all three cases, we have a physically meaningful upper bound on the area of glaciers for which we apply the power law imposed by topography - the glacier distribution where glacier thickness is small relative to local topography is fundamentally different to the distribution when glaciers begin to subsume the underlying topography, so we cannot continue the distribution observed for most mid-sized glaciers to areas represented by smaller numbers of extremely large glaciers. In our analysis, we find that we put a practical upper bound

on the power law of $10^{2.6}$ km^2, so we can fix $n = 10^{2.6}$ and do not need to worry about the convergence of these intervals as n varies. At the lower end of glacier areas, we do not have a physically meaningful cutoff for minimum glacier size m. We fix a lower limit of $10^{-2.0}$ km^2 due to this being the smallest glacier size represented in RGIv5, but this is purely a limitation of the data set, so in order to have physically plausible power laws, we should expect convergence in some of these integrals as m tends to zero. In equations (3.2) and (3.3), convergence is necessary as the total area and total volume of glaciers gloabally must be finite regardless of how small we make our minimum limit on glacier size, but equation (3.1) should not necessarily converge, since dropping the threshold for what we consider to be glaciers can plausibly add huge numbers of increasingly small ice masses. In essence, we can continue to add significant numbers of increasingly small glaciers as long as they do not contribute a significant overall area or volume. As $N(S)$ is proportional to S^b for the power law exponent b, in order for equations (3.2) and (3.3) to converge as m tends to zero, we require, respectively:

$$b + 1 > -1 \tag{3.4}$$

$$b + 1.375 > -1 \tag{3.5}$$

Equation (3.5) is satisfied comfortably by every value of the exponent for all the power laws we generate, meaning that the total ice volume is at least theoretically consistent in every case. Equation (3.4) is satisfied comfortably for both the *missing* glacier power laws with and without A&S glaciers, so the power law explanation of 2015 glaciers is theoretically consistent. Both with and without A&S glaciers, the upper bound power laws based on 1901 glacier areas to derive *disappeared* glacier contributions have error margins that straddle the b = -2 threshold for area convergence, and the corresponding power law for the lower bound is below but extremely close to the b = -2 threshold. This means there is uncertainty over whether the power law is too steep to be an accurate description of a possible 1901 glacier distribution if the minimum glacier size approaches zero. However, we do recognise that the inability of the model to account for the fact that separate modern glaciers may actually have been part of the same ice masses in the past when they were larger may 'bunch up' the distribution of smaller glaciers (and we note a slightly smaller exponent for the lower bound, where this effect is lessened). We therefore trust the estimate of the *missing* glacier SLE mass loss contribution more than the *disappeared* glacier contribution, but choose to include the figures as part of a consistent whole due to them originating from the same theoretical basis.

3.3.7 Data availability

The RGIv5 dataset used for glacier area distribution data is available from GLIMS at https://www.glims.org/RGI/randolph50.html with identifier doi:10.7265/N5-RGI-50. The updated glacier model output is available from the corresponding author upon reasonable request.

3.3.8 Addendum

This research is funded by the Austrian Science Fund (FWF) project P25362.

D.P. and B.M conceived and designed the study; B.M. performed the glacier model experiments, D.P. the developed and applied the upscaling techniques and performed the analysis; D.P. wrote the manuscript with contributions by B.M.

The authors declare that they have no competing financial interests.

Correspondence and requests for materials should be addressed to David Parkes. (email: david.parkes.88@gmail.com).

3.4 Additional Figures

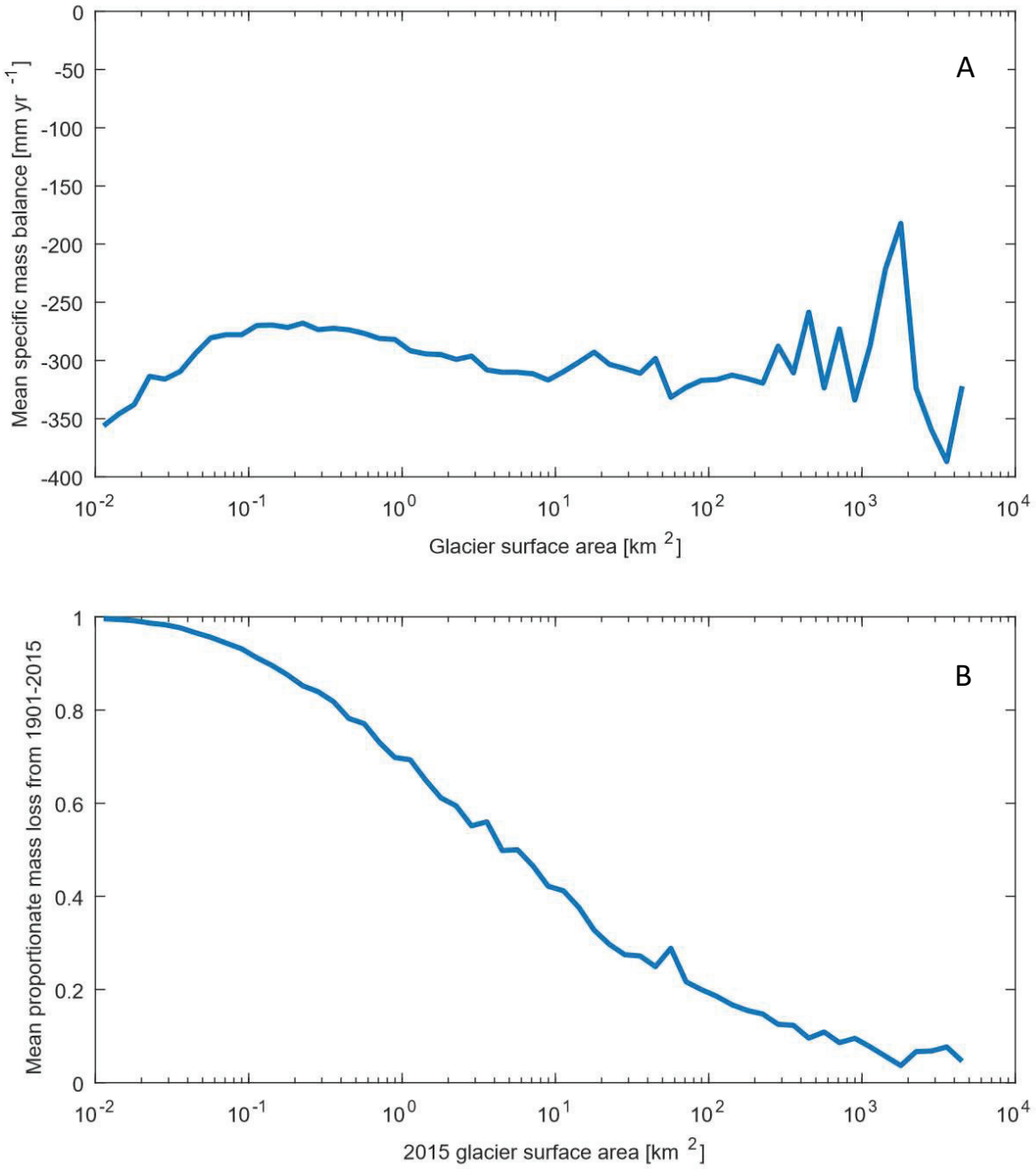
A
Mean specific mass balance [mm yr -1]
0
-50
-100
-150
-200
-250
-300
-350
-400
10-2
10-1
100
101
102
103
104
Glacier surface area [km 2]
B
Mean proportionate mass loss from 1901-2015
1
0.8
0.6
0.4
0.2
0
2015 glacier surface area [km 2]

Figure 3.3: **(A)** Mean specific glacier mass balance by glacier size class. The fact that this graph is relatively flat suggests that differing mass balance between small glaciers and larger glaciers does not play a significant role in small glaciers (and by extension *missing* glaciers) contributing a large amount to SLE mass loss relative to their current ice mass. Glacier size does not strongly impact mean specific mass balance, and this weak dependence is also shown in observations from literature [18] **(B)** Mean proportion of 1901 mass lost between 1901 and 2015 as a function of glacier size class. The smallest glaciers that exist in 2015 typically lost almost all of their 1901 mass, with the proportion dropping consistently as 2015 glacier size increases, up to the largest glaciers in 2015 which have seen an average of less than 10% of their mass disappear since 1901.

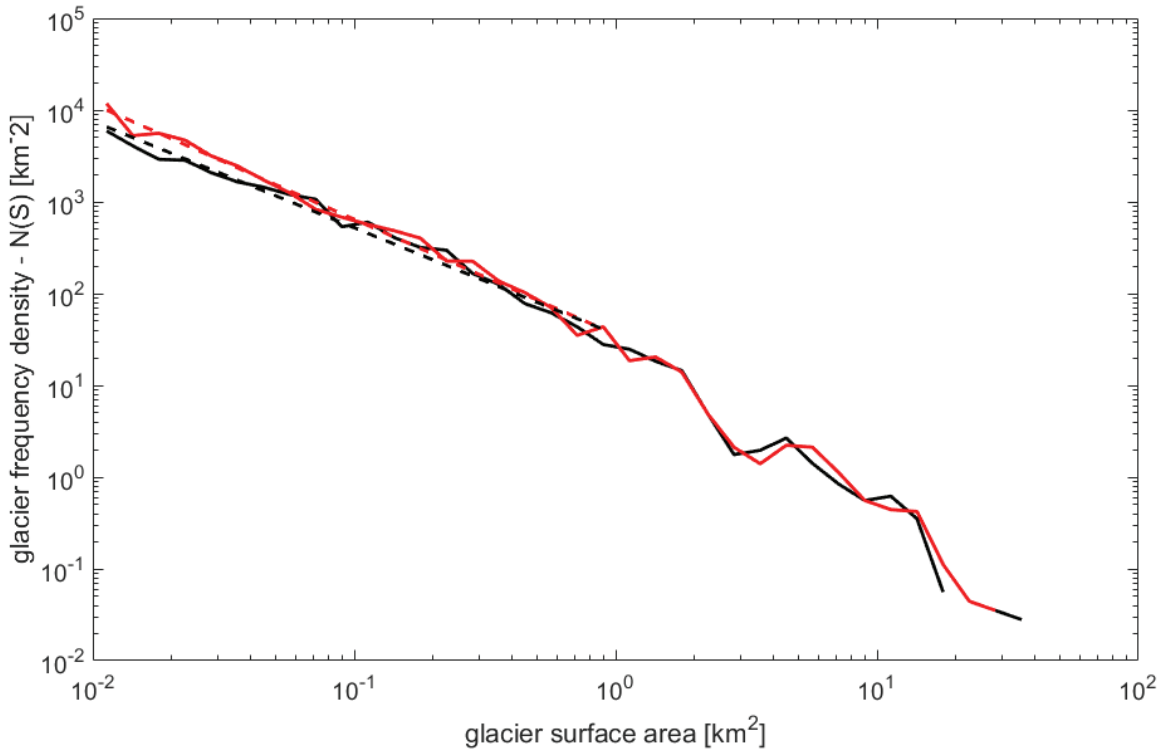

Figure 3.4: Glacier distribution for Switzerland, a region where we believe the RGI (red) to have much better representation of small glaciers, thanks to high resolution mapping efforts (such as the Swiss Glacier Inventory [17] shown in black). The power laws for the RGI and SGI (dashed red and dashed black respectively) are calculated for the 10^{-2} to 10^{0} km^2 range, and show that a credible power law exists in this region down to the smallest glacier sizes, albeit with reduced exponents (1.26 and 1.16 respectively)

Chapter 4

Paper 3: The Fractal Dimension of Spatial Glacier Distribution on Regional Scales

David Parkes[1] & Ben Marzeion[1]

[1]Institute of Geography, University of Bremen, Bremen, Germany

Manuscript to be submitted to *The Cryosphere*

4.1 Abstract

Like many aspects of the earth system, the distribution of glaciers potentially displays fractal properties. Scaling relationships across glacier populations play a significant role in glacier modelling, due to relatively sparse direct measurements of glacier properties, and fractal dimension is effectively another scaling relationship for glacier populations that can contextualise our understanding of other laws for glacier scaling and how representative they might be. We find that in most glacierised regions, we can derive reasonable estimates of the fractal dimension of the regional glacier distribution, with a mean estimated dimension of 1.34±0.08. The estimated regional dimensions take a broad range of values, from 0.88±0.06 to 1.62±0.06, suggesting considerable variability in the nature of the distributions between regions. We find that the mean of regional fractal dimension when weighted by total regional glacierised area is significantly different to the mean weighted by the number of available glacier measurements per region, raising the question of whether commonly-used scaling laws taken to hold for glaciers globally are in fact biased due to being derived largely from regions which are not representative of spatial patterns of glacier distribution globally. We also compare the fractal dimension model of spatial distribution of glacierised area to an existing approach based on percolation theory, and find that the percolation theory approach cannot adequately describe the fractal dimension exhibited by glacierised regions on larger scales, but also that the percolation theory approach is more applicable on smaller scales, which the description of fractal dimension in this paper is not equipped to deal with. An effective description of the way glacierised area is distributed spatially may result from a randomised percolation theory approach at small scales, constrained at larger scales by structures of fractal dimension. A first attempt at combining percolation theory and fractal dimension to generate a model of glacierised area is presented, but is found to be of limited value without further enhancements.

4.2 Main Text

4.2.1 Introduction

Self-similarity and fractal dimension have been usefully employed in understanding properties and scaling relationships in the earth system - for example, in coastlines [35], and in river networks [63] and watersheds [16] - and glacier modelling has often employed empirically determined scaling relationships between glacier properties to compensate for relatively limited numbers of direct measurements in comparison to the number of glaciers globally [4, 54, 41, 34, 39, 50]. It is therefore natural to investigate whether glaciers - individually and as regional or global distributions of ice mass - exhibit fractal properties, and whether these properties can be used to better understand scaling relationships and regional differences for the purposes of glacier modeling and measurement.

Fractal dimension represents an additional metric by which to characterise glacierised regions, for the purpose of either constructing or validating models. As even the most comprehensive global glacier inventories are incomplete at the smallest scales [6, 50], the scale-independent properties implied by fractal behaviour can inform our ability to upscale or even repopulate regions where representation of glaciers is lacking. Further, characterising glacierised regions with small numbers of numerical parameters - if this can be done accurately - is a step towards statistical glacier models operating over grid cells that are both more efficient and more flexible than those which explicitly model each glacier of an inventory discretely. While these models are likely to sacrifice sophistication, they may be important for integrating glacier modelling into global circulation models (for which efficiency is a huge concern) and for modelling glaciers in climates that differ considerably from today. The further a climate used for modelling is from the climate in which glaciers inventoried exist, the less we can reasonably rely on the individual locations of modern glaciers as a basis. This is particularly the case in colder-than-current climates, where glaciers may exist in locations they do not today, meaning they cannot be represented in models explicitly based on modern inventories.

The distribution of glaciers is primarily a function of topography and local climate, in the form of snow deposition and surface energy balance (with temperature often used as a proxy) [49, 29, 61]. Provided glaciers have thickness less than the typical variability of their surrounding topography, they are largely constrained to flow within topographical basins [5] in the same way as rivers, and their locations are dependent on the distribution of precipitation. Of course, glaciers also differ from river networks in many ways, so while qualitiatively we might expect glaciers to exhibit fractal behaviour from what we know about rivers, we cannot assume their dimension is related to the dimension of river systems, even in the same areas. The more viscous nature of ice flow means glaciers have thickness

and width that scale much more rapidly with length than is typical for rivers - at first estimation, these properties mean we would expect glaciers to be less sensitive to the roughnes of topography at the smallest scales.

In this paper, we focus on the fractal dimension of total glacierised area on the largest scales, looking at how the pattern of glaciers across first order Randolph Glacier Inventory version 6.0 (RGIv6) [57] regions may exhibit fractal behaviour. We first generate an estimate of fractal dimension for the glacier distribution in each region, and assess in which of the regions this estimate is indicative of genuinely fractal behaviour. We then look at how differences in fractal dimension between regions may be related to other properties of regional glacier distribution, and what context this provides for the distribution of direct measurements of glaciers that have been collected historically. We also look at how the estimated fractal dimensions here compare to the implied dimension from an existing model of spatial glacier distribution [7].

4.2.2 Determining fractal dimension

We employ a 'box counting' approach to estimate the fractal dimension of glacierised area within each region [36]. This is two-dimensional analog of the one-dimensional 'measuring stick' approach used, for example, to estimate the fractal dimension of coastlines. Glaciers in a region are mapped onto a square grid, and as the grid is made increasingly fine, the relationship between the linear scale (side length) of each grid cell, L and the number of grid cells, N which contain any glacierised area should scale with fractal dimension d, according to:

$$N \propto L^{-d} \tag{4.1}$$

So, by graphing $log(N)$ against $log(L)$, the slope of the line of best fit gives an approximation of $-d$.

Given the large scale of entire RGI regions, the method used to project the curved surface of the earth onto a 2D plane for the purposes of box counting is significant. We choose to project onto an area-preserving (so that all boxes on a grid are equally sized) but not distance-preserving grid. For each grid, cells have some constant height C in degrees latitudinally, and a width of $C/cos(lat)$ (so for any grid cell, the width - in degrees - at the top and bottom will be different). This is aligned so the vertical line through the centre of the grid has fixed longitude, but other lines of fixed longitude will curve in towards the top (in the Northern Hemisphere) or bottom (in the Southern Hemisphere). This is a region-restricted equivalent of a the Craster Parabolic (Putnin's P4) projection, except that in our regional grids the central meridian is not the 0th, but the central longitude of each region.

We project the glaciers onto the grids with the area and centre point given by the RGIv6 database, but not the glacier outlines given by the corresponding shapefiles - instead we simply use a square. This is for several reasons; firstly, within the the RGI shapefiles, some glaciers already have arbitrary outlines (e.g. circles) instead of actual outlines from observations, so we cannot sensibly use glacier outlines without excluding these glaciers, which would damage the primary aim of understanding the large scale fractal properties of the regional distribution of glaciers. Secondly, as we are interested in properties on the scale of glacierised regions, rather than properties on the scale of individual glacier outlines/surfaces (which may well also exhibit fractal properties, but with no necessary reason to share the same dimension as the region as a whole), using simple square glaciers allows us to very easily visualise the cutoff between fractal properties of the distribution and properties relating to individual glaciers: fixing glacier shapes as square ensures that as the grid scale becomes small enough that glacier outlines dominate over regional distribution, the estimated dimension tends to 2, making the transition obvious in the log-log graphs, assuming there are no regions where the glacier distribution exhibits dimension close to 2 (in practice, no regions do). Finally, it is simply increasingly computationally expensive to use smaller and smaller grids over such large regions, and square glaciers in a near-square grid make the sorting of glaciers into grid squares considerably easier, allowing us to use grids down to 0.001 degrees latitude ($\approx$0.1 km) per side in reasonable time and without specialised computing facilities. The impact of using squares over another shape is small at larger grid scales (where the spatial distribution of the set of glaciers dominates over the geometry of individual glaciers), and results in a more rapid convergence to a dimension of 2 at the smallest grid scales, as the near-square grid can more readily converge to the shape of the square glaciers.

We define 10 area-preserving grids across each region from cell side length 1 degree ($\approx$111 km) down to 0.001 degrees ($\approx$0.1 km) - with all uses of 'degrees' pertaining to the grid representing the mean earth-surface distance spanned by one degree of latitude. These grids gives us a maximum cell area of $\approx$12,300 km^2, larger than the largest ice mass recorded in RGIv6, and a minimum cell area of $\approx$0.01 km^2, as small as the lower limit of recorded RGIv6 glaciers. Coarser or finer grids than these are not likely to give any greater insight into the distribution, as we do not have either extant glaciers (at the top end) or high-resolution global data (at the bottom end) to continue to observe any fractal properties beyond these scales. In addition, extending the grid cell side length in either direction may actually *reduce* our ability to distinguish fractal properties, as at measurement scales much larger than the phenomena being observed, the apparent fractal dimension will converge to 0 (the entire measurement area contained in a single cell) and at measurement scales much smaller than the phenomena being observed, the apparent fractal dimension will converge to the dimension of the minimum measuring unit (in this case, a 0.01 km^2 square, so dimension 2). The 4 panels of fig. 4.1 show the shape of the glacier-filled cells for the first 4 grid cell scales (1 degree, 0.5 degrees, 0.2 degrees, and 0.1 degrees respectively) for RGI region 13 -

Central Asia.

Related to the phenomenon of apparent dimension converging to zero for grid cell scales much larger than the scale of the phonemenon being measured, we have removed a small subset of glaciers from RGI region 10 - Low Latitudes. There are a very small number of tiny, isolated African and South East Asian glaciers in this region which result in the region, as defined, having the largest area in the RGI, and being the only region to span multiple continents. These 41 glaciers represent only 7 km^2 of glacierised area, in comparison to the remainder of the region (all in South and Central America) containing 2898 glaciers representing 2335 km^2 of glacierised area. As these 41 glaciers are such a tiny component of an already small (in terms of ice-covered surface area) glacierised region, we exclude them due to the potential to skew the distribution by adding isolated cells of glacierised area from which we cannot reliably draw any scaling relationships. The effect of removing these glaciers is to restrict RGI region 10 to a much more manageably sized section of northern South America and Central America, more in line with other regions.

After processing of the box counting data, we made a decision to restrict the range of L for the generation of a line of best fit for the relationship of $log(N)$ against $log(L)$ to the first 6 of our 10 grid scales (1 degree to 0.02 degrees) based on the linearity of the relationship appearing to weaken in many regions as the grid scale was reduced below 0.02 degrees. This means each line of best fit is calculated from a set of 6 points. We expect the linearity to deteriorate at some grid scale, as the fractal dimension will tend to 2 as the scale becomes very small, but the scale at which this deterioration becomes apparerent varies by region and may be partly due to the completeness of the inventory at the smallest glacier sizes. We do not generate errors through the standard formula for calculating a line of best fit, because we do not have a set of independent observations, but instead a nested, non-independent sequence of box counts, and we are interested more in how much the slope may vary than in how far points may fall from the line. Instead, for each region, we take the slope between each pair of adjacent points (1 degree to 0.5 degrees, 0.5 degrees to 0.2 degrees, ... , 0.05 degrees to 0.02 degrees) - 5 slope values in total - and calculate the standard deviation of these values, which is then stated as the error in estimated fractal dimension. In practice, this results in a good separation between regions with high error values, where it is clear from the log-log graphs that there is little claim to an observed linear relationship from which to draw an estimated fractal dimension, and regions with low error values, where there is a convincing linearity to the section of the log-log graph where the line of best fit is drawn (see fig. 4.2).

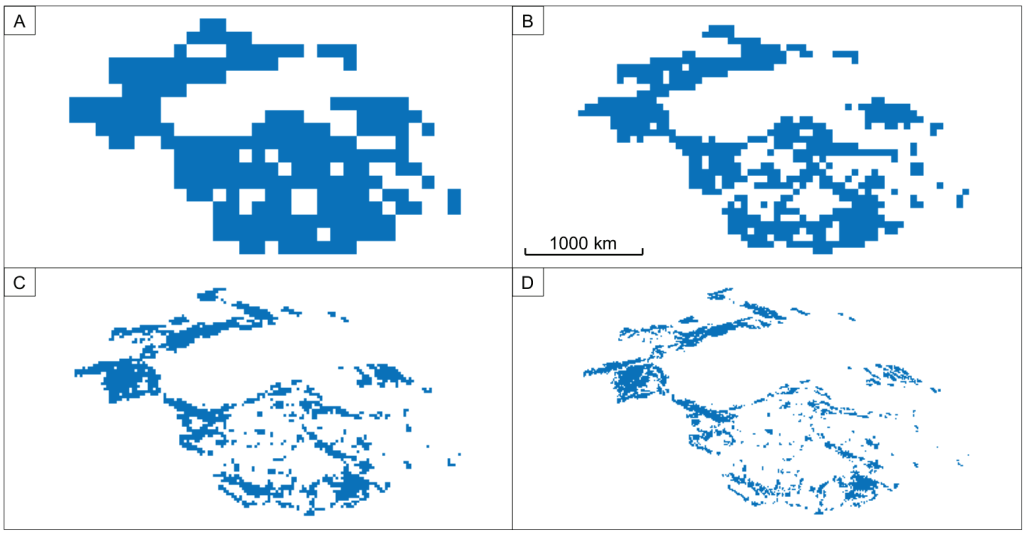

Figure 4.1: Illustration of the shrinking grid used for the box-counting approach to determining fractal dimension for RGI region 13 - Central Asia. Grid sizes for **(A)**, **(B)**, **(C)**, and **(D)** are 1 degree, 0.5 degrees, 0.2 degrees, and 0.1 degree respectively. These are only 4 of the 10 grid scales used, with the smallest scale being 0.001 degrees. The estimated fractal dimension values are derived from the line of best fit for the first 6 grid scales, from 1 degree to 0.02 degrees.

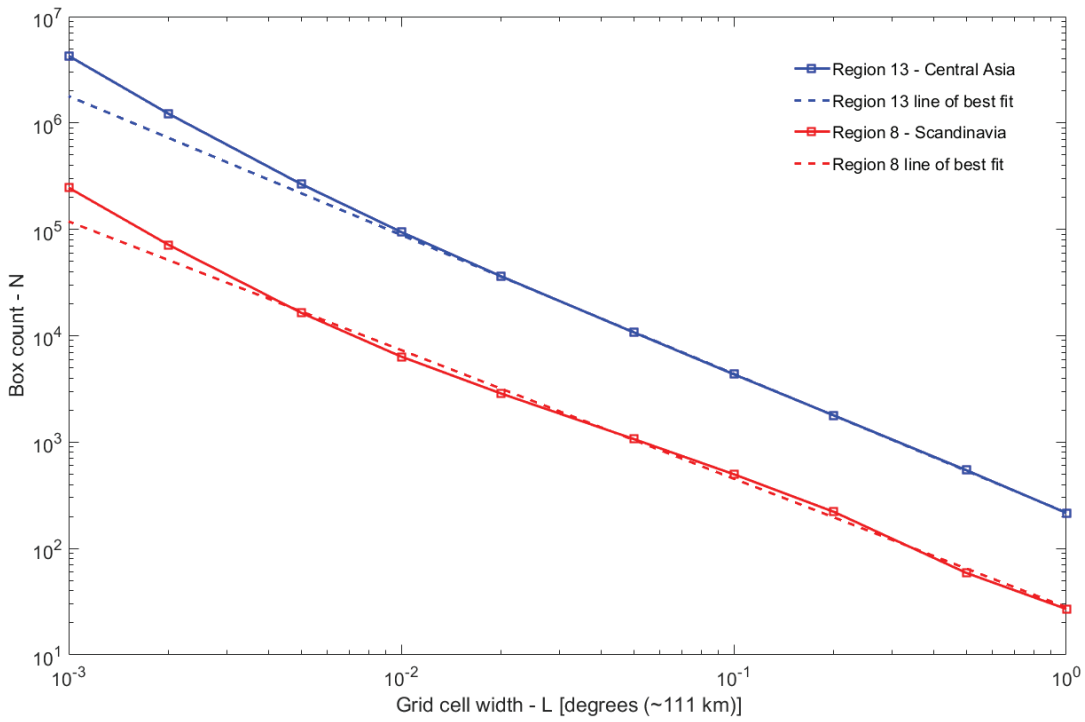

Figure 4.2: Box count vs grid cell width for the regions with the most confident estimated fractal dimension (Region 13 - Central Asia, with dimension 1.30±0.02) and the least confident estimated fractal dimension, excluding the 5 regions showing an insufficiently clear relationship (Region 8 - Scandinavia, with dimension 1.21±0.15). The confidence in the plotted line of best fit for all other regions lies somewhere between these two.

4.2.3 Fractal dimension results

Table 4.1 shows the estimated fractal dimension for each RGI region. In 5 regions (6, 9, 12, 18, and 19), we find graphs that are not consistent with a well-defined estimated fractal dimension in the 1 degree to 0.02 degree range - they do not exhibit a convincing linear relationship within this range - and these correspond to the regions with error values in the estimated fractal dimension of more than ±0.15. In the remaining 14 regions, a credible value of an estimated fractal dimension exists. In fig. 4.2, we show the $Log(N)$ vs $Log(L)$ graph for the region with the smallest error value (region 13 - Central Asia, with dimension 1.30±0.02), and the region with the largest error value (excluding regions with no apparent fractal dimension), region 8 - Scandinavia - with dimension 1.21±0.15. The values for estimated fractal dimension across the 14 regions ranges from 0.88±0.06 (region

10 - Northern Asia) and 0.90±0.12 (region 16 - Low Latitudes, restricted to the Americas) to 1.62±0.06 (region 3 - Arctic Canada North) and 1.57±0.08 (region 14 - South Asia West). The unweighted mean estimated fractal dimension across all regions (excluding 6, 9, 12, 18, and 19) is 1.34±0.08, which is close to the fractal dimension derived from the sum of box counts across all regions, at 1.37±0.11.

The considerable variation in estimated fractal dimension suggests major differences in the spatial distribution of glaciers between regions. Fractal dimension does not uniquely determine the shape of a distribution - two shapes with the same fractal dimension can be radically different - but different fractal dimension does imply difference in shape, and considerably different dimensions do suggest considerably different shapes. In the two regions where the estimated fractal dimension is less than 1 (10 and 16), we might expect a very sparse spatial distribution relative to typical glacier sizes, and potentially glaciers arrayed in narrow lines, rather than covering areas, as we see in the sample box counting grid for region 16 (fig. 4.3a). At the other end of the scale, we have 6 regions where the estimated fractal dimension is greater than or equal to 1.5 (regions 1, 3, 4, 5, 7, and 14). In the cases where the fractal dimension is closer to 2, we expect the distribution to come closer to having 'space filling' properties, with a denser clustering of glaciers. This is shown clearly for region 3 (fig. 4.3b), and a side-by-side comparison shows considerable qualitative difference between fig. 4.3a's sparse distribution and 4.3b's densely packed glacierised area.

The distribution of glacier sizes plays a key role in determining fractal dimension, so we compare our estimated fractal dimensions to some properties of the distribution for each region. In fig. 4.4, we show the estimated fractal dimension of each region as a function of mean, median, and total glacierised area for each region. For mean and median regional glacier area, we do not find any statistically significant correlation at the 5% level, but for total regional glacierised area, we do find a moderate positive correlation of 0.58. This suggests, fairly intuitively, that regions with more glacierised area tend to have more tightly packed structures of glaciers in their distribution, but it is important to recognise that the total glacierised area in a region is heavily dependent (more so than mean or median glacierised area) on the definition of the region boundaries, which are partly artificially drawn for human convenience rather than geographical significance. While there are some first-order RGI regions that define themselves fairly naturally through geographical isolation (e.g. Svalbard), there are others which split glaciers within the same underlying large-scale topography into separate regions (e.g. Central Asia, South Asia West, and South Asia East) or contain glaciers from areas that do not have any apparent link in terms of large scale features (e.g. North Asia), even straddling more than one continent (Low Latitudes, although here we restrict this region to the Americas).

RGI Region	**Estimated dimension of regional glacier distribution**
1 - Alaska	1.50±0.11
2 - Western Canada and US	1.25±0.08
3 - Arctic Canada North	1.62±0.06
4 - Arctic Canada South	1.51±0.07
5 - Greenland Periphery	1.50±0.07
6* - Iceland	1.34±0.27
7 - Svalbard	1.58±0.13
8 - Scandinavia	1.21±0.15
9* - Russian Arctic	1.49±0.23
10 - North Asia	0.88±0.06
11 - Central Europe	1.18±0.09
12* - Caucasus and Middle East	0.98±0.18
13 - Central Asia	1.30±0.02
14 - South Asia West	1.57±0.08
15 - South Asia East	1.34±0.03
16** - Low Latitudes (Americas)	0.90±0.12
17 - Southern Andes	1.38±0.04
18* - New Zealand	1.22±0.31
19* - Antarctic and Subantarctic	1.32±0.33
Region Mean (excl. 6, 9, 12, 18, 19)	**1.34±0.08**
Global Dimension	**1.37±0.11**

Table 4.1: The various RGI regions show considerable variation in estimated fractal dimension, derived from the slope of the box-counting graph between 1 degree and 0.02 degrees, and in the uncertainty of these dimensios, derived from the variability in this slope. The 'region mean' is an unweighted mean across all of the listed regions, while the 'global dimension' is the estimated fractal dimension derived from the slope of a box-counting graph summing boxes across all regions. Neither the region mean nor global figures are necessarily good representations of a true global distribution, but are included for context. *Regions 6, 9, 12, 18, and 19 do not show a convincing estimated fractal dimension. We show the fractal dimension calculated for these regions, but leave them out of the mean across regions and do not consider their fractal dimension values to be meaningful for the purposes of our discussion. **RGI region 16 has been restricted to the Americas only, as the region covers multiple continents with only 41 glaciers with a total area of 7 km outside the Americas. These heavily skew any potential fractal relationship observed compared to the other (largely contiguous or at least geographically coherent) RGI regions, as explained in the text.

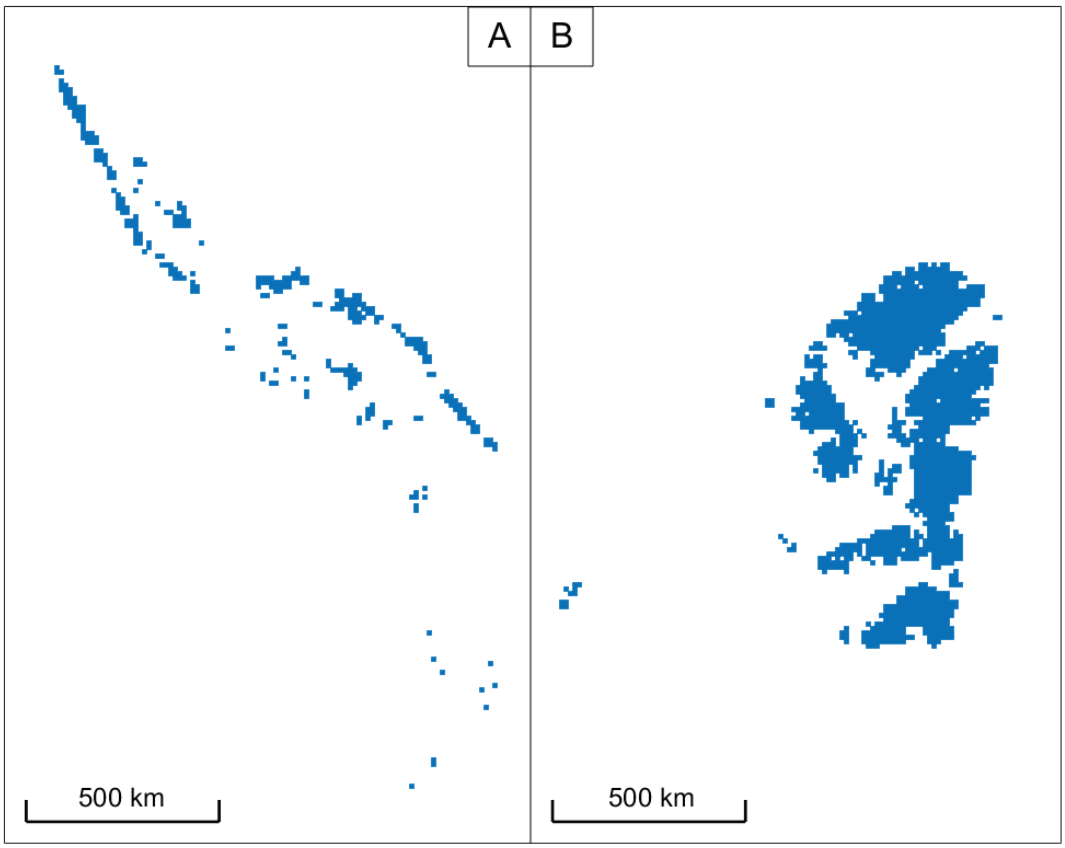

Figure 4.3: Box counting grids at 0.1 degree scale for **(A)** part of RGI region 16 - Low Latitudes, restricted to the Americas, and zoomed in on the densest part of the distribution, centred on Peru, and **(B)** RGI region 3 - Arctic Canada North. This shows the contrast between a region of low fractal dimension (A) and a region with high fractal dimension (B), with the glacierised area in A much sparser.

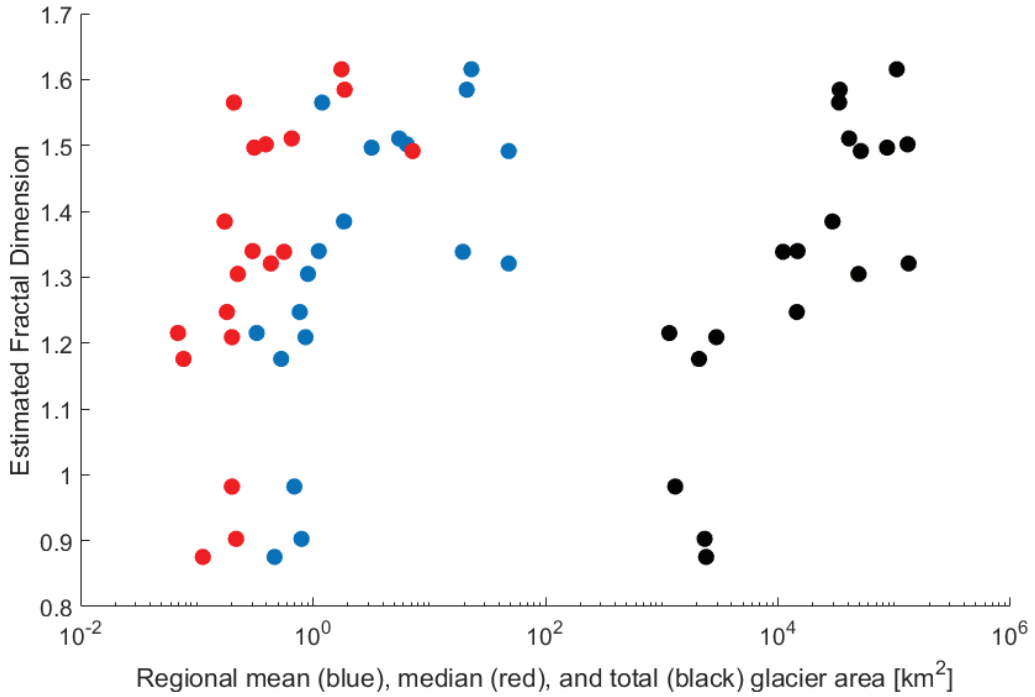

Figure 4.4: Estimated fractal dimension by region as a function of several numerical properties of regional glacier distribution. Only total glacier area (black) shows a statistically significant correlation with estimated fractal dimension.

4.2.4 Comparison to distributions of direct measurements

Direct measurements of glacier properties are relatively rare [11, 67, 33], and may be distributed unevenly, with a bias towards glacierised regions which are smaller and more accessible. If glacier modelling is to derive universal scaling relationships from small, spatially non-representative samples of glacier measurements, we need to have confidence that the observed scaling relationships are properties of glaciers in general, and not properties that vary considerably by region. Of course, the only complete solution to this problem is increased coverage of glacier observations, but collection of the data is time-consuming and technology-limited, so in the interim we must look at what comprehensive measurements we do have, and determine whether the data supports the idea that the glaciers from which we draw direct measurements are representative enough globally to support the posited scaling relationships. We believe RGIv6 to be fairly representative (except possibly at the smallest glacier scales [6, 50]) of glacier areas and locations globally, with over 200,000 glaciers represented, but we do not believe observation-based data sets of similar size exist for many

other important properties for glacier modelling (ice thickness, surface mass balance, or flowlines, for example). One way we can test the idea that regions with more dense observations are representative of regions with sparse observations is to compare the distribution of glacier areas between regions. Comparison of fractal dimension is a new way to assess representativity, beyond the obvious statistics such as mean, median, or maximal glacier area; it incorporates the structure of the underlying topography for the glacierised region, and the spatial pattern of glacier locations by size. We expect - but cannot prove, without the additional direct observations mentioned - that two regions where glaciers follow similar scaling relationships will be of similar fractal dimension.

The WGMS Global Glacier Change Bulletin [65] provides global data for glacier length (2475 series with 44969 data points), and glacier mass balance from both glaciological (446 series withand geodetic sources, with 6503 data points) and geodetic (4275 series with 5319 data points) sources. We generate a 'representativity index' for each RGI region and each measurement type, by dividing the number of data points in the region by the total glacierised area (given by RGIv6) in the region. 'Representativity index' could equally be considered 'measurement density'. In fig. 4.5 we show the representativity indices against estimated fractal dimension, and also show the mean of regional dimension weighted by various methods (and unweighted). We do not directly find a correlation (at 5% confidence level) between estimated fractal dimension and representativity index for length, glaciological mass balance, or geodetic mass balance measurements, but we do find quite a variation in mean of regional estimated fractal dimension depending on the weighting. The unweighted mean of regional fractal dimension is 1.34±0.08, but weighted by the total glacierised area in each region, this rises considerably to 1.49±0.07. Weighted by measurement counts, the mean of regional estimated fractal dimension is 1.20±0.09 (length), 1.26±0.09 (glaciological mass balance), or 1.37±0.09 (geodetic mass balance). Of particular significance here is that there is no overlap in the confidence intervals for mean of regional estimated fractal dimension weighted by total glacierised area and the means weighted by either length measurements or glaciological mass balance measurements.

Leclercq et al. [33] find that there are 4 RGI regions where the percentage of glacierised area accounted for by glaciers with direct length measurements exceeds 10% - Central Europe (38.4%), Southern Andes (29.7%), Caucasus (24.9%), and Scandinavia (12.6%) - while the global average figure is only 2.8%. Because of the longer observation periods as well as the larger number of glaciers observed, the data for glaciers in Central Europe makes up 59% of the total number of data points globally. In our results, we find that Central Europe has an estimated fractal dimension (1.18±0.09) that is lower than both the mean of regions (1.34±0.08) and global estimated fractal dimension (1.37±0.11), though the confidence intervals do very slightly overlap, so we cannot conclude that the fractal dimension of Central Europe differs from the global figures with confidence.

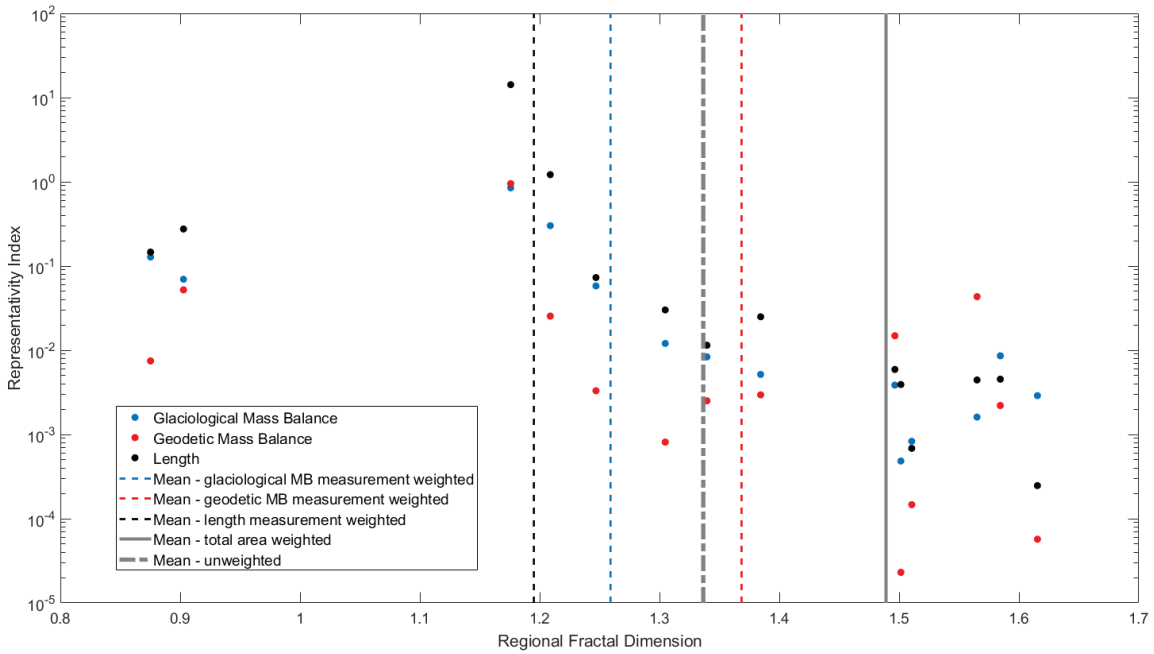

Figure 4.5: Representativity of several types of glacier measurement by region, compared with estimated fractal dimension. The representativity index is calculated by dividing the number of measurements (all taken from the WGMS Global Glacier Change Bulletin [65]) for the region by the total glacierised area within the region (from RGIv6 [57]). The vertical lines show the mean of regional fractal dimension weighted by various methods; we see that the mean of regional estimated fractal dimension weighted by glacierised area differs considerably from the mean of regional estimated fractal dimension weighted by glaciological and geodetic mass balance measurements, and most significantly length measurements.

4.2.5 Comparison to percolation theory

The statistical distribution of glaciers has previously received attention from a theoretical perspective [7], and power law behaviour of frequency density as a function of glacier area has been observed on regional [6] and global [50] scales. These observational approaches did not, however, take into account the spatial distribution of glaciers, which is an additional factor in estimating fractal dimension. In the theoretical work [7], a model for the spatial distribution was constructed based on percolation theory, which provides valuable insight into the spread of glacier sizes, but has a spatial distribution that does not match the observed estimated fractal dimension we find in any RGI regions. In the simple 2D percolation array model, the dimension of glacier distribution is easily shown to be 2: all sites

are occupied with uniform non-zero probability p, so as the size for box-counting becomes considerably larger than the percolation grid scale, the probability of any box containing some occupied site tends to 1. No correlation length scales exist, so no scale-independent features can exist either - intuitively, as you zoom out from a simple 2D percolation array, less and less structure is apparent. The dimension for the modified 2D percolation array, given correlation length r, is less obvious, but will still tend to 2 as the ratio of r to the distance across the region tends to 0. By definition r is less than or equal to the mean glacier radius (so πr^2 is less than or equal to the mean glacier area), and from our data, mean glacier sizes by region are typically on the order of 1 km^2 ($\approx$0.01 degrees * 0.01 degrees) while regions have dimensions in the 10s of degrees, so a modified percolation model on the scale of entire RGI regions would still have dimension approaching 2, and could not show structure on a scale much greater than 0.01 degrees.

Clearly, a model of glacier distribution requires structure to glacierised regions on scales larger than typical glacier dimension in order to accurately represent the observed fractal dimension for large glacierised regions, but this does not discredit the strengths of the percolation theory approach. By design, the percolation theory approach attempts to explain the numerical distribution of glacier (and snow patch) sizes, and does not claim to explain larger scale spatial distribution features. It is also constructive, generating potential distributions from scratch with a simple parameterisation, while the estimated fractal dimension presented in this paper is at present only descriptive. There is potential for a hybrid approach to understanding glacier distribution, whereby on small scales, local random or pseudorandom processes determine the distribution of snow accumulation, constrained by structured phenomena of fractal dimension (such as areas with topography above a calculated equilibrium line altitude) at larger scales.

In fig. 4.6, we show a first attempt at constructing a map of glacierised area utilising fractal dimension, using the starting point of the 1 degree box-counting grid for region 13 (Central Asia) for easy comparison with fig. 4.1. The 4 scales of grid shown are 1 degree, 0.5 degrees, 0.25 degrees, and 0.125 degrees, because we need each progressively fine grid to be an extension of the larger grids. Given the estimated fractal dimension d of the region (in this case, 1.30), we generate a probability $p = 2^{d-2}$ (in this case, 0.62), which is the probability that any cell in the 0.5 degree, 0.25 degree, and 0.125 degree grids contains glacierised area if the 1 degree, 0.5 degree, and 0.25 degree cell, respectively, containing it also contains glacierised area. The grids are filled in sequentially, starting with the largest grid and getting smaller. This ensures the correct fractal dimension is observed under a box counting approach. While we see in fig. 4.6 that this approach does create different scales of structure in the glacierised area (more so than a pure percolation theory approach applied to a grid of 0.125 degrees), it is clear when comparing to fig. 4.1 that the lack of directionality to the structures in the distribution and the absence of any parameterisation of correlation length (beyond the correlation length implied by the 'nesting' of the grids)

results in a distribution that is not particularly realistic. Without enhancements to account for these features, which are beyond the scope of this paper, this approach to constructing glacierised area with a hybrid percolation theory/fractal dimension method is of limited value.

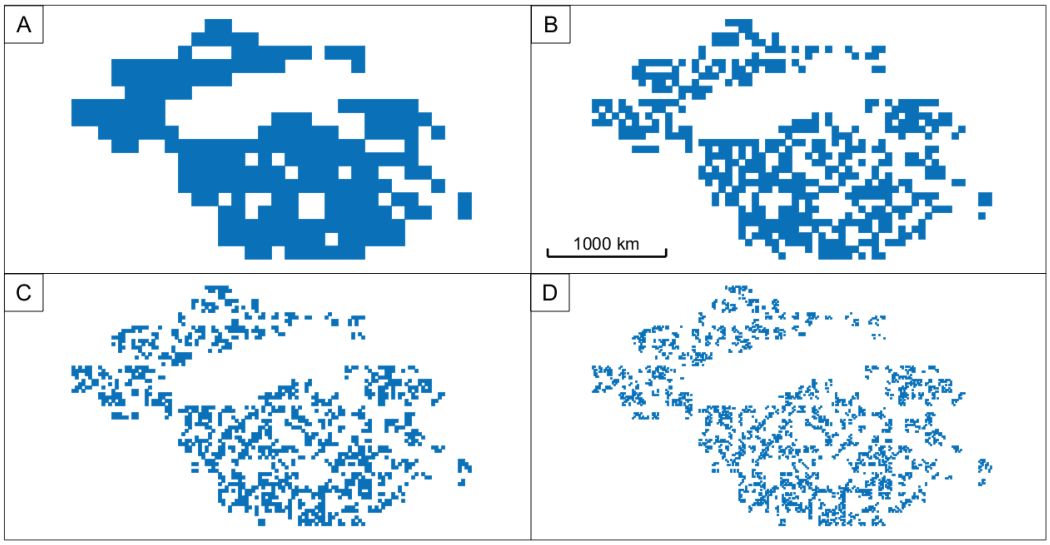

Figure 4.6: Construction of glacierised area maps using a hybrid percolation theory and fractal dimension approach. **(A)** 1 degree grid based on RGIv6 data, the same as shown in fig. 4.1a. **(B), (C), (D)** 0.5 degree, 0.25 degree, and 0.125 degree grids, respectively, using the hybrid construction approach.

4.2.6 Conclusions

We find compelling evidence that the spatial distribution of glaciers can be understood as a phenomenon of fractal dimension in a majority of RGI regions. Variations in the estimated dimension between regions is considerable, and we suggest, but do not yet prove, that this is largely due to variation in the topography and climate that determine where glaciers can exist. Because the distribution of glaciers, and associated numerical scaling relationships, are integral to most forms of large-scale glacier modelling, it should be of concern to modellers that the fractal dimensions of regions where available direct glacier measurements are most concentrated are considerably different to the fractal dimensions of regions where glacierised area is most concentrated; this is potentially evidence that the well-known quantitative bias of measurements towards a few, small regions is also a qualitative bias in the nature of the spatial distribution being sampled from. As ever, this

is an issue which, ultimately, only more representative global measurements can resolve.

An understanding of the fractal nature of glacier distribution provides an additional constraint for generating models of glacierised area that are not reliant on existing inventories, and we show that it can be used to enhance an existing simple percolation theory approach. However, this new method still has considerable problems, and more work is needed to create a method which can generate realistic maps of glacierised area. The ability to reconstruct the numerical and spatial distribution of glaciers from limited data is significant for glacier modelling - as we know that in practice even the most comprehensive inventories are incomplete - and for climate modelling as a whole, as the integration of glaciers into global circulation models is much easier if their distribution can be simply parameterised with reasonable accuracy, instead of requiring considerable resources for discretely modelling each member of a glacier inventory and correcting for associated biases. From our initial investigation, it seems likely that a comprehensive parameterisation of correlation length for the separation of glaciers, and of directionality in large-scale features will be necessary in order to synthetically generate representative glacier distributions suitable for modelling.

4.2.7 Data availability

The RGIv6 dataset used for glacier area distribution data is available from GLIMS at https://www.glims.org/RGI/rgi60_dl.html with identifier doi:10.7265/N5-RGI-60

4.2.8 Addendum

This research is funded by the Austrian Science Fund (FWF) project P25362.

Author contributions D.P. and B.M conceived and designed the study; D.P processed the data; D.P. wrote the manuscript with contributions by B.M.

Competing Interests The authors declare that they have no competing financial interests.

Correspondence Correspondence and requests for materials should be addressed to David Parkes. (email: david.parkes.88@gmail.com).

Chapter 5

Conclusions

5.1 Summary

The three papers presented here tell us that glacier mass changes, and their associated contribution to GMSLR, have been increasingly impacted over the last century by anthropogenic climate change; that there are potentially large deficiencies in the representation of small glaciers, which result in significant contributions to GMSLR that have not previously been calculated; and that the spatial distribution of glaciers demonstrates structure on a large scale which can be quantified (in part) using fractal dimension, with considerable differences between regions suggesting that regions with the most measurements are not representative of the majority of glacierised area globally. Taken together, these papers paint a picture of important statistical and spatial structure to glacier distributions, potentially beyond what we are able to capture directly with current remote sensing techniques, with these glaciers forming a component of recent GMSLR which is both sensitive to anthropogenic climate change and a major part of the 20th century GMSLR budget. The demonstrated relationships and structures that apply on regional - or even global - scales to the distribution of glaciers can be quantified with sufficient confidence, and have sufficient impact on GMSLR estimates, to deserve representation in models or large-scale glacier mass changes and to be worthy of further investigation.

5.2 Impact and Repercussions

We know that glaciers are a major component of the GMSLR budget, and that their mass losses are now mostly due to human activity, but despite the best efforts of the remote-sensing community, the underrepresentation of small glaciers matters more than their current size might suggest. Moreover, the skewing of direct measurements such as glacier length and mass balance is not only quantitative (sampling heavily from regions that have smaller total glacierised area), but also qualitative, sampling heavily from regions with estimated fractal dimension significantly lower than the mean weighted for total glacierised area. The uncertainties represented by these large-scale, statistical concerns over glacier distribution for the estimation of recent and ongoing glacier mass-changes cannot directly be tackled by enhancements to discretised glacier models. The overall impact of this new understanding is to weaken confidence in how representative regional- or global-scale estimates based on existing glacier measurements can be.

The repercussions for glacier modelling are not wholly negative, however. It is clear that the large-scale distributions of glaciers on both regional and global scales do show structure and do satisfy some relatively simple numerical relationships, which suggests good things for the 'knowability' of how these uncertainties impact mass change estimations. From

paper 2, we have a credible upper bound for how uncharted glaciers affect the mass change output from a global glacier model, and the same method of upscaling can be applied regardless of glacier model type. There is not yet such a neat solution for augmenting spatial distributions, but the finding that regional distributions typically satisfy the conditions for fractal properties is a step towards understanding where these uncharted glaciers exist (or previously existed). A better understanding of glacier distribution also allows for improved targeting of glacier measurements in the future in order to achieve more representative datasets, and for improved understanding of the representativity of existing datasets.

5.3 The Future of Large-Scale Glacier Modelling

State-of-the-art glacier models are always growing in sophistication. Models add complexity in terms of the physical processes they can represent, improved access to high-powered computing allows greater developmental freedom (or allows models developed with smaller applications in mind to be extended to larger data sets), and the data available for calibration and validation is always growing in both accuracy and volume. However, these natural progressions and refinements can be limited in value if there are problems with the modelling paradigm, and the evidence set out in this thesis suggests that glacier-by-glacier modelling based on fixed glacier data sets, which has been the norm for the era of remote-sensing data sets (around the past 30 years [66]), is not sufficient for many of the purposes that motivate large-scale glacier modelling in the first place. Future large-scale glacier models need to account for the statistical and spatial distribution of glaciers beyond what is explicitly recorded in inventories, in order to account not only for the deficiencies in the inventories themselves, but also for the systematic bias that comes from working from a snapshot of glacier distribution in a particular year and then working backwards or forwards.

Much of the work presented here is in some way a first-attempt or proof-of-concept for methods aimed at influencing such a shift in modelling paradigm. The exact implementation and results are therefore arguably less significant than the ideas presented: in paper 2, for example, while the headline figure of a contribution to GMSLR can inform future work on sea-level budgets, from a glacier modelling perspective it is hopefully the importance of providing some form of upscaling or other accounting for uncharted glaciers that is the main takeaway.

The avenues for extension of the material in the 3 papers vary based on the scope of the papers. As paper 1 is an attribution study using an established model, the scope for natural extension of the work specific to the paper is limited; greater interest lies in the further development of the model, which is already taking place in the form of the OGGM [40]

project that grew out of the original Marzeion et al. [39] model used in the attribution study, and now has a large active development team.

In paper 2, the upscaling method presented is a possible addition to large-scale glacier models of any type. One aspect of the future work based on this paper could actually lie in working with existing or new glacier model developers to implement upscaling for uncharted glaciers. The upscaling presented in the paper is straightforward, and could be applied as a post-processing measure in many cases, but a bespoke approach that works with the idiosyncracies of individual models would likely be more accurate, and would help to ingrain uncharted glacier upscaling as part of the modelling process, rather than an optional extra. There is still work to be done investigating the power law, both in terms of validation against remote-sensing data (this is done in a limited way with data from Switzerland in the paper, but more is possible, though this is contingent on inventories of sufficient quality) and in terms of creating a good model for why glaciers have the power law distribution observed. The percolation theory approach [7] offers a starting point, but as we see in paper 3, there are aspects of this approach that are not consistent with the observed distribution on the largest scales.

The content of paper 3 is perhaps the most extensible, largely because it is not as concrete as the work in the other papers. It is the only paper that does not explicitly relate to GMSLR contributions, instead indirectly relating to glacier mass change modelling through its impact on the understanding of glacier distributions and the representativity of regions glacier measurements are taken from. Further characterisation of glacierised regions through correlation length and directionality of glacier distribution may yield useful results. Eventually, a model to generate a realistic spatial distribution of glaciers from scratch is desirable; this is of interest not only to offer insights into real distributions, but also to help with parameterisations of glacier area that may be of use in GCMs.

The parameterisation of glacierised area - and the ability to accurately model from parameter sets without relying on data for the individual glaciers that are represented by the parameterisation - are of great importance for the integration of glacier modelling into GCMs. This is because GCMs are highly computationally expensive - and therefore highly optimised - and typically run over grid cells of area much larger than typical glaciers. Modelling glaciers within the framework of GCMs allows the effects of feedbacks between ice mass changes and the climate system which cannot otherwise be captured by offline modelling (feeding a glacier model with pre-generated climate results). The papers in this thesis do not go as far as specifying a translation between a traditional discretised glacier model and a distributed, parameter-based model that can be run on the scale of GCM grid cells, but working towards this would be a productive use of the effort to characterise the large-scale statistical and spatial properties of glacier distributions.

Bibliography

[1] Arendt, A., Bliss, A., Bolch, T., Cogley, J., Gardner, A., Hagen, J.-O., Hock, R., Huss, M., Kaser, G., Kienholz, C., Pfeffer, W., Moholdt, G., Paul, F., Radić, V., Andreassen, L., Bajracharya, S., Barrand, N., Beedle, M., Berthier, E., Bhambri, R., Brown, I., Burgess, E., Burgess, D., Cawkwell, F., Chinn, T., Copland, L., Davies, B., De Angelis, H., Dolgova, E., Earl, L., Filbert, K., Forester, R., Fountain, A., Frey, H., Giffen, B., N.Glasser, Guo, W., Gurney, S., Hagg, W., Hall, D., Haritashya, U., Hartmann, G., Helm, C., Herreid, S., Howat, I., Kapustin, G., Khromova, T., König, M., Kohler, J., Kriegel, D., Kutuzov, S., Lavrentiev, I., LeBris, R., Liu, S., Lund, J., Manley, W., Marti, R., Mayer, C., Miles, E., Li, X., Menounos, B., Mercer, A., Mölg, N., Mool, P., Nosenko, G., Negrete, A., Nuimura, T., Nuth, C., Pettersson, R., Racoviteanu, A., Ranzi, R., Rastner, P., Rau, F., Raup, B., Rich, J., Rott, H., Sakai, A., Schneider, C., Seliverstov, Y., Sharp, M., Sigurdsson, O., Stokes, C., Way, R., Wheate, R., Winsvold, S., Wolken, G., Wyatt, F., and Zheltyhina, N. Randolph Glacier Inventory – A Dataset of Global Glacier Outlines: Version 5.0. Global Land Ice Measurements from Space, Boulder Colorado, USA. Digital Media, 2015.

[2] Arendt, A., Bolch, T., Cogley, G., Gardner, A., Hagen, J. O., Hock, R., Kaser, G., Paul, F., Radic, V., Bliss, A., Fountain, A., Mercer, A., Negrete, A., Giffen, B., Menounos, B., Kienholz, C., Mayer, C., Nuth, C., Burgess, D., Hall, D., Kriegel, D., Berthier, E., Burgess, E., Cawkwell, F., Wyatt, F., Hartmann, G., Wolken, G., Frey, H., Brown, I., Howat, I., Lund, J., Rich, J., Filbert, K., Andreassen, L., Copland, L., Beedle, M., Koenig, M., Sharp, M., Moelg, N., Sigurdsson, O., Rastner, P., Forester, R., LeBris, R., Pettersson, R., Wheate, R., Herreid, S., Vorogushin, S., Winsvold, S., Chinn, T., Hagg, W., and Manley, W. Randolph Glacier Inventory 1.0: A Dataset of Global Glacier Outlines. Global Land Ice Measurements from Space, Boulder Colorado, USA. Digital Media, 2012.

[3] Bahr, D. Global distributions of glacier properties: a stochastic scaling paradigm. *Water Resourc. Res. 33*, 7 (1997), 1669–1679.

[4] Bahr, D., Meier, M., and Peckham, S. The physical basis of glacier volume-area scaling. *J. Geophys. Res. 102*, 20 (1997), 355–362.

[5] Bahr, D., and Pfeffer, T. Crossover scaling phenomena for glaciers and ice caps. *J. Glaciol. 62*, 232 (2016), 299–309.

[6] Bahr, D., and Radic, V. Significant contribution to total mass from very small glaciers. *The Cryosphere 6* (2012), 763–770.

[7] Bahr, D. B., and Meier, M. F. Snow patch and glacier size distributions. *Water Resourc. Res. 36* (2000), 495–501.

[8] Church, J., Clark, P., Cazenave, A., Gregory, J., Jevrejeva, S., Levermann, A., Merrifield, M., Milne, G., Nerem, R., Nunn, P., Payne, A., Pfeffer, W., Stammer, D., and Unnikrishnan, A. Sea level change. In *Climate Change 2013: The Physical Science Basis. Contribution of Working Group I to the Fifth Assessment Report of the Intergovernmental Panel on Climate Change*, T. Stocker, D. Qin, G.-K. Plattner, M. Tignor, S. Allen, J. Boschung, A. Nauels, Y. Xia, B. V., and P. Midgley, Eds. Cambridge University Press, Cambridge, United Kingdom and New York, NY, USA, 2013.

[9] Church, J. A., Monselesan, D., Gregory, J. M., and Marzeion, B. Evaluating the ability of process based models to project sea-level change. *Environ. Res. Lett. 8*, 1 (2013), 014051.

[10] Clarke, G., Jarosch, A., Anslow, F., Radic, V., and Menounos, B. Projected deglaciation of western Canada in the twenty-first century. *Nature Geosci. 8* (2015), 371–377.

[11] Cogley, J. Geodetic and direct mass-balance measurements: comparison and joint analysis. *Ann. Glaciol. 50* (2009), 96–100.

[12] Cogley, J. G., and Adams, W. Mass balance of glaciers other than the ice sheets. *J. Glaciol. 44*, 147 (1998), 315–325.

[13] Dangendorf, S., Marcos, M., Woeppelmann, G., Conrad, C., Frederikse, T., and Riva, R. Reassessment of 20th century global mean sea level rise. *P. Natl. Acad. Sci. USA 114*, 23 (2017), 5946–5951.

[14] Ehlschlaeger, C. Using the a^t search algorithm to develop hydrologic models from digital elevation data. In *International Geographic Information Systems (IGIS) Symposium* (1989), vol. 89, pp. 275–281.

[15] Farinotti, D., Huss, M., Bauder, A., Funk, M., and Truffer, M. A method to estimate the ice volume and ice-thickness distribution of alpine glaciers. *J. Glaciol. 55*, 191 (2009), 422–430.

[16] Fehr, E., Kadau, D., Araújo, N. A. M., Andrade, J. S., and Herrmann, H. J. Scaling relations for watersheds. *Phys. Rev. E 84* (2011).

[17] Fischer, M., Huss, M., Barboux, C., and Hoelzle, M. The new swiss glacier inventory sgi2010: relevance of using high-resolution source data in areas dominated by very small glaciers. *Arctic, Antarctic and Alpine Research 46*, 4 (2014), 933–945.

[18] Fischer, M., Huss, M., and Hoelzle, M. Surface elevation and mass changes of all swiss glaciers 1980–2010. *The Cryosphere 9* (2015), 525–540.

[19] Flato, G., Marotzke, J., Abiodun, B., Braconnot, P., Chou, S., Collins, W., Cox, P., Driouech, F., Emori, S., Eyring, V., Forest, C., Gleckler, P., Guilyardi, E., Jakob, C., Kattsov, V., C., R., and Rummukainen, M. Evaluation of climate models. In *Climate Change 2013: The Physical Science Basis. Contribution of Working Group I to the Fifth Assessment Report of the Intergovernmental Panel on Climate Change*, T. Stocker, D. Qin, G.-K. Plattner, M. Tignor, S. Allen, J. Boschung, A. Nauels, Y. Xia, B. V., and P. Midgley, Eds. Cambridge University Press, Cambridge, United Kingdom and New York, NY, USA, 2013.

[20] Frederikse, T., Riva, R., Kleinherenbrink, M., Wada, Y., van den Broeke, M., and Marzeion, B. Closing the sea level budget on a regional scale: Trends and variability on the Northwestern European continental shelf. *Geophys. Res. Lett. 43*, 20 (2016), 10864–10872.

[21] Fricker, H., and Padman, L. Ice shelf grounding zone structure from ICESat laser altimetry. *Geophys. Res. Lett. 33*, 15 (2006).

[22] Gardner, A. S., Moholdt, G., Cogley, J. G., Wouters, B., Arendt, A. A., Wahr, J., Berthier, E., Hock, R., Pfeffer, W. T., Kaser, G., Ligtenberg, S. R. M., Bolch, T., Sharp, M. J., Hagen, J. O., van den Broeke, M. R., and Paul, F. A reconciled estimate of glacier contributions to sea level rise: 2003 to 2009. *Science 340*, 6134 (2013), 852–857.

[23] Giesen, R. H., and Oerlemans, J. Climate-model induced differences in the 21st century global and regional glacier contributions to sea-level rise. *Climate Dyn. 41*, 11-12 (2013), 3283–3300.

[24] Gregory, J. M., White, N. J., Church, J. A., Bierkens, M. F. P., Box, J. E., van den Broeke, M. R., Cogley, J. G., Fettweis, X., Hanna, E., Huybrechts, P., Konikow, L. F., Leclercq, P. W., Marzeion, B., Oerlemans, J., Tamisiea, M. E., Wada, Y., Wake, L. M., and van de Wal, R. S.

Twentieth-century global-mean sea-level rise: is the whole greater than the sum of the parts? *J. Climate 26* (07/2013 2013), 4476–4499.

[25] Harris, I., Jones, P., Osborn, T., and Lister, D. Updated high-resolution grids of monthly climatic observations – the CRU TS3.10 Dataset. *Int. J. Climatol. 34* (2014), 623–642.

[26] Harrison, W., Elsberg, D., Echelmeyer, K., and Krimmel, R. On the characterization of glacier response by a single time-scale. *J. Glaciol. 47*, 159 (2001), 659–664.

[27] Hartmann, D., Klein Tank, A., Rusticucci, M., Alexander, L., Brönnimann, S., Charabi, Y., Dentener, F., Dlugokencky, E., Easterling, D., Kaplan, A., Soden, B., Thorne, P., Wild, M., and Zhai, P. Observations: Atmosphere and surface. In *Climate Change 2013: The Physical Science Basis. Contribution of Working Group I to the Fifth Assessment Report of the Intergovernmental Panel on Climate Change*, T. Stocker, D. Qin, G.-K. Plattner, M. Tignor, S. Allen, J. Boschung, A. Nauels, Y. Xia, B. V., and P. Midgley, Eds. Cambridge University Press, Cambridge, United Kingdom and New York, NY, USA, 2013.

[28] Hay, C. C., Morrow, E., Kopp, R. E., and Mitrovica, J. X. Probabilistic reanalysis of twentieth-century sea-level rise. *Nature 517*, 7535 (2015), 481–484.

[29] Hock, R. Temperature index melt modelling in mountain areas. *J. Hydrol. 282*, 1-4 (2003), 104–115.

[30] Immerzeel, W. W., van Beek, L. P. H., and Bierkens, M. F. P. Climate change will affect the Asian water towers. *Science 328* (2010), 1382–1385.

[31] Jóhannesson, T., Raymond, C., and Waddington, E. Time-scale for adjustment of glaciers to changes in mass balance. *J. Glaciol. 35*, 121 (1989), 355–369.

[32] Kaser, G., Grosshauser, M., and Marzeion, B. Contribution potential of glaciers to water availability in different climate regimes. *P. Natl. Acad. Sci. USA 107*, 47 (2010), 20223–20227.

[33] Leclercq, P. W., Oerlemans, J., Basagic, H. J., Bushueva, I., Cook, A., and Le Bris, R. A data set of worldwide glacier length fluctuations. *The Cryosphere 8*, 2 (2014), 659–672.

[34] Leclercq, P. W., Oerlemans, J., and Cogley, J. G. Estimating the glacier contribution to sea-level rise for the period 1800–2005. *Surv. Geophys. 32* (2011), 519–535.

[35] Mandelbrot, B. How long is the coast of Britain? Statistical self-similarity and fractional dimension. *Science 156*, 3775 (1967), 636–638.

[36] Mandelbrot, B. *The Fractal Geometry of Nature*. W. H. Freeman and Co., 1982.

[37] Marcos, M., Marzeion, B., Dangendorf, S., Slangen, A. B., Palanisamy, H., and Fenoglio-Marc, L. Internal variability versus anthropogenic forcing on sea level and its components. *Surv. Geophys. 38*, 1 (2017), 329–348.

[38] Marzeion, B., Jarosch, A. H., and Gregory, J. M. Feedbacks and mechanisms affecting the global sensitivity of glaciers to climate change. *The Cryosphere 8* (2014), 59–71.

[39] Marzeion, B., Jarosch, A. H., and Hofer, M. Past and future sea-level change from the surface mass balance of glaciers. *The Cryosphere 6* (2012), 1295–1322.

[40] Maussion, F., Butenko, A., Eis, J., Fourteau, K., Jarosch, A., Landmann, J., Oesterle, F., Recinos, B., Rothenpieler, T., Vlug, A., Wild, C., and Marzeion, B. The Open Global Glacier Model (OGGM) v1.0. *Geosci. Model Dev. Discuss. - in review* (2018).

[41] Meier, M. F., Dyurgerov, M. B., Rick, U. K., O'Neel, S., Pfeffer, W. T., Anderson, R. S., Anderson, S. P., and Glazovsky, A. F. Glaciers dominate eustatic sea-level rise in the 21st century. *Science 317* (2007), 1064.

[42] Meinshausen, M., Smith, S. J., Calvin, K., Daniel, J. S., Kainuma, M., Lamarque, J., Matsumoto, K., Montzka, S., Raper, S., Riahi, K., et al. The RCP greenhouse gas concentrations and their extensions from 1765 to 2300. *Climatic Change 109*, 1-2 (2011), 213–241.

[43] Mitchell, T. D., and Jones, P. D. An improved method of constructing a database of monthly climate observations and associated high-resolution grids. *Int. J. Climatol. 25* (2005), 693–712.

[44] Myhre, G., Shindell, D., Bréon, F.-M., Collins, W., Fuglestvedt, J., Huang, J., Koch, D., Lamarque, J.-F., Lee, D., Mendoza, B., Nakajima, T., Robock, A., Stephens, G., T., T., and Zhang, H. Anthropogenic and natural radiative forcing. In *Climate Change 2013: The Physical Science Basis. Contribution of Working Group I to the Fifth Assessment Report of the Intergovernmental Panel on Climate Change*, T. Stocker, D. Qin, G.-K. Plattner, M. Tignor, S. Allen, J. Boschung, A. Nauels, Y. Xia, B. V., and P. Midgley, Eds. Cambridge University Press, Cambridge, United Kingdom and New York, NY, USA, 2013.

[45] New, M., Lister, D., Hulme, M., and Makin, I. A high-resolution data set of surface climate over global land areas. *Clim. Res. 21* (2002), 1–25.

[46] Oerlemans, J. Simulation of historic glacier variations with a simple climate-glacier model. *J. Glaciol. 34*, 118 (1988), 333–341.

[47] Oerlemans, J. Extracting a climate signal from 169 glacier records. *Science 308* (2005), 675–677.

[48] Oerlemans, J., Dyurgerov, M., and van de Wal, R. S. W. Reconstructing the glacier contribution to sea-level rise back to 1850. *The Cryosphere 1* (2007), 59–65.

[49] Ohmura, A. Physical Basis for the Temperature-Based Melt-Index Method. *J. Appl. Meteorol. 40* (2001), 753–761.

[50] Parkes, D., and Marzeion, B. Major 20th century contribution to sea-level rise from uncharted glaciers. *In review* (2018).

[51] Paul, F., Bolch, T., Kääb, A., Nagler, T., Nuth, C., Scharrer, K., Shepherd, A., Strozzi, T., Ticconi, F., Bhambri, R., Berthier, E., Bevan, S., Gourmelen, N., Heid, T., Jeong, S., Kunz, M., Lauknes, T., Luckman, A., Merryman Boncori, J., Moholdt, G., Muir, A., Neelmeijer, J., Rankl, M., VanLooy, J., and Van Niel, T. The glaciers climate change initiative: Methods for creating glacier area, elevation change and velocity products. *Remote Sens. Environ. 162* (2015), 408–426.

[52] Pfeffer, W. T., Arendt, A. A., Bliss, A., Bolch, T., Cogley, J. G., Gardner, A. S., Hagen, J. O., Hock, R., Kaser, G., Kienholz, C., Miles, E. S., Moholdt, G., Mölg, N., Paul, F., Radic, V., Rastner, P., Raup, B. H., Rich, J., and Sharp, M. J. The Randolph Glacier Inventory: a globally complete inventory of glaciers. *J. Glaciol. 60* (2014), 537–552.

[53] Radić, V., Bliss, A., Beedlow, A., Hock, R., Miles, E., and Cogley, J. Regional and global projections of twenty-first century glacier mass changes in response to climate scenarios from global climate models. *Climate Dyn. 42*, 1-2 (2014), 37–58.

[54] Raper, S., and Braithwaite, R. Low sea level rise projections from mountain glaciers and icecaps under global warming. *Nature 439* (2006), 311–313.

[55] Rastner, P., Bolch, T., Mölg, N., Machguth, H., Le Bris, R., and Paul, F. The first complete inventory of the local glaciers and ice caps on greenland. *The Cryosphere 6*, 6 (2012), 1483–1495.

[56] Reichert, B. K., Bengtsson, L., and Oerlemans, J. Recent glacier retreat exceeds internal variability. *J. Climate 15* (2002), 3069–3081.

[57] RGI Consortium. Randolph Glacier Inventory (RGI) - A Dataset of Global Glacier Outlines: Version 6.0., 2017.

[58] Richardson, S. D., and Reynolds, J. M. An overview of glacial hazards in the Himalayas. *Quaternary Int. 65* (2000), 31–47.

[59] Roe, G., and O'Neal, M. The response of glaciers to intrinsic climate variability: observations and models of late-Holocene variations in the Pacific Northwest. *J. Glaciol. 55*, 193 (2009), 839–854.

[60] Schutz, B., Zwally, H., Shuman, C., Hancock, D., and DiMarzio, J. Overview of the ICESat mission. *Geophys. Res. Lett. 32*, 21 (2005).

[61] Sicart, J., Hock, R., and Six, D. Glacier melt, air temperature, and energy balance in different climates: The Bolivian Tropics, the French Alps, and northern Sweden. *J. Geophys. Res. 113*, D24 (2008), D24113.

[62] Slangen, A., Church, J., Agosta, C., Fettweis, X., Marzeion, B., and Richter, K. Anthropogenic forcing dominates global mean sea-level rise since 1970. *Nature Clim. Change 6* (2016), 701–705.

[63] Tarboton, D., Bras, R., and Rodriguez-Iturbe, I. The Fractal Nature of River Networks. *Water Resourc. Res. 24*, 8 (1988), 1317–1322.

[64] Vaughan, D., Comiso, J., Allison, I., Carrasco, J., Kaser, G., Kwok, R., Mote, P., Murray, T., Paul, F., Ren, J., Rignot, E., Solomina, O., K., S., and Zhang, T. Observations: Cryosphere. In *Climate Change 2013: The Physical Science Basis. Contribution of Working Group I to the Fifth Assessment Report of the Intergovernmental Panel on Climate Change*, T. Stocker, D. Qin, G.-K. Plattner, M. Tignor, S. Allen, J. Boschung, A. Nauels, Y. Xia, B. V., and P. Midgley, Eds. Cambridge University Press, Cambridge, United Kingdom and New York, NY, USA, 2013.

[65] WGMS 2017. *Global Glacier Change Bulletin No. 2 (2014-2015).* World Glacier Monitoring Service, Zurich, Switzerland, 2017.

[66] WGMS (World Glacier Monitoring Service) and NSIDC (National Snow and Ice Data Center). World Glacier Inventory. available at: `http://nsidc.org/data/glacier\_inventory/index.html`, 1989.

[67] Zemp, M., Frey, H., Gärtner-Roer, I., Nussbaumer, S. U., Hoelzle, M., Paul, F., Haeberli, W., Denzinger, F., Ahlstrøm, A. P., Anderson, B., Bajracharya, S., Baroni, C., Braun, L. N., Cáceres, B. E., Casassa, G., Cobos, G., Dávila, L. R., Granados, H. D., Demuth, M. N., Espizua, L., Fischer, A., Fujita, K., Gadek, B., Ghazanfar, A., Hagen, J. O., Holmlund, P., Karimi, N., Li, Z., Pelto, M., Pitte, P., Popovnin, V. V., Portocarrero, C. A., Prinz, R., Sangewar, C. V., Severskiy, I., Sigurdsson, O., Soruco, A., Usubaliev, R., and Vincent, C. Historically unprecedented global glacier decline in the early 21st century. *J. Glaciol. 61* (2015), 745–762.